Title

Structural Studies of Polypeptide: Mechanism of Immunoglobin Catalysis and Helix Propagation in Hybrid Sequence, Disulfide Containing Peptides

Author

Storrs, R.W.

Publication Date

1992-08-01

LBL-33152
UC-408

Lawrence Berkeley Laboratory
UNIVERSITY OF CALIFORNIA

CHEMICAL BIODYNAMICS DIVISION

Structural Studies of Polypeptides: Mechanism of Immunoglobin Catalysis and Helix Propagation in Hybrid Sequence, Disulfide Containing Peptides

R.W. Storrs
(Ph.D. Thesis)

August 1992

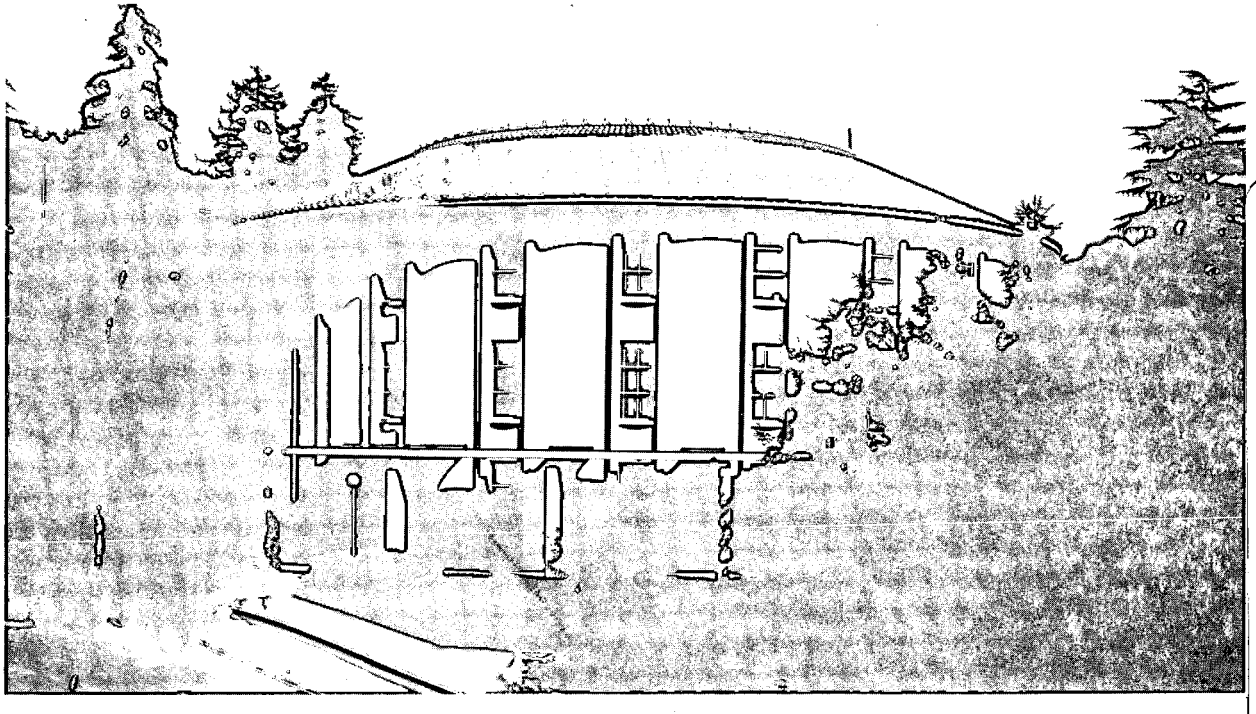

Prepared for the U.S. Department of Energy under Contract Number DE-AC03-76SF00098

DISCLAIMER

LBL-33152

Structural Studies of Polypeptides: Mechanism of Immunoglobin Catalysis and Helix Propagation in Hybrid Sequence, Disulfide Containing Peptides

Richard Wood Storrs

(Ph.D. Thesis)

Department of Chemistry
University of California
and
Structural Biology Division
Lawrence Berkeley Laboratory
University of California
Berkeley, California 94720

August 1992

This work was supported by the Director, Division of Energy Biosciences, Office of Basic Energy Sciences, U. S. Department of Energy under contract DE-AC03-76SF00098

Structural Studies of Polypeptides: Mechanism of Immunoglobin Catalysis and Helix Propagation in Hybrid Sequence, Disulfide Containing Peptides

by

Richard Wood Storrs

Structural Studies of Polypeptides:
Mechanism of Immunoglobin Catalysis
and
Helix Propagation in Hybrid Sequence, Disulfide Containing Peptides

by

Richard Wood Storrs

Abstract

The structures of several polypeptides were investigated using Nuclear Magnetic Resonance spectroscopy. Catalytic immunoglobin fragments were studied to identify amino acid residues responsible for the catalytic activity. Small, hybrid sequence peptides were analyzed for helix propagation following covalent initiation. These peptides were analyzed for biochemical activity related to the protein from which the helical sequence was derived.

Hydrolysis of *p*-nitrophenyl carbonates and esters by specific immunoglobins is thought to involve charge complementarity. The pK of the transition state analog *p*-nitrophenyl phosphate bound to the immunoglobin fragment was determined by ^{31}P-NMR to verify the juxtaposition of a positively charged amino acid to the binding/catalytic site. Binding to the immunoglobin did not alter the pK of this species. No evidence was seen for charge complementarity.

Optical studies of immunoglobin mediated photoreversal of *cis, syn* cyclobutane thymine dimers implicated tryptophan as the photosensitizing chromophore. The current work shows the chemical environment of a single tryptophan residue is altered upon binding

of the thymine dimer. This tryptophan residue was localized to within 20 Å of the binding site through the use of a nitroxide paramagnetic species covalently attached to the thymine dimer.

A hybrid sequence peptide was designed and synthesized based on the bee venom peptide apamin in which the helical residues of apamin were replaced with those from the recognition helix of the bacteriophage 434 repressor protein. Oxidation of the disufide bonds occured uniformly in the proper 1-11, 3-15 orientation, stabilizing the 434 sequence in an α-helix. The glycine residue stopped helix propagation.

Helix propagation in 2,2,2-trifluoroethanol mixtures was investigated in a second hybrid sequence peptide using the apamin-derived disulfide scaffold and the S-peptide sequence (residues 3-20 of ribonuclease A). The "helix-stop" signal previously observed in the free S-peptide was not observed in the NMR NOESY spectrum. Helical connectivities were seen throughout the S-peptide sequence.

The apamin/434 hybrid peptide did not bind to DNA. The apamin/S-peptide hybrid did bind to the S-protein (residues 21-166 of ribonuclease A) and reconstituted enzymatic activity.

Table of Contents

List of Figures

Acknowledgments

Firstly, I wish to thank my mentor Prof. David Wemmer, for the guidance and opportunity to pursue these studies. Without his steady hand at the tiller little of the following would have come to fore.

Dave leads an eclectic group of characters all of whom have shared in my personal scientific development. Ann is always sharp as a tack and quite usually right on the money. Joe has always had a knack for explaining the intricacies of a procedure with exquisite clarity. Vasant invariably adds a fresh perspective to any issue. They, along with Jeff, Beth, Debbie, and Milton all shaped my approach to science, and I am grateful to share their friendship. The "new crew", played in my time by Patty, Brian, Marty, Mark, Valérie, and Ho, had big shoes to fill, but they also had big feet.

The friendships and educations I developed during my eight years at the Round House are far too numerous to succinctly itemize. I only hope I have adequately expressed my gratification personally to the legion of scientists and support staff who have made my tenure here enjoyable and productive.

And thanks, Mom and Pops, and Charlie, too. Without their love and support I might have succumbed to one of those doubting thoughts.

Lastly, I thank my late lover Will, who taught me more about life than could be written herein.

ENJOY!

Chapter 1: Introduction to NMR of Polypeptides

Polypeptides are essential for life. They function as building blocks providing structure and organization to living systems, as engines by which molecules are constructed and transported, and as messengers regulating these events. They consist of several to several hundred amino acids linked up in a (usually linear) chain via peptide bonds (figure 1.1). The peptide backbone twists and turns to form specific three-dimensional matrices of the amino acids, whose side chain and peptide moieties interact to perform the necessary chemistry. The functions of these ubiquitous molecules of life, therefore, are intimately associated with their structures.

NMR is a spectroscopic technique which measures the magnetic environment of atomic nuclei with non-zero spin. Of the few methods developed for obtaining structural information on polypeptides, nuclear magnetic resonance (NMR) is perhaps the most powerful. As described below and extensively reviewed elsewhere (Wüthrich, 1986; Ernst *et al.*, 1987; Slichter, 1978), NMR can provide structural and dynamic information on a molecular scale by measuring the magnetic interaction of spin 1/2 nuclei. This information can be interpreted in terms of specific molecular or intermolecular interactions, or can be combined piecemeal to give a dynamic model of the equilibrium molecular structures.

The most common nucleus with non-zero spin is hydrogen-1, or the proton. Protons are ubiquitous and abundant in the amino

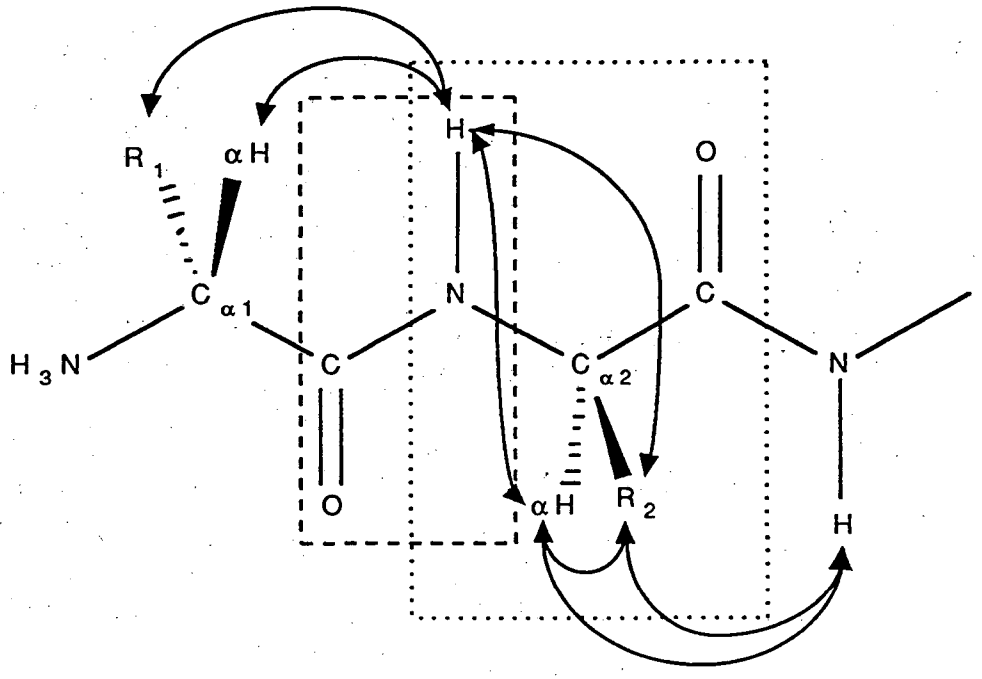

Figure 1.1 - Bonding of the peptide backbone. The dotted box encircles one amino acid. The dashed box encircles one peptide bond. The arrows designate interproton connectivities important to NMR assignments and structural characterization. R_i: amino acid side chains.

acids which comprise polypeptides, and therefore are the most useful in the study of polypeptide structure by NMR. Other nuclei can also provide useful information as demonstrated in Chapter 2, where ^{3}H and ^{31}P are utilized to probe the local environment of a very large polypeptide. Additionally, the stable isotopes ^{15}N and ^{13}C are often utilized in the study of biomolecules. All of these nuclei have spin 1/2, yet each has a very different magnetic moment owing to different values of charge and mass, and consequently they have distinguishable NMR spectra.

NMR works by measuring the interaction of the magnetic dipole of the nucleus with other magnetic dipoles. The dipole of the nucleus arises from the quantum mechanical behavior of the protons and neutrons of which it is composed. Each proton and neutron has a spin quantum number of 1/2, which for a nucleus add in a vector manner to yield the overall nuclear spin quantum number, I. This quantum number is associated with 2I+1 spin states for a nucleus, each of which has a characteristic angular momentum. When placed in an external magnetic field the normally degenerate spin states of a given nucleus split into 2I+1 energy levels, whose energy is given by

$$E_{m_I} = -\gamma h m_I H_o / 2\pi$$

where H_o is the magnitude of the external magnetic field, m_I is the projection of the nuclear spin on H_o, and γ is the magnetogyric ratio of the given nucleus in Hz/Tesla. This latter quantity relates the charge of the nucleus to its moment of inertia, and is a constant for a given nuclear species. This splitting of energy levels is diagrammed

in figure 1.2.

The Boltzmann distribution describes the population of these states, which differ only slightly (but perceptibly) at room temperature. For protons in a magnetic field of 1.4 Tesla, the relative populations are:

$$N_+/N_- = \exp[-(E_- - E_+)/kT] = 0.999998$$

where N_+ the population of the higher energy (E_+) state, N_- is the population of the lower energy (E_-) state, T is the absolute temperature (298 K in the calculation above), and k is Boltzmann's constant. Thus the populations differ by about two in a million spins at room temperature. This makes NMR an inherently insensitive spectroscopy, requiring large numbers of identical molecules to create detectable signals. The input of electromagnetic radiation with energy matching the separation in spin energy drives transitions between spin states which differ by one unit in m_I, and in doing so perturb the populations from their equilibrium distribution. By interacting with a randomly fluctuating magnetic field, generally of chemical origin, the energy levels are no longer static and the spin state populations can relax back to their equilibrium distribution. Consideration of mechanisms for this relaxation will become important in the analysis of NMR data, as discussed below.

Nuclear spin may be envisioned in a classical mechanical model as a magnetic dipole, as any charged particle in motion establishes a magnetic field. The spinning of positive charge will establish a stationary magnetic dipole, as diagrammed in figure 1.3a.

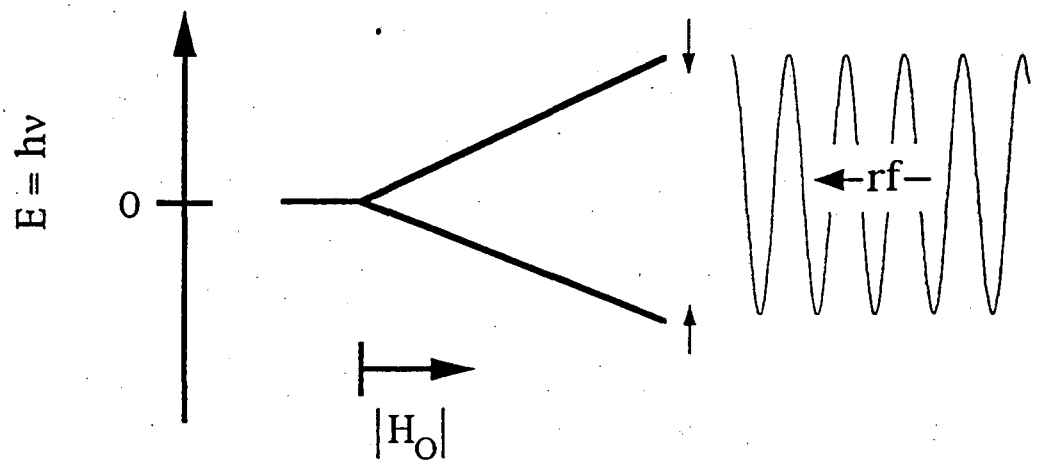

Figure 1.2: Energy of nuclear spin quantum levels in an external magnetic field, Ho. Radio frequency radiation (rf) can induce transitions between spin states when matched in energy to the spin state splitting.

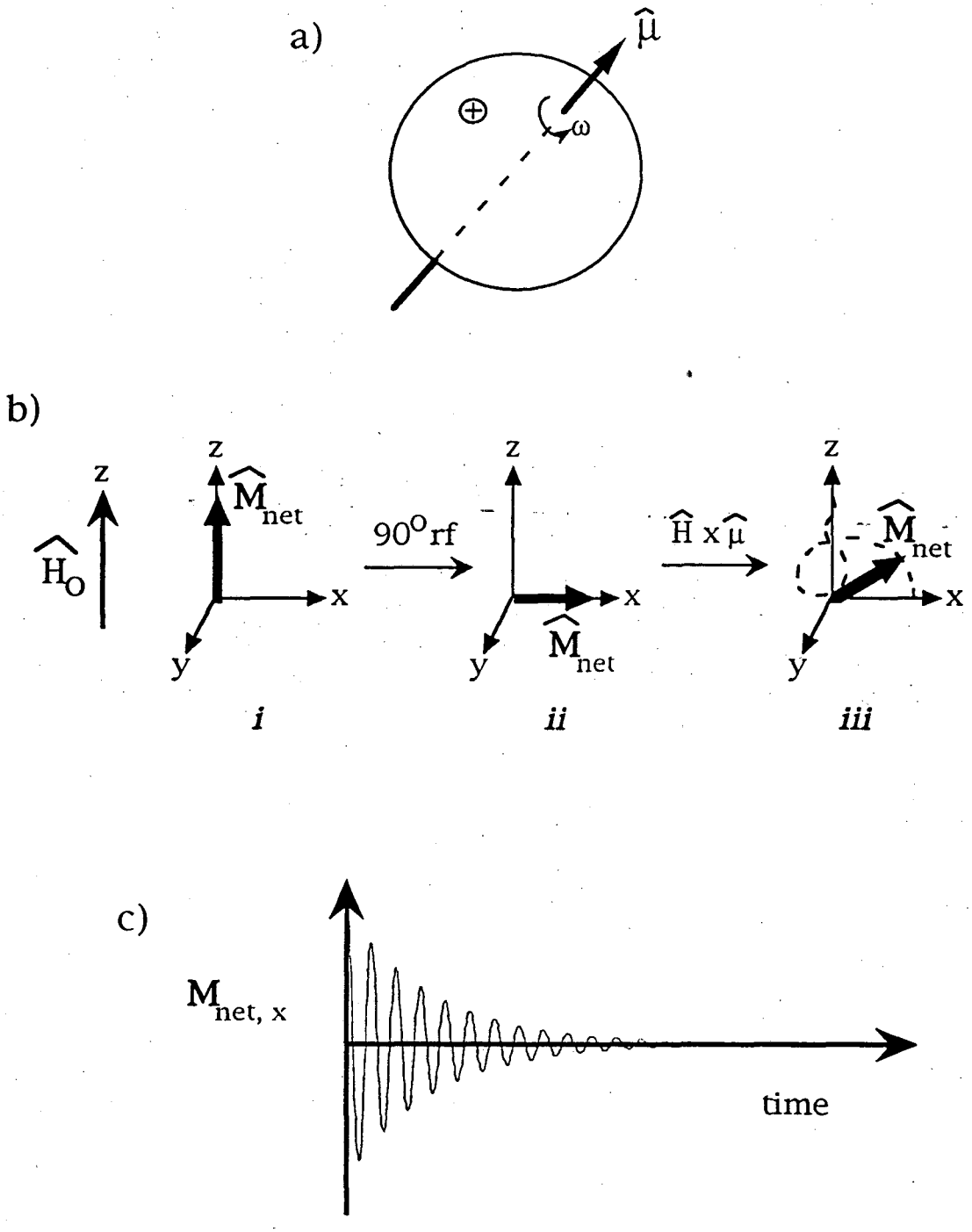

Figure 1.3 - a) Magnetic dipole, μ, generated by the spin of a proton.
b) Orientation and evolution of net nuclear magnetic vector, M, from a collection of protons in a magnetic field, Ho.
i: equilibium. *ii*: following a 90 degree rf pulse.
iii: precession due to interaction with applied magnetic field.
c) x-component of net nuclear magnetization in *iii* as a function of time, known as Free Induction Decay (FID).

This classical view is justified as long as other couplings involving the spin are weaker than coupling to the field. A collection of nuclei with non-zero spin may then be described by a net magnetization vector whose magnitude is the vector sum of the magnetic moments of the individual spins. In the absence of an external magnetic field, there is no preferred orientation of the magnetic dipoles and hence no net magnetization vector. Application of such a field not only creates such a vector, but aligns it with the external magnetic field. This direction is generally defined to be the z-axis.

In this classical description, the state of lowest energy occurs when the net magnetization vector is aligned with the applied magnetic field. This corresponds to the equilibrium Boltzmann distribution. The radiation applied to perturb this distribution acts as a second force, "tipping" the magnetic vector away from its parallel, equilibrium orientation. As there remains a force from the external magnetic field, a torque is applied to the vector. This causes precession about the z-axis with a frequency dependent on the magnitude of the external magnetic field, as diagrammed in figure 1.3b. The frequency of precession is given by the Larmor equation,

$$\omega_o = -\gamma H_o$$

The presence of suitable relaxation mechanisms, other fluctuating magnetic dipoles or other magnetic fields, then allows the perturbed vector to "relax" back to the equilibrium configuration parallel to H_o.

What makes this phenomenon useful in structure determination is that the effective external magnetic field felt by a

given nucleus is highly dependent on the immediate electronic environment of the nucleus. Recalling the fact that moving charges produce magnetic fields, it is easy to see that the electrons around and between nuclei, as well as the presence of other nuclei, will alter the magnetic field affecting a given nucleus. Because the splitting of spin energy levels is dependent on the magnitude of the effective external magnetic field, the spin state energy splittings of a given nucleus will depend on its chemical environment. If the applied magnetic field is strictly homogeneous, any variation in energies absorbed by the nuclear ensemble of a sample can be attributed to the chemical environment of each nucleus. This is the phenomenon known as chemical shift, and can be defined as follows:

$$\Delta E = \gamma H_{eff} = \gamma H_o (1 - \sigma).$$

σ, the chemical shift, quantitates the amount a given nucleus is deshielded, relative to a reference standard, from the applied field by nearby electrons. The energy splitting and resonant frequency remain proportional to H_o but are scaled by σ. This scaling is typically on the order of 10^{-6} x H_o, and so σ is generally given in unitless denominations of parts per million, or ppm. This convention allows comparisons of chemical shift independent of the operating field (H_o) of the spectrometer.

By observing the distribution of frequencies absorbed by a sample, much structural information can be obtained. To a first approximation a given chemical functionality will give rise to a characteristic chemical shift. For example, a representative ^{1}H-NMR

spectrum of the 2.5 kDa peptide described in chapter 5 is given in figure 1.4. On the left hand, or downfield, side of the spectrum are the amide protons resonating at relatively large values of σ. These are the most deshielded because the high electronegativity of the amide nitrogen yields little shielding electron density on the proton. Next to them on the right, at somewhat smaller values of σ, are protons on aromatic rings. These protons experience a downfield shift from the magnetic field caused by circulation of the aromatic π-bonding electrons. Further upfield at smaller values of σ are the peptide Cα protons, then the side chain aliphatic protons. These resonate at progressively smaller values of σ in keeping with the increasing electron density of the C-H bonding electrons at the ^1H nucleus. For similar reasons methyl protons are typically found furthest upfield.

Experimentally, this amplitude vs. frequency profile can be obtained in two ways. The most straightforward of these is to apply a constant supply of radiation at a specific frequency to a sample in a homogeneous magnetic field. When the frequency of applied radiation matches the energy splitting of the spin states for a given nucleus, resonance occurs and transitions are induced between the spin states:

$$\Delta E = h\nu = \gamma H_o (1-\sigma).$$

The energy absorption is measured by the electric current induced in a receiver coil by the precessing net magnetization vector. By sweeping either the frequency of irradiation or the applied magnetic

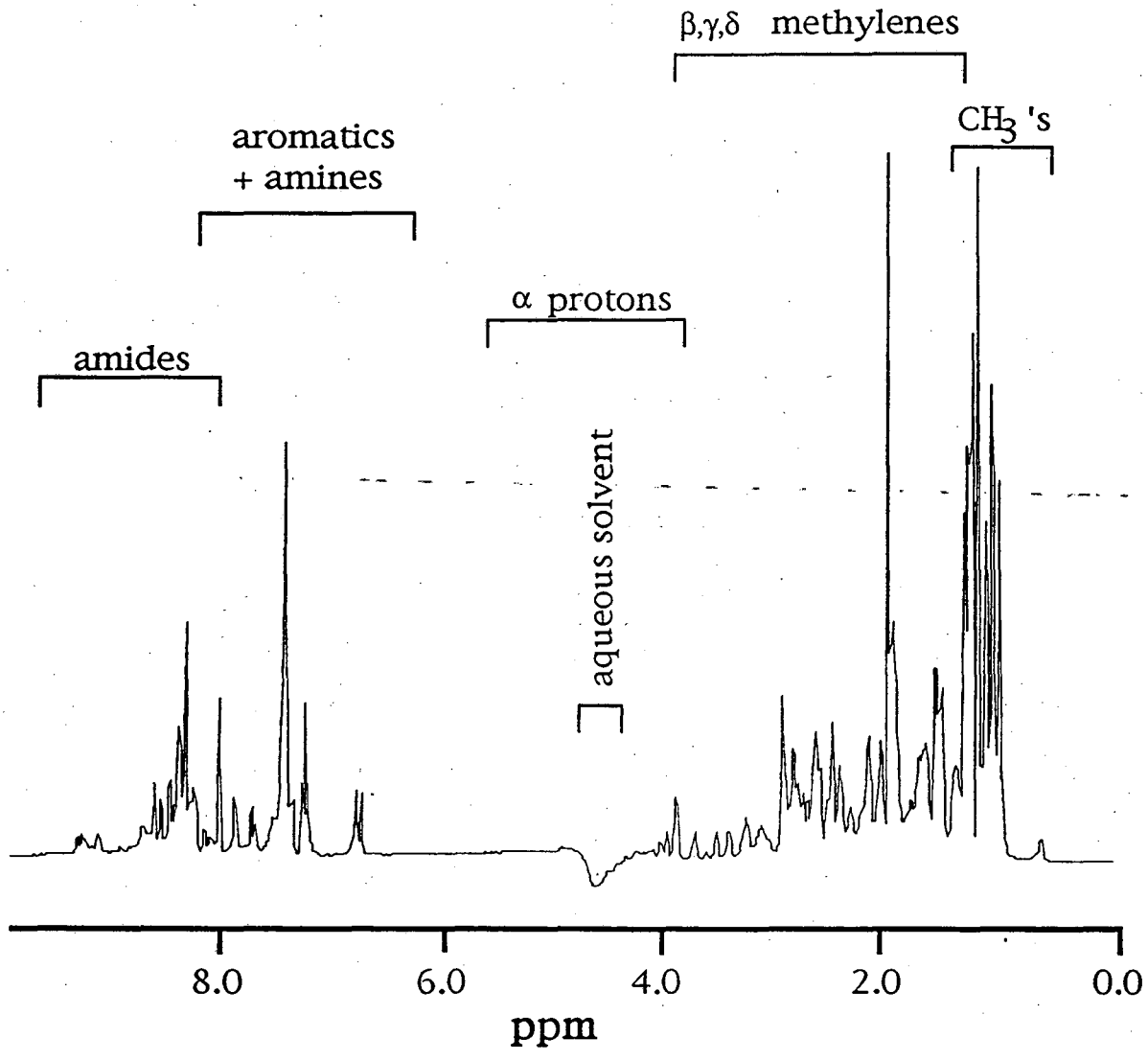

Figure 1.4 - Proton-NMR spectrum of the 25 amino acid peptide described in Chapter 5. Typical positions at which the protons of amino acids appear are indicated.

field the appropriate absorption vs. energy spectrum can be procured. Modern NMR spectrometers have a magnetic field strength of 2.35-14.1 Tesla, which give protons a spin resonant frequency of 100-600 MHz. These frequencies are in the radio frequency (rf) band of the electromagnetic spectrum. Because the rf waves are applied continuously, this method is known as Continuous Wave Nuclear Magnetic Resonance, or CW-NMR. This method, while simple in description and application, has many shortcomings not the least of which is limited sensitivity.

The alternative method is to apply a discrete pulse of radio frequency radiation and monitor the precession of the tipped net magnetization vectors of all nuclei of a given type simultaneously. These vectors then precess at the frequency characteristic of their individual chemical shifts, as described by the Larmor equation. The measured oscillation in current of a detector wire is then a linear combination of all the precessional frequencies of each chemically shifted nuclear ensemble. With the relaxation of the magnetic vectors the precessional amplitude decays. Hence the term Free Induction Decay (FID) is given to the amplitude vs. time data and is shown in figure 1.3b. By performing a Fourier Transform on the FID, we may change the dependent variable from time to frequency, deriving the same information as is obtained directly in CW-NMR. This procedure is known as FT-NMR.

For the added costs and complexity, FT-NMR has many advantages. Not the least of these is the time efficiency of data accumulation. The Fourier transformation can result in a high resolution spectrum from a single FID. The capability of averaging

multiple FID accumulations on a single sample drastically increases the signal to noise ratio and allows spectra to be obtained from very dilute samples. The main advantage of the FT-NMR technique, however, is in its ability to directly measure the rate of magnetic relaxation.

Following perturbation from its equilibrium state, a spin system requires some mechanism for angular momentum transfer in order to return to the equilibrium Boltzmann distribution. Fluctuating magnetic fields arising from molecular motions provide the means for this transfer. Of the many such fields experienced by a nucleus, in general only those arising from nearby nuclei or unpaired electrons are large enough to contribute significantly to the relaxation of protons in liquids. The coupling of one magnetic dipole with another nearby dipole allows direct transfer of angular momentum, and hence facilitates spin relaxation. Such dipolar coupling is dependent on the relative orientation of the dipoles with respect to H_0, an effect which averages to zero in liquids but is still important for the relaxation of each nucleus. An exception to this dictum is the ^{31}P isotope. This I=1/2 nucleus has a very asymmetric electron distribution which allows it to self-relax. This will be explained in greater detail in Chapter 2.

Consider two I=1/2 nuclei, I and S, in a static magnetic field as in an FT-NMR experiment. There correspond four energy levels E_i, as diagrammed in figure 1.5, each with a characteristic equilibrium population P_i. When I and S are the same nuclear species E_2-E_3 is so small that P_2 and P_3 may be considered equal. There are six possible transitions between these spin states, each described by a transition

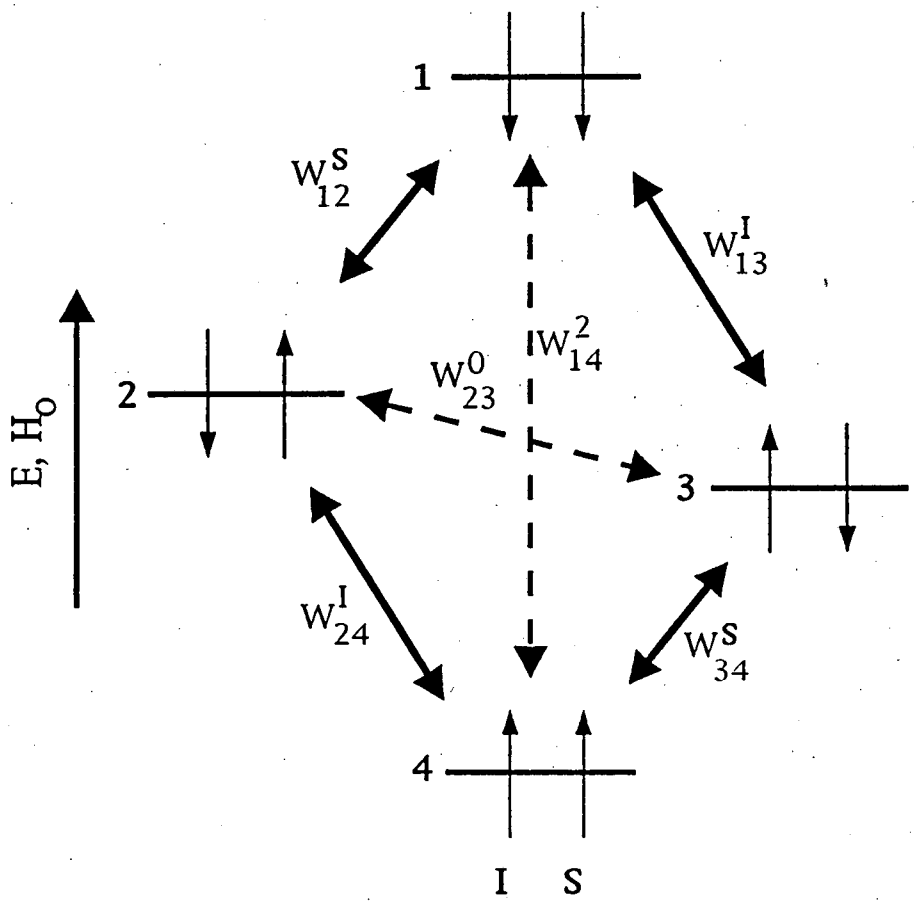

Figure 1.5 - Spin orientation, energy levels, and observed transitions for two spins, I and S in a magnetic field. The solid double arrows represent the allowed, single quantum transitions, while the dashed double arrows represent the "forbidden" zero and double quantum transitions allowed through dipolar coupling of the spins.

probability, W_{ij}. Radio frequency radiation can only induce transitions on a single nucleus following the selection rule $\Delta m_I=\pm 1$ with a probability $W_I=W_{13}=W_{24}$ and $W_S=W_{12}=W_{34}$, each transition with a characteristic rate given by

$$R_{ij} = W_{ij}(P_j-P_i).$$

Dipolar coupling, however, is a perturbation of the isolated spin quantum description and can induce transitions between all spin energy levels. By irradiating nucleus S at its resonant frequency its spin populations are altered, so that $P_1=P_2$ and $P_3=P_4$. In the isolated spin case, the populations of spin I are unaffected. But if the two spins are close enough their magnetic dipoles can couple, and double and zero quantum transitions can be induced by the dipolar interaction. As P_1 and P_4 become more equal, the zero and double quantum transitions become more important in re-establishing a steady state of the populations. $P_1(=P_2)$ is decreased with double quantum transitions, while $P_4(=P_3)$ increases. The resulting difference in populations for spin I is increased, as is the magnitude of energy absorption. Zero quantum transitions also occur, however, as P_2 is no longer equal to P_3. The net effect on the intensity of signal I is therefore complex, as the double quantum transition increases this intensity, while the zero quantum transition reduces it.

Zero and double quantum transitions also correspond to rather different magnitudes of ΔE. In a qualitative manner one can then estimate that the double quantum transitions will be facilitated by rather fast fluctuations in magnetic environment, while the zero

quantum transitions will be helped by slow motions. This analysis correctly predicts that for small molecules, which tumble quickly in solution, spin I will be enhanced because the double quantum transition is favored, while large molecules will show negative enhancement of spin I due to more efficient zero quantum transitions. The practical result is that when S is irradiated, the intensity of I is affected, an effect known as the nuclear Overhauser effect, or NOE.

If the molecular tumbling causes fluctuations of the local field at a frequency near the Larmor frequency of the nuclear transition, relaxation can occur. Intramolecular motions can also contribute to relaxation, particularly for large molecules. The extent or probability of magnetic interaction leading to relaxation is determined by the power or spectral density of motions at the Larmor frequency. The extent to which the frequency of these fluctuations matches the energy of transition is best described by a correlation function relating the position of a given nucleus at some time τ relative to the position at any earlier time:

$$K_i(\tau) = K_i(0) \exp [- |\tau|/\tau_c],$$

where τ_c is the correlation time describing the motion. Fourier analysis of the correlation function leads to a spectral density function $J(\omega)$ which provides a theoretical basis for determining the efficiency of relaxation.

$$J(\omega) = \int K_i(\tau) \exp [-i\omega\tau] \, d\tau$$

$$= A [\tau_c/(1 + \omega^2\tau_c^2)]$$

where A is a combination of constants. The spectral density function $J(\omega)$ describes the amplitude of fluctuation at a given frequency, ω,

and by evaluating this function at the appropriate frequencies the rate of relaxation may be calculated.

As described above, the NOE is dependent on the sum of zero and double quantum transitions. In the homonuclear case the energy splitting for the zero quantum transition W_{23}, $\Delta E = E_2 - E_3 \sim 0$. The spectral density at this frequency becomes proportional to τ_c. For the double quantum transition a simplification of this term can be obtained if $\omega\tau_c >> 1$, in which case the entire spectral density term approaches zero. This is consistent with the observation that for large molecules, with long correlation times, the double quantum transitions do not compete successfully with the zero quantum transitions. The dipolar magnetic field falls off radially as r^{-3}. The interaction of two dipolar fields, which gives rise to the NOE, is dependent on r^{-6}. Therefore the amplitude of an NOE cross peak $\sigma(f_1,f_2)$ for a large polypeptide is given by

$$\sigma(f_1,f_2) = B\,[\,\tau_c/r^6\,]$$

where B is a collection of experimental constants. Thus the NOE serves as a sensitive yardstick for measuring internuclear distances.

NOE's can be detected by selectively irradiating an isolated resonance with a discrete rf pulse and observing the changes in peak intensities of other resonances following excitation by a broad band rf pulse. This approach can be taken only when the irradiated resonances are well resolved, however, as unambiguous interpretation is possible only if the first, discrete rf pulse affects only a single resonance. Additionally this approach requires careful

selection of irradiation frequencies and execution of multiple experiments to obtain all the NOE data for a given sample. More complex systems often exhibit correspondingly complex spectra so that many resonances are not sufficiently resolved to allow selective irradiation.

A complete NOE profile can be obtained in a single experiment by utilizing two dimensional (2D) spectroscopy. The introduction of a second independent time variable in 2D spectroscopy allows the correlations between spins to be detected simultaneously. A generic 2D pulse sequence is diagrammed in figure 1.6. The preparation period establishes the spin ensemble in a desired population state. This may include time for the magnetization to completely relax to equilibrium and/or selective irradiation for elimination of large solvent resonances. The t_1 time period following the first (usually) 90° pulse allows the net magnetization vectors to evolve under chemical shift and scalar couplings (*vide infra*), and serves in the most general sense to frequency label the magnitude of the net magnetization vector following the second 90° pulse. The t_1 time period is incremented in successive experiments (or blocks) of a single 2D data set. The frequency-labeled magnetization is then allowed to mix, or communicate with other spins, during the time τ_m, resulting in the exchange of magnetization between two (or more) dipolar coupled spins. Finally the resultant magnetization is detected as a FID after the third 90° pulse in a second variable time domain, t_2. Thus the complete 2D data set consists of a series of FIDs modulated by the time period t_1.

This time domain data $S(t_1,t_2)$ is converted into the frequency

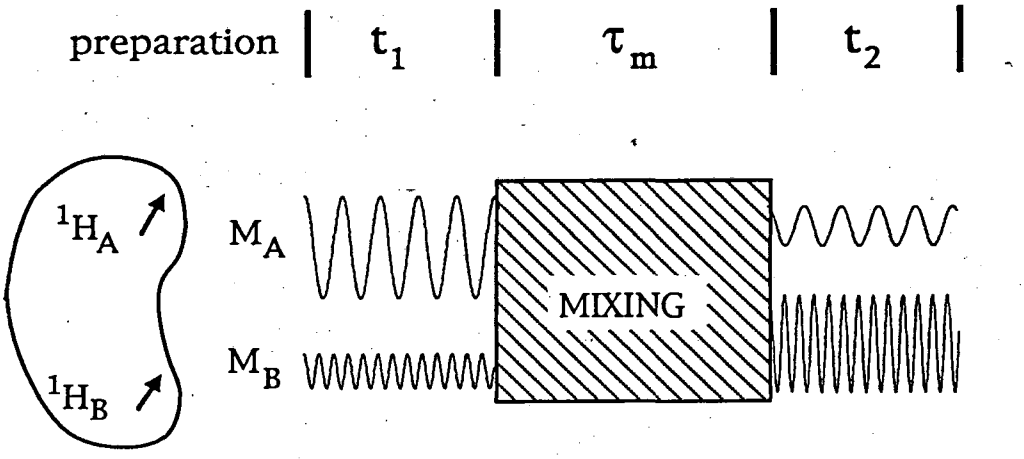

Figure 1.6 - Generic two-dimensional NMR experiment. The magnetization (M_i) of one nuclear spin (depicted as proton A) is exchanged with that of another (proton B) during the mixing period.

domain by Fourier transformation first in t_2 then in t_1. The resulting matrix in frequency space $S(f_1,f_2)$ exhibits intensity along the diagonal ($f_1=f_2$), corresponding to the unmodulated, one dimensional spectrum, and off-diagonal intensity or cross peaks [$S(f_1,f_2)$, $f_1 \neq f_2$] which reflect the mixing or exchange of magnetization between a spin resonating at frequency f_1 during t_1 with one resonating at f_2 during t_2. This type of frequency domain data is usually presented as a topographical contour plot, where the intensity is reflected in the number of contours.

The 2D-NOE or NOESY (for Nuclear Overhauser Effect SpectroscopY) experiment is the workhorse of structural NMR, for it provides direct information on which protons are close to one another in space. (In practice, "close" means within 5Å.) The pulse sequence is diagrammed in figure 1.7a, and can be rationalized using the classical model. As described above, the preparation period involves establishment of equilibrium and often the saturation of large solvent resonances. The first 90° pulse establishes transverse magnetization, which evolves under chemical shift during t_1. Part of the magnetization is returned to the z axis by the second 90° pulse, its magnitude now modulated by the chemical shift evolution during t_1. During the mixing time, τ_m, dipolar relaxation occurs, mixing z magnetization. The extent of this mixing is determined by the t_1-modulated populations of spin states. The third 90° pulse returns the resultant magnetization to the transverse plane, allowing detection in t_2. However, this information is of little value if the chemical identity of the protons exhibiting NOE's are unknown. From the resonant frequency one can get a rough chemical assignment for

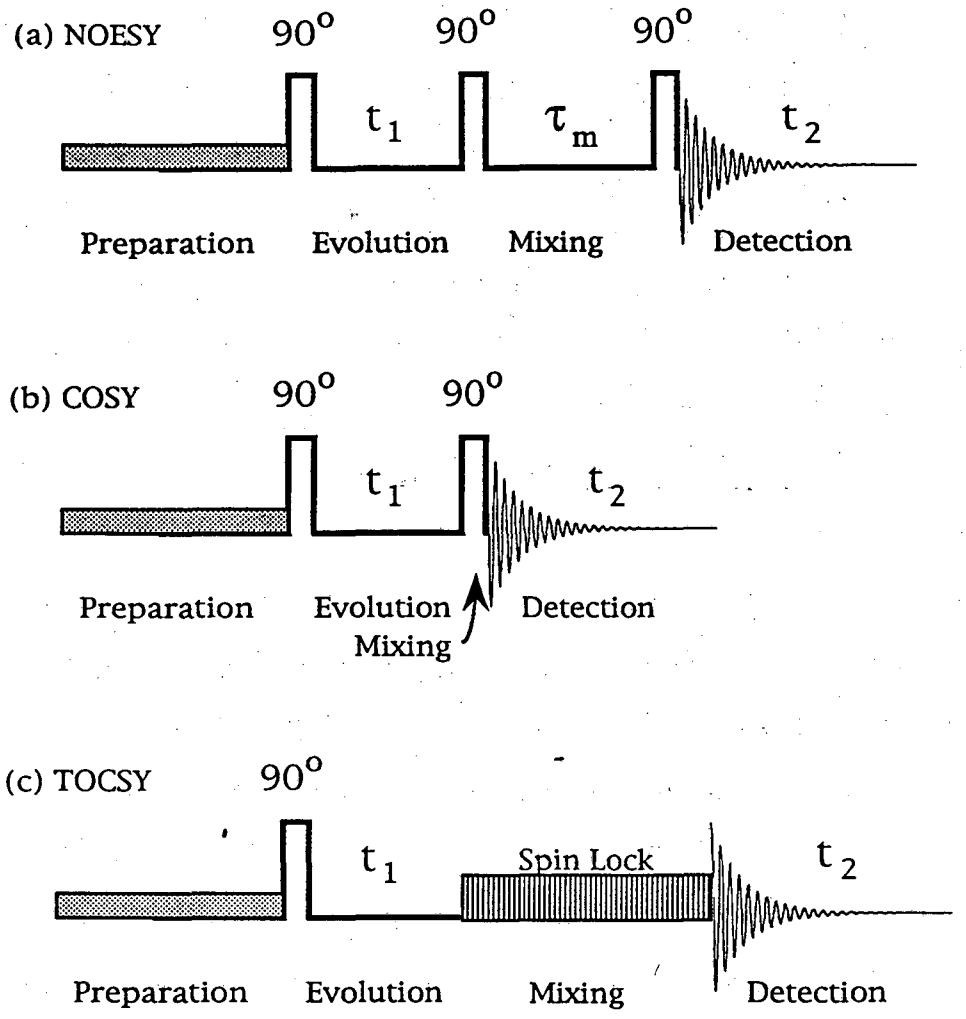

Figure 1.7 - Pulse sequences for the two-dimensional experiments used in this work. The preparation period in most of the data presented included saturation of the solvent resonance by selective irradiation.
(a) NOESY - Nuclear Overhauser Effect SpectroscopY which measures dipolar (or through-space) connectivities of <5Å.
(b) COSY - COrrelated SpectroscopY which measures scalar (or through-bond) connectivities of < four bonds.
(c) TOCSY - TOtal Correlation SpectroscopY which measures scalar connectivities through multiple bonds in a non-linear fashion.

the proton, however biological molecules are polymers of chemically similar groups. Clearly more information is necessary to assign a resonance to a particular proton in a polypeptide.

This information is obtained through the use of COrrelated SpectroscopY, or COSY data. The COSY experiment and the related TOCSY (for TOtal COrrelation SpectroscopY) experiment are 2D experiments in which magnetization is exchanged not through dipolar coupling but by scalar or through-bond coupling. Scalar coupling arises from the interaction of the nuclear magnetic dipole with the bonding electrons, with the consequence that the dipolar field is transmitted through the bonding network. This alters the effective field of spin I so that its resonant frequency reflects the spin state of spin S, to which it is connected by covalent bonds. Because the S spins can only be up or down, the I spins are split into two frequencies. Fortunately this effect, like the NOE, is limited in range. In practice, homonuclear ^{1}H-^{1}H couplings are limited to those protons connected by three or fewer bonds for COSY data. The TOCSY experiment extends this range considerably, but in a non-linear fashion. The TOCSY correlation map often has hard-to-predict holes which can only be observed with multiple experiments at various mixing times.

The evolution of magnetization in COSY and TOCSY experiments cannot be demonstrated using the classical net magnetization vector model. Like the NOESY these experiments incorporate two independent time variables which can be analyzed by analogous procedures. The useful information in the resulting contour plot is again contained in the cross peaks, but this information now reflects

the through bond interaction of the two spins rather than the through space interaction. This information is convoluted by the dependence of scalar coupling on the dihedral angles of bonds, and the magnitude of these cross peaks does not directly reflect the proximity of the two protons. The angular dependence of scalar coupling is well behaved, following a relationship derived by Karplus, and can yield information which is often useful in structure determination.

By combining the through-bond information of correlated experiments with the through space information of the NOE experiment a complete picture of the three dimensional structure of the molecule can be obtained. Using a computer algorithm a model can be constructed which is consistent with all the observed couplings. This process is rigorous yet time consuming, and care must be taken in interpreting the resulting model. Often one is interested only in local structure, or in structural changes. Much of the pertinent information concerning local structure can be derived directly from one- and two-dimensional data sets, without modeling the entire structure. This approach is used in Chapter 5 to investigate peptide helix propagation in an aqueous alcohol solvent.

A special situation of dipolar relaxation arises from paramagnetic species. Paramagnets are molecules which have an unpaired electron. This electron has spin angular momentum, just as the spinning nucleus does. The mass of the electron, however, is much smaller than that of the proton, resulting in a 660 fold difference in the magnetic moment between the two. This difference manifests itself in an NMR experiment by extremely rapid relaxation

of nuclei within 20Å of the unpaired electron. The rapid relaxation of the tipped net magnetic vector disallows protracted precession, and the FID decays so rapidly that it is undetectable. The advantage of this effect is that it can be detected over a longer range than internuclear dipolar relaxation, up to 20Å, and that unpaired electrons are rare in most biological systems (in the absence of transition metal cofactors) so that one must be specifically introduced into the experiment. In this way the spectral effects, broadening or elimination of resonances, can be interpreted in terms of distances to the added paramagnetic species. In Chapter 3 this effect is used to determine the proximity of particular spins to the antigen binding site of an antibody fragment.

Ernst, R.R., Bodenhousen, G., & Wokaun, A. (1987) *Principles of Nuclear Magnetic Resonance*, Oxford University Press, New York.

Slichter, C.P. (1978) *Principles of Magnetic Resonance*, Springer-Verlag, New York.

Wüthrich, K. (1986) *NMR of Proteins and Nucleic Acids*, Wiley, New York.

Chapter 2: Mechanism of Immunoglobin Catalysis I Transition State Stabilization

Immunoglobins are a class of structurally related proteins which bind a broad array of ligands with high affinity and great specificity (Pressman & Grossberg, 1968; Goodman, 1975; Amzel & Poljak, 1979). A typical immunoglobin (Ig) has a molecular mass of about 150 kDa, with over 5,000 protons distributed amongst some 1300 amino acids. As diagrammed in figure 2.1, Igs are composed of four peptide chains. These chains fold into domains with roughly 110 amino acids from each of two chains. Structural stability is acheived by hydrophobic packing between domains of separate polypeptide chains in a pairwise fashion. Ligand binding occurs in a pocket formed at the interface of the N-terminal domains, where the amino acid sequence is highly variable.

Igs are produced in mammals in response to exposure to foreign substances, or immunogens. Their physiological role is to bind specifically to these substances, marking them for neutralization and elimination from the host. Modern monoclonal technology allows the production of large quantities of immunoglobins with defined specificity and homogeneous composition (Kohler & Milstein 1975). The exquisite specificity and high affinity of immunoglobins has been combined with modern transition state theory to generate novel chemical catalysts (reviewed in Catalytic Antibodies, 1991). A stable molecule which mimics in charge, size, and shape the rate limiting

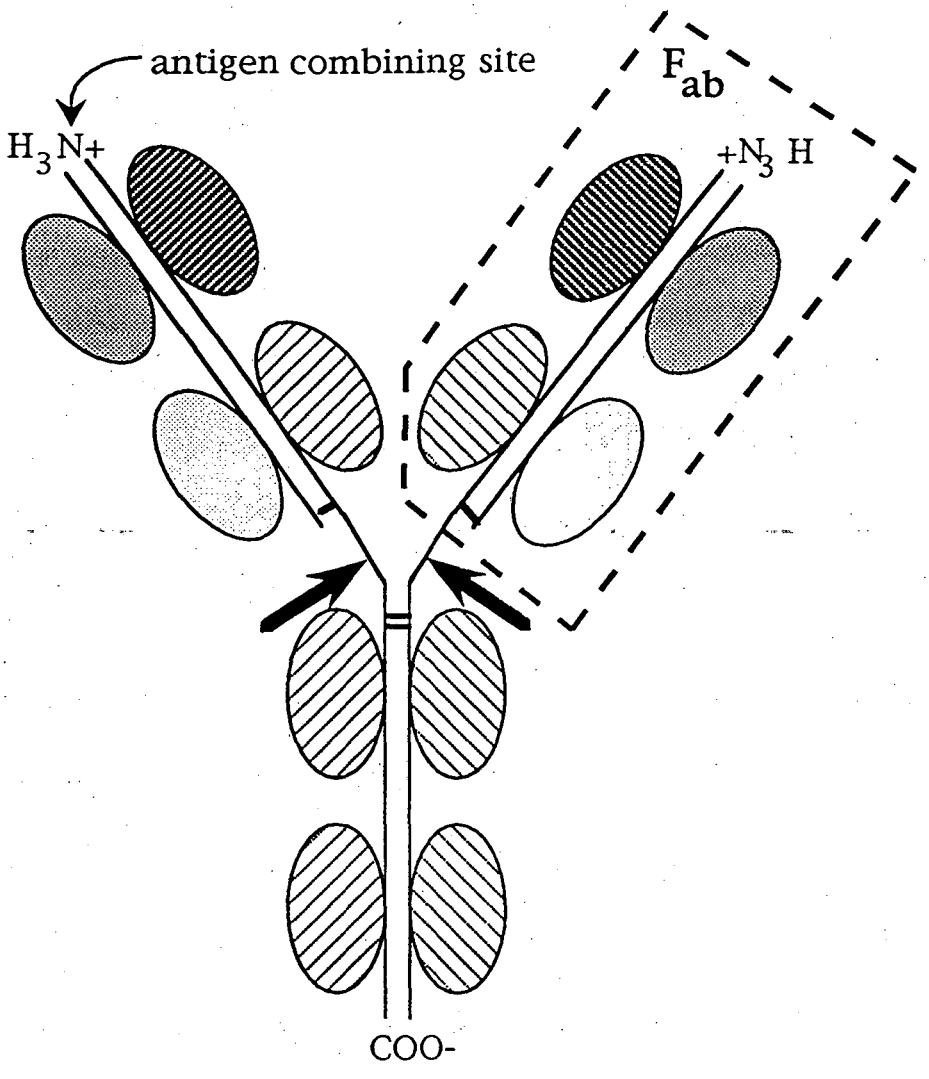

Figure 2.1 - Representative Ig structure. The site of papain cleavage is marked by the bold arrows. One of the two identical antigen binding Fab fragments is enclosed in the dashed box. The two identical heavy chains are crosshatched, the two identical light chains are stippled. The variable sequence N-terminal domains of the heavy and light chains are colored darker. Each domain consists of about 110 amino acid residues, with one disulfide bond.

transition state for a chemical reaction can elicit Igs which catalyze the reaction when presented with the substrate. Often these designed molecules are too small to elicit a strong immunoglobin response, and are eliminated directly through the kidneys. Specific antibodies can be elicited to these molecules if they are bonded with a larger molecule to form the immunogen. The small molecule is now termed a hapten, and will often bind to the antibodies with similar affinity as the immunogen.

To date a diversity of chemical reactions have been catalyzed with monoclonal antibodies. These reactions include ester and carbonate hydrolysis, amide bond formation, Claisen rearrangements, acyl group transfer, β-elimination and redox reactions (Shokat & Schultz, 1990). Often this catalysis is quite specific, in some cases facilitating chemistry in a stereospecific fashion.

Binding lowers the overall free energy of the immunogen / immunoglobin complex. If the immunogen is a transition state analog, and is recognized preferentially over the substrate of the corresponding reaction, some of the binding energy can be utilized for catalysis (Figure 2.2). If the products have low affinity for the antibody they will be released and true enzyme-like turnover can occur. The binding energy can arise from a number of forces, including van der Waals and hydrophobic forces, charge complementarity, and hydrogen bonding. The specific role these forces play in promoting catalysis requires experimental analysis to implicate particular residues in binding and catalysis. The development and optimization of new protein catalysts necessitates

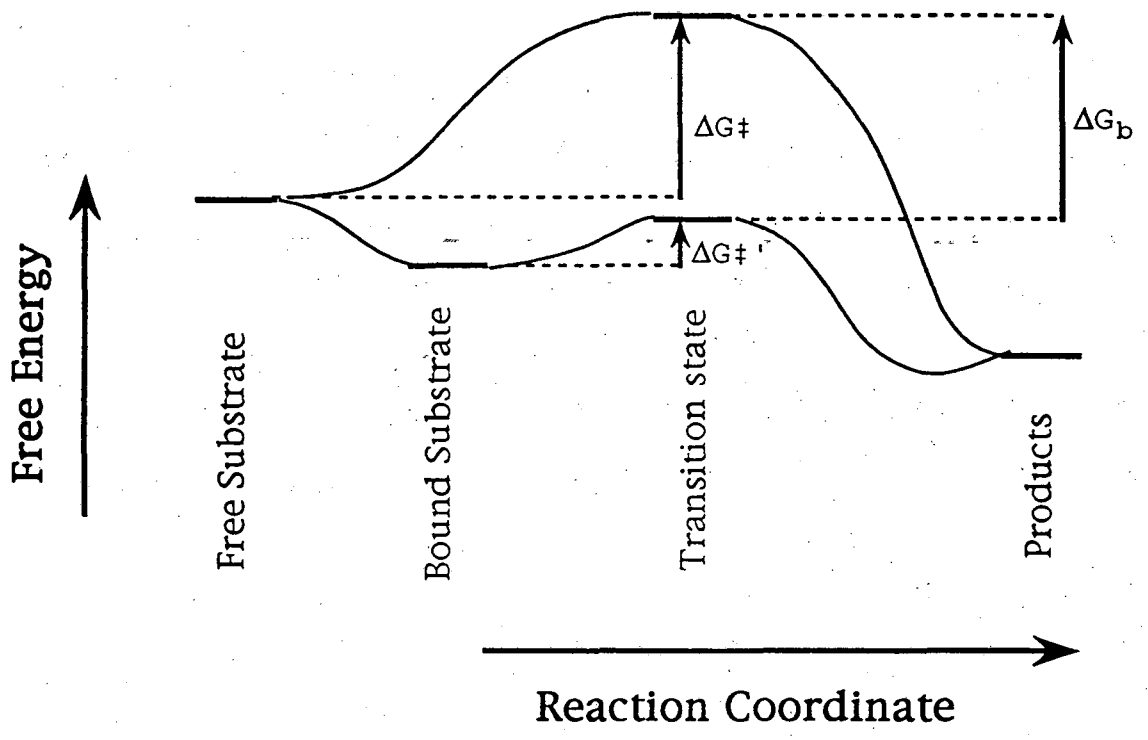

Figure 2.2 - General Reaction Coordinate diagram showing catalysis by preferential binding of transition state over substrate or products.

an understanding of the mechanisms by which chemistry occurs in the binding pocket. Hence experimental identification of the amino acid residues involved in binding and catalysis is central to the design of new immunogens and the development of new catalysts.

One of the first reactions observed to be catalyzed by immunoglobins is the hydrolysis of nitrophenyl carbonate esters (Jacobs *et al.*, 1987, Jacobs, 1988). The solution chemistry of this reaction is fairly facile and has been extensively studied. Kinetic data are consistent with an *sn*-2, base catalyzed mechanism where the carbonate is directly attacked by hydroxide (Figure 2.3a; Bruice & Benkovic, 1965). In this mechanism the central carbon is transiently bonded to four oxygen atoms. This unstable transition state is tetrahedral and negatively charged, and in these respects it resembles a phosphate diester. The central phosphorous atom in a phosphodiester is also bonded to four oxygens in a tetrahedral conformation, and is stable and negatively charged at neutral pH.

To be a successful catalyst the immunoglobin must also bind the substrate. In this example the acyl groups attached to the phospho-immunogen must provide other recognition elements to provide sufficient binding energy and specificity to bind the carbonate substrate. The recognition of these elements, or epitopes, must be balanced against recognition of the tetrahedral phosphate epitope to allow turnover of the corresponding carbonate substrate. In this example the carbonate must have enough affinity to bind specifically, but not so much that the release of hydrolysis products is too slow. Choice of acyl groups is therefore important in designing an immunogen. Nitrophenyl groups have long been recognized to

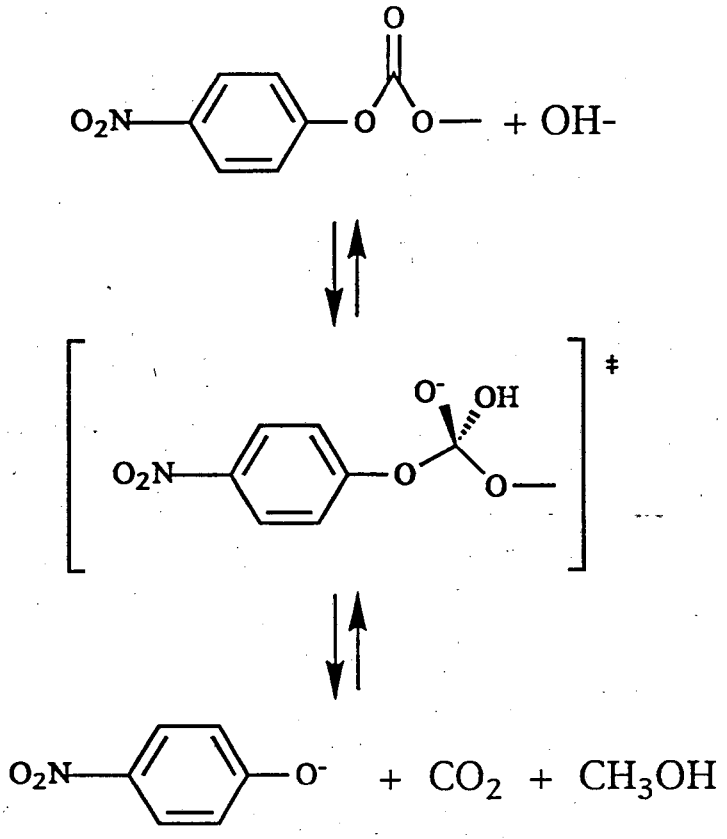

Figure 2.3a - Mechanism of solution hydrolysis of 4-nitrophenyl methyl carbonate. Bracketed structure is the unstable transition state.

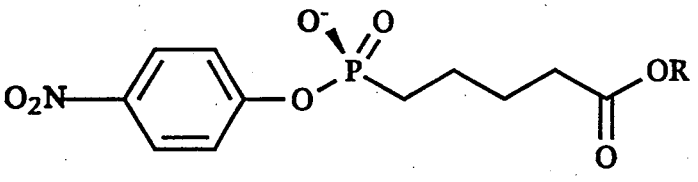

Figure 2.3b - Immunogen used to elicit the G5 antibody (JWJ-1/KLH; R = keyhole limpet hemocyanin).

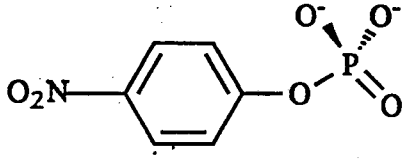

Figure 2.3c - Hapten used in these experiments, 4-nitrophenyl phosphate (4NPP). The phosphate is doubly ionized at neutral pH.

stimulate strong humoral immune responses, and have the additional benefit of being a chromophore (Pressman & Grossberg, 1968). These properties made it an excellent choice for inclusion in the design of a catalytic immunogen.

Phosphates, however, are readily hydrolyzed by phosphatases in the bloodstream. This short half-life limits their applicability as an immunogen as phosphate esters would be hydrolyzed before a full immune response can be educed. Phosphonates, however, are widely recognized as transition state inhibitors for these enzymes and retain the desired negative charge and near tetrahedral geometry desired in the design of the immunogen. In designing a transition state analogue for the induction of hydrolytic immunoglobins a nitrophenyl phosphonate was an attractive candidate (Figure 2.3b).

4-nitrophenyl butanoic phosphonate coupled to the carrier protein keyhole limpet hemocyanin (KLH) served as the immunogen in Balb/c mice (Jacobs *et al.*, 1987; Jacobs, 1988). When polyclonal sera exhibited hapten-inhibitable catalytic hydrolysis of the corresponding nitrophenyl carbonates, monoclonal antibodies were generated using standard techniques (Jacobs, 1988). Several of the clones were found to promote hydrolysis, and the one with the highest catalytic rate was chosen for further study. This antibody, JWJ-1/4A1, catalyzes the hydrolysis of 4-nitrophenyl ethanoic carbonate at a rate 10,000 times the background rate. It did not significantly catalyze hydrolysis of 2-methyl, 4-nitrophenyl ethanoic carbonate, nor that of 2-nitrophenyl ethanoic carbonate. This demonstrates the exquisite substrate specificity of immunoglobin

catalysts.

The reaction was found to be first order in hydroxide ion, indicating a mechanism of direct hydroxide attack on the carbonate carbon (Jacobs, 1988). Other reaction mechanisms are also possible, such as general base hydrolysis or a covalent acyl-immunoglobin intermediate. The rate vs. pH profile was strictly linear over the range of pH 6 - 9, showing no inflection to indicate the titration of a general base. This evidence argues against a mechanism of general base catalysis. Similarly there is no initial burst or lag of product release upon addition of substrate, as might be expected if an acyl-antibody intermediate was formed. Direct hydroxide attack on the carbonyl, therefore, is the most likely mechanism for carbonate hydrolysis by this immunoglobin.

The proposed mechanism of direct hydroxide attack on the carbonate carbon suggests two likely effects of substrate binding in the immunoglobin's protein fold. Antibodies to phosphate esters often contain positively charged residues in the binding site (Padlan *et al.*, 1976). The positively charged side chains attract the negatively charged phosphate and contribute up to several kcal/mol to the overall free energy of association (Anderson *et al.*,1990). Immunoglobins to a phosphate diester would catalyze hydrolysis of the corresponding carbonate if the developing negatively charged transition state is stabilized in a similar fashion. Secondly, attack at the carbonate by the hydroxide ion could be further facilitated if some of the binding energy can be harnessed to distort the carbonate geometry towards the tetrahedral configuration of the transition state, making it more accessible to the attacking hydroxide ion.

However, steric distortion effects alone are not likely to produce as significant a rate enhancement while still providing for high substrate affinity. The 10^5-fold acceleration of carbonate hydrolysis by the JWJ-1/4A1 immunoglobin suggests that charge neutralization is critical in lowering the activation barrier. This chapter describes experiments designed to verify the hypothesis of a positive charge from the immunoglobin contributing to the binding energy of the phosphate immunogen/inhibitor.

Of the 1300 or so amino acids constituting an Ig, only a handful are in a position to interact with and perform chemistry on a specific ligand. Their spectroscopic signature is lost amid the text of less interesting, but critical structural residues. Some of these structural residues can be removed by proteolytic cleavage. The two identical 50 kDa F_{ab} domains containing the binding/catalytic site (see figure 2.1) still contain ~440 amino acids, or about 1800 protons. Identifying the involvement of one or a few of these residues in binding and catalysis is still a formidable obstacle.

Observing the effects of hapten binding on the positively charged side chains with ^{1}H-NMR is further complicated by the rapid solvent exchange of the protons on the positively charged amino or guanidino groups of lysine and arginine, respectively (Wüthrich, 1986). Deuterons substituted in these positions will be rapidly exchanged with protons from the solvent, and the isotopic label will therefore be lost. Labeling the non-exchangeable methylenes of these side chains is possible, but these are further removed from the locus of positive charge and the environmental perturbation invoked by hapten binding will not be as great. ^{15}N amino acids provide an

alternative NMR probe for these positively charged residues, with the additional advantage of having a minimal background from its low natural abundance. However incorporating isotopically labelled amino acids into the immunoglobin requires extensive adaptation of the hybridoma cell line to growth on media supplemented with minimal exogenous growth factors and proteinaceous nutrients.

Initial attempts to adapt the JWJ-1/4A1 cell line to growth on minimal media appeared to be successful. This cell line continued to grow, albeit slowly, in 2% fetal calf serum (FCS; see appendix). The culture medium reacted strongly on ELISA plates coated with the immunogen. Antibodies were produced at a level of about 5 μg/ml as estimated by ELISA titers. However, upon purification of F_{ab} fragments hapten binding was not observed in the NMR experiment. Neither were these fragments catalytically active. This preparation of F_{ab}'s was titered a second time on JWJ-1/BSA coated ELISA plates, using a goat anti-mouse κ-light chain Ig/biotin conjugate for the secondary antibody. The titer thus obtained closely matched the concentration of F_{ab} estimated from UV/VIS spectroscopy (see appendix).

These results indicated that the antibody isolated from cell cultures is already bound to some ligand. The data are consistent with a culture-derived ligand binding with an affinity intermediate between the hapten used in the NMR experiments (4NPP; figure 2.3c) and the hapten/BSA conjugate used in the ELISA experiment (figure 2.3b). In this scenerio the latter ligand successfully competes for the JWJ-1/4A1 binding site, while the former does not.

Identification of the proposed culture-derived ligand was

attempted in several ways, all unsuccessful. Attempts to compete out this moiety in the NMR sample with the tightest binding hapten, the phosphonate of figure 2.3b where R = H, were unsuccessful even at a ten-fold excess of this hapten. The only spectral changes observed were of the added hapten free in solution. Several likely candidates for the culture-derived ligand were identified in the composition of the culture medium. These included free amino acids, the pH indicator, and the buffer. The indicator and buffer were ruled out by producing JWJ-1/4A1 in a custom media in which the indicator was omitted and the buffer changed to sodium carbonate, the major physiological buffer in mammals. These alterations had no impact on the binding behavior of the antibody, nor did growth on media from several different suppliers.

The amino acids are necessary for cell growth, and so cannot be substituted in the manner described above. However, interference of these compounds with binding to the desired hapten, 4NPP can be detected in an ELISA experiment. To this end, JWJ-1/4A1 Ig produced in ascites, which behave predictably in these experiments, was multiply titered on a JWJ-1/BSA conjugate ELISA plate. In separate titer series, however, each aromatic amino acid was added to the buffer. These additions should interfere with the titer in the same manner as they might interfere with the culture-derived F_{ab}. No interference was detected in these experiments. All titer series gave the same result, as monitored by the Ig dilution producing half-maximal ELISA response.

Despite the failure to produce active immunoglobins in cell culture, initial NMR experiments were conducted with unlabelled

immunoglobins from ascites fluid. The intent of these initial experiments is to determine the sensitivity and applicability of ^1H-NMR to Ig systems (see Chapter 3). Of particular interest is the magnitude of chemical shift changes ($\Delta\delta$) that occur upon hapten binding as well as the ability of modern high field spectrometers to detect these shifts within the generally featureless proton spectra of such large polypeptides.

The focus of this investigation is on the positively charged amino acids, lysine and arginine. The ε-methylenes of lysine side chains and the δ-methylenes of arginine have a characteristic chemical shift, around 2.9-3.1 ppm, and appear as triplets with a coupling constant of 5-7 Hz. With this distinct spectral signature it was hoped that the involvement of a lysine might be discerned in the absence of isotopic labelling. Indeed, titration with hapten of the immunoglobin F_{ab} fragment produced in mice from ascites fluid (see appendix) resulted in difference spectra which exhibited two triplets in the 3.0 ppm region. As expected, signal to noise of these difference features was limited due to the large background signal from lysines and arginines far from the binding site. It is also possible that the difference intensity was reduced because the affected resonances shifted by less than their linewidth, cancelling some of their intensity in the difference spectra. In the absence of isotopic labels, it was judged that this approach would not likely produce useful, unequivocable information.

These initial experiments did encourage the investigation of other spectroscopic techniques to identify a positively charged residue interacting with the hapten. The interaction of a positively

charged residue with the hapten phosphate should shift the pK_a of the phosphate towards lower values. A study of phosphocholine (PC) binding immunoglobins found just this effect. Binding to the immunoglobins M603 or W3207 lowered the pK_{a2} of PC by 0.4 units. Conversely, the binding of PC to the antibody M167 raised the pK_{a2} by 1.5 units. (Goetze & Richards, 1978) X-ray crystallographic data of the latter complex show the interaction of a negatively charged aspartic acid with the hapten phosphate in this system. (Padlan *et al.*, 1976) The resulting unfavorable charge repulsion is compensated by several hydrogen bonds from other residues. From this work it was postulated that the interaction of 4-nitrophenyl phosphate (4NPP, Figure 2.2c) with the immunoglobin JWJ-1/4A1 would result in a significant and measurable shift in the pK_a's of the charged groups.

^{31}P is an NMR active nucleus with a nuclear spin of 1/2 and 100% natural abundance. This, combined with a chemical shift range of some 300 ppm, makes ^{31}P-NMR an attractive candidate for spectroscopic determination of the hapten pK_a. The frequency of a phosphodiester ^{31}P resonance shifts by nearly 4 ppm upon titration (Goetze & Richards, 1978). Unfortunately the electron distribution around the ^{31}P nucleus is very asymmetric which gives rise to a dependence of the chemical shift on the orientation of the bonding electrons with respect to the external magnetic field. Termed chemical shift anisotropy, this effect broadens the ^{31}P resonances in a field dependent manner and limits the resolution of ^{31}P-NMR spectra. However, there are no ^{31}P nuclei in immunoglobins, eliminating confounding background signals, and ^{31}P-NMR spectra have been obtained successfully from other immunoglobin systems

(Goetze & Richards, 1978). Finally, there is a significant change in ^{31}P chemical shift upon titration of phosphates, about 2.5 ppm. These considerations make ^{31}P-NMR an attractive candidate for monitoring the pH behavior of 4-nitrophenyl ethanoic phosphate when bound to the catalytic immunoglobin JWJ-1/4A1.

Methods and Materials:

JWJ-1/4A1 immunoglobins were produced via ascites induction in mice. 5 x 10^7 hybridoma cells/mouse were harvested from standard cell cultures in RPMI-1640, 10% FCS in mid-log phase growth by mild centrifugation, resuspended in 0.5 ml of cold PBS/mouse, and injected into the peritoneae of 10-14 week old Balb/c mice with a syringe fitted with a 22 gauge needle. Ten to fourteen days following, once the soft tumors interfered with hind leg mobility, the ascites fluid was drained by insertion of an 18 gauge needle directly into the tumor. An average of 1.5 ml of ascites fluid per mouse was collected in polyethylene tubes, incubated for 30 minutes at 37°C, and clarified of cells by centrifugation. The fluid was stored in this state for up to several weeks at -20°C.

The immunoglobin was purified from the ascites fluid by Protein A chromatography. After thawing, the coagulated lipids were removed from the fluid with a wooden stick and the fluid was diluted 1:1 or 1:2 with binding buffer (see appendix). This was applied to the Protein A column through a glass wool filter in a pasteur pipet at a rate of 1 drop every 4 sec. Extraneous proteins, mostly albumins, were washed from the column by extensive flushing with binding buffer. Elution of purified immunoglobin was accomplished by standard protocols once the optical density at

280nm of the eluant dropped below 0.05 (see appendix). Production of F_{ab} fragments proceeded as previously described (see appendix). 17 ml of clarified ascites fluid produced 32mg of purified F_{ab}'s, which were dialyzed extensively against 20mM succinate, 50mM NaCl, pH 7.5 with 0.05% NaN_3. 150µl, or 10% of the sample's volume, of ^2H_2O was added for frequency locking. The concentration of F_{ab}, about 420 µM, was estimated by $\varepsilon^{0.1\%}$=1.37 at 280nm, and the 1.5 ml sample was titrated to 1:1 stoicheometry with 4-nitrophenyl phosphate (4NPP; Sigma). Stoicheometry was determined by monitoring the aromatic region of the ^{1}H-NMR spectrum for the appearance of the sharp doublets of unliganded hapten.

^{31}P-NMR spectra were collected at 121.5 MHz on an IBM AC-300 spectrometer equipped with a 10mm broadband probe equilibrated at 30°C. An average of 8000 transients were averaged per pH value, for a total time of 50 minutes per pH point. A 10kHz spectral width was used with 8k points for each spectrum. The chemical shift was referenced to an external standard of 100% H_3PO_4. The pH was adjusted by µl additions of the succinate buffer at pH 0.7. The pH was monitored with a Corning Digital 112 pH meter before and after signal acquisition. The two readings always agreed within 0.05 pH units.

Following these experiments the F_{ab} sample was overtitrated with 4NPP, and ^{31}P-NMR spectra were collected under similar conditions as described above at several pH values bracketing the observed pK_a to confirm the relative pK_a's of free and bound 4NPP.

The pK_a of free 4NPP was determined in the succinate

buffer by ^{1}H-NMR spectroscopy on a GN-500 spectrometer. The chemical shift of the phenyl ring proton resonances shift by 0.035 ppm (15Hz) upon titration of the phosphate. These resonances were monitored as a function of pH in 10% $^{2}H_2O$ solution, and the spectra were referenced to internal TSP. The pH in this experiment was monitored on a Radiometer Copenhagen PHM-80 pH meter with no correction made for the ^{2}H.

Results:

The chemical shift behavior with pH for bound 4NPP (^{31}P chemical shifts) and free 4NPP (^{1}H chemical shifts) is shown in figure 2.4. Both chemical shifts exhibit sigmoidal dependence on pH with an apparent pK_a of 5.6. The identity of the bound ^{31}P resonance and the equality of the apparent pK_a's for free and bound were confirmed by overtitration of the F_{ab} sample with 4NPP. Upon addition of excess 4NPP a new peak appeared in the ^{31}P spectrum about 1.78 ppm upfield from the previously observed resonance (figure 2.5). The linewidth of the new, upfield resonance was consistently 5-8 Hz less than the downfield resonance, although the linewidth varied between spectra because of differences in magnetic field homogeneity.

Ascribed to the excess 4NPP, the appearance of this new peak confirms the assignment of the broader resonance to bound 4NPP. Furthermore, the observation of two distinct peaks indicates that exchange of 4NPP between free and bound states occurs slowly on the NMR timescale, so the two species can be studied independently yet simultaneously with ^{31}P-NMR spectroscopy. ^{31}P-NMR spectra were collected at several pH values bracketing the observed pK_a and

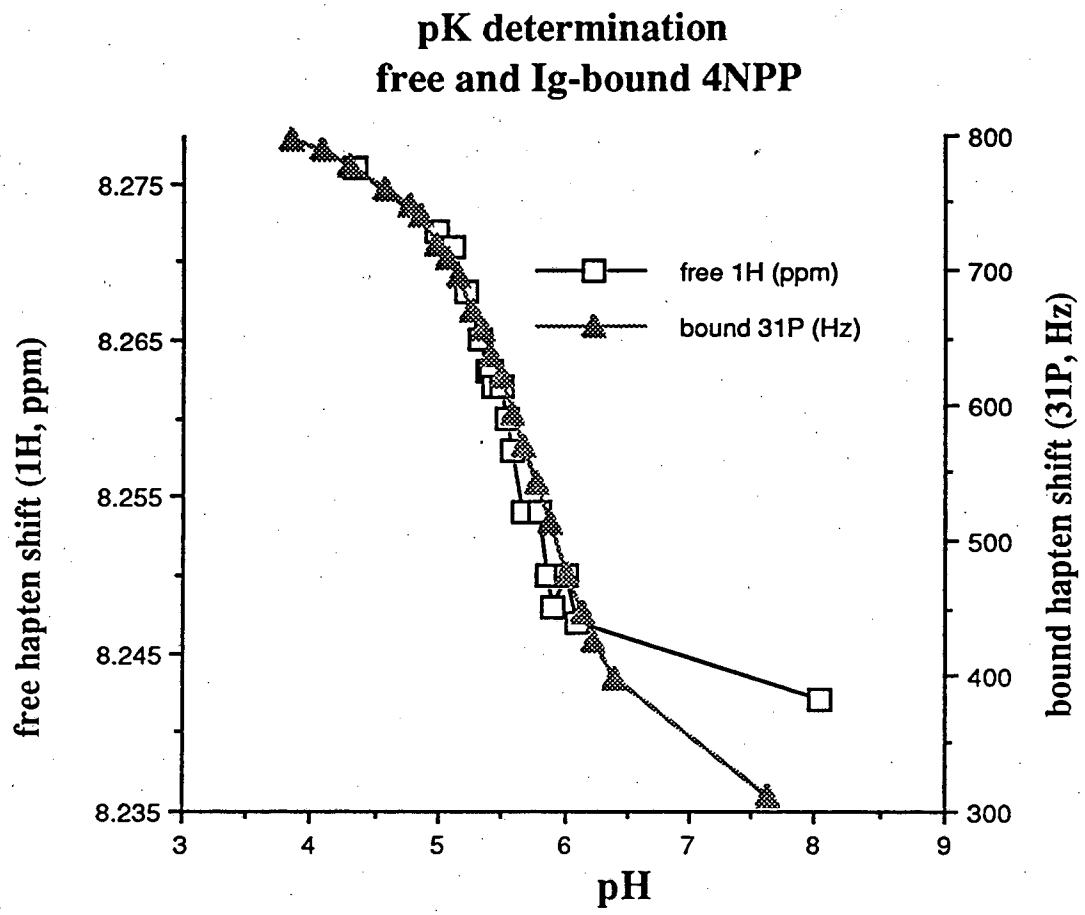

Figure 2.4 - Chemical shift of 4NPP as a function of pH.
Square symbols - 4NPP free in aqueous solution. Data are ^{1}H chemical shift in ppm of protons *meta* to the phosphate on the aromatic ring.
Triangular symbols - 4NPP bound to the Fab. Data are ^{31}P frequency in Hz of the phosphate.
Data are not normalized with respect to each other.
Asymptotic chemical shifts were not obtained due to hydrolysis of 4NPP or denaturation of the protien.

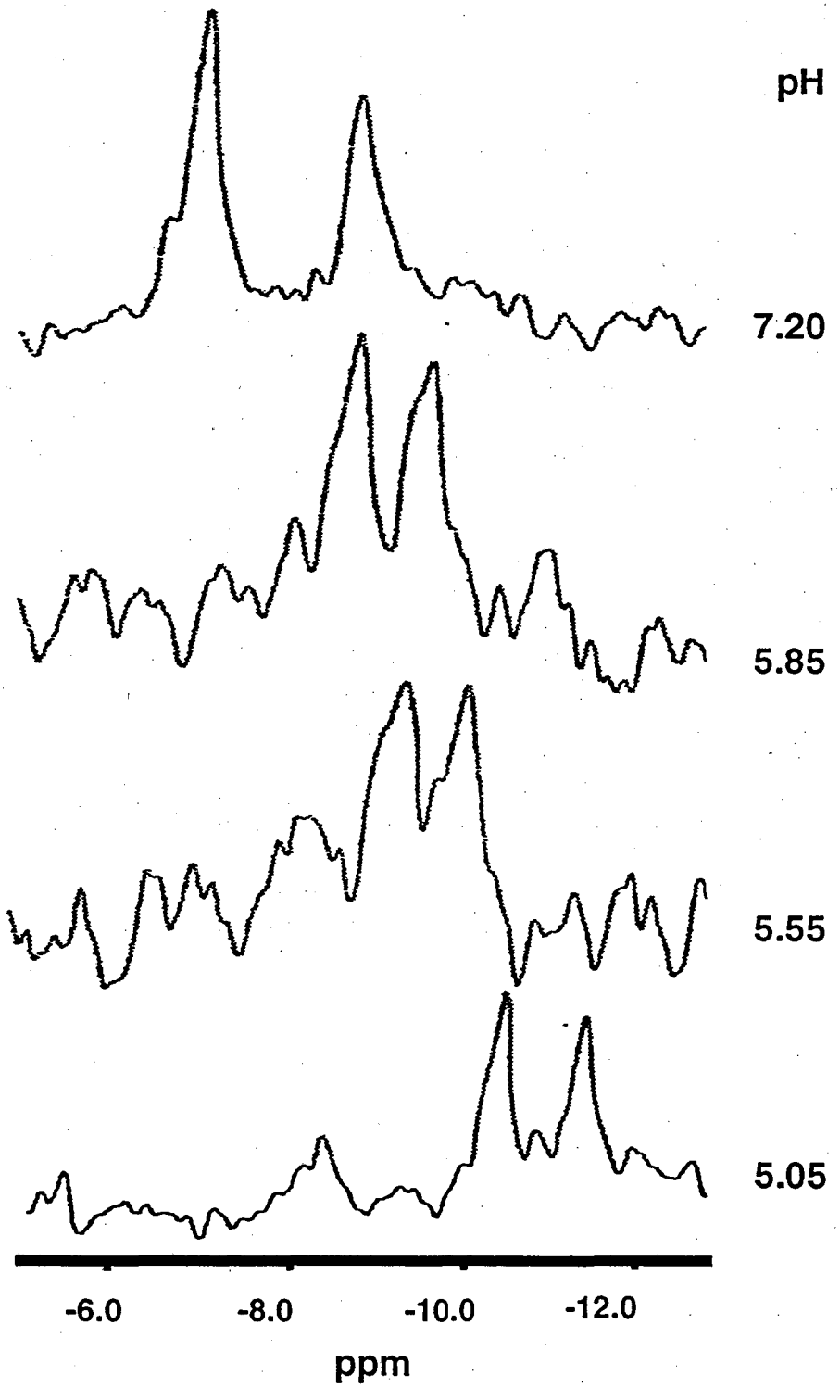

Figure 2.5 - ^{31}P spectra of 4NPP in excess of Fab as a function of pH. The signal on the right arises from 4NPP bound to the Fab. The pK of free 4NPP is 5.6. Chemical shift is referenced to neat phosphoric acid.

the two peaks were observed to move in unison (figure 2.5). This confirms that the pK_a of 4NPP is not altered by binding to the F_{ab} JWJ-1/4A1, an observation at odds with the prevailing theory for the mechanism for catalysis of carbonate hydrolysis by this immunoglobin.

Discussion:

The pK_a of 4NPP is not shifted significantly upon binding. This indicates that the negative charge on the phosphate group is not countered by a complimentary positive charge localized on the immunoglobin, as predicted by the proposed mechanism for catalysis (Jacobs, 1988). This hypothesis predicts that direct hydroxide attack at the carbonate would be facilitated through stabilization of the developing negative charge in the transition state by a positively charged amino acid residue. This stabilization should also be seen in the negatively charged phosphate analog. That the pK_a of the latter is not perturbed upon binding to the immunoglobin makes this interaction improbable. In the unlikely event that such stabilization is occuring, the effects on the phosphate would have to be serendipitously countered by an equal and opposite effect from a neighboring negatively charged residue. In addition to being unlikely, such interactions would not contribute favorably to the catalytic rate.

In the course of initial characterization of the NMR behavior of JWJ-1/4A1 preparations, it was observed that 4NPP is cleanly removed from the binding site by competition with 4-nitrophenyl methyl phosphate, the methyl ester of 4NPP. Following titration to 1:1 stoicheometry with 4NPP, addition of 4NPP-methyl ester results

in two sharp doublets in the aromatic region centered at 8.30 ppm and 7.35 ppm, the chemical shift of the ring protons of unbound 4NPP. Overtitration with 4NPP-methyl ester gives rise to a second set of doublets, just downfield from the first at 8.35 ppm and 7.38 ppm. This is also the chemical shift of the ring protons on unbound 4NPP-methyl ester. Concommitant changes were observed in other spectral regions as well. Titration of F_{ab} with 4NPP results in a peak at -0.2 ppm moving to -0.3 ppm. Competition with 4NPP-methyl ester causes this peak to move further upfield to -0.4 ppm. This shift was separately observed to occur upon 4NPP-methyl ester binding. Using this upfield-shifted resonance as a marker of ligand binding, it was determined that 4NPP-TEMPO spin label (see figure 3.1b[II]) similarly competes out the smaller 4NPP-methyl ester. These observations indicate that hydrophobic or van der Waals interactions with the secondary ester group contribute significantly to the binding energy of these compounds.

The observation that phosphodiesters have a higher affinity for this immunoglobin than 4NPP argues against significant charge stabilization by a positively charged residue. The formation of a single salt bridge can confer up to 3-4 kcal/mol to the stability of a protein fold, and results in pK shifts of 2.5-3.5 units for the residues involved (Anderson *et al.*, 1990). These values are derived from a charged interaction mostly removed from the solvent in a hydrophobic protein matrix, and so represents an upper limit for the energy of unlike charge attraction in proteins. At neutral pH 4NPP is doubly anionic, while the methyl ester has only a single negative charge. It is not known whether the increasing the charge difference

from 2 to 3 (from -1 with +1 to -2 with +1) scales in energy proportionately to the change from 1 to 2 as investigated by Anderson and coworkers. It is possible that the second negative charge on 4NPP is localized on a phosphate oxygen at a greater distance from the putative positive charge in the binding site than the first charge, reducing the energy of attraction.

The additional hydrophobic interactions proffered by a single methyl group more than offset the reduced energy of interaction from lowering the charge on the phosphate. An upper limit on the binding energy arising from the additional charge complementarity of 4NPP with the F_{ab} in this system can be estimated by the energy of hydrophobic interactions. The energy of hydrophobic interaction of a single methyl group is estimated to be 1-2 kcal/mol (Tanford, 1980). This value is derived from the transfer of long chain acyl alcohols (C_6-C_{12}) from neat solution into dilute aqueous solutions. It is likely that, when bound to the F_{ab}, the methyl group on 4NPP-methyl ester is still somewhat solvent exposed, since this is the site of attachment to the carrier protein when the Ig was originally elicited. The additional binding energy due solely to hydrophobic interactions with the methyl group will be less than 2 kcal/mol. To account for the roughly ten-fold less affinity for 4NPP relative to the methyl ester, the additional charge on the former can account for no more than 1 kcal/mol in binding energy.

The Michaelis constant K_m reflects the binding energy of substrates. This parameter has been determined for several substrates and show a dependence on the alkyl chain (Jacobs, 1989). However, the effect of chain length was not studied systematically,

and the data presented do not show a simple correlation of chain length to K_m.

Binding to the immunoglobin does not affect the pK_a of 4NPP, yet the difference in linewidth and ^{31}P chemical shift between free and bound states indicates some perturbation of the chemical environment of the phosphate by the immunoglobin. The 1.78 ppm downfield shift observed upon binding is significant, and can be the result of altered hydrogen bonding. Determinination of hydrogen bonding effects based on changes in chemical shift is difficult. However, it has been observed in cosolvent aqueous mixtures that the chemical shift of phosphodiesters moves progressively downfield as the hydrogen bonding potential of the cosolvent decreases (Lerner & Kearns, 1980). The most dramatic shift occured with the non-hydrogen bonding solvent DMSO, which induced a 3 ppm downfield shift at 80% (mol/mol). Based on the direction of the chemical shift this evidence implies that the phosphate is sequestered from hydrogen bonding with the solvent when bound to JWJ-1/4A1.

The phosphate would appear to bind in an uncharged, non-hydrogen bonding environment of the F_{ab}. Such an environment should not be favored by the charged, electron dense phosphate diesters, and is worse for the dianionic phosphomonoester 4NPP. This would explain the weaker binding of the latter hapten. However, there is significant binding energy attributable to the phosphate epitope, as 4NPP binds with μM dissociation constant, while the product, *p*-nitrophenylate anion, binds with about mM K_d. (Jacobs, 1988).

Analysis of chemical shifts is problematic, however, because

many environmental effects can contribute to the overall chemical shift. The ^{1}H-NMR titration data show that several aromatic residues are perturbed upon binding of the 4NPP ligand. Ring currents from these or other nearby residues could also cause the change in chemical shift. Although ring current shifts are generally small for phosphates, owing to the distancing effects of the oxygen atoms surrounding the phosphorous, several aromatic residues could constructively contribute to the overall shift. Shifts of this magnitude are not unprecedented for these types of systems (Gorenstein, 1984).

Little structural information can be discerned from the chemical shift alone. Certainly the phosphate is not freely solvated when bound by the protein. On the other hand, it is affected by the bulk pH of the solvent, and therefore has some solvation. Some specific interaction can be inferred from the binding affinity of the protein for 4NPP versus the reaction product, *p*-nitrophenol. The experiment described in this chapter, however, rules out the proposed mechanism of catalysis primarily by charge complementarity between the negatively charged transition state and a positively charged residue juxtaposed in the binding/catalytic site. How this catalysis is acheived awaits further investigation.

Amzel, L.M. & Poljak, R.J. (1979) *Annu. Rev. Biochem.* **48**, 961-997.

Anderson, D.E., Becktel, W.J., & Dahlquist, F.W. (1990) *Biochemistry* **29**, 2403-2408.

Bruice, T. & Benkovic, S.; (1965) *Bioorganic Chemistry* vol. 1, Benjamin, New York.

Catalytic Antibodies c. 1991, J.Wiley and Sons, Chichester.

Goetze, A.M. & Richards, J.H. (1978) *Biochemistry* **17**, 1733-9.

Goodman, J.W. (1975) in *The Antigens*, vol. 3, pp. 127-187; Sela M, ed. Academic Press, New York.

Gorenstein, D.G. (1984) *Phosphorus-31 NMR : principles and applications*, Academic Press, Orlando, Fla.

Jacobs, J., Schultz, P.G., Sugasawara, R., & Powell, M. (1987) *J. Am. Chem. Soc.* **109**, 2174-2176.

Jacobs, J.A. (1988) Ph.D. dissertation, UC Berkeley.

Kohler, G. & Milstein, C. (1985) *Nature (London)* **256**, 495-497.

Lerner, D.B. & Kearns, D.R. (1980) *J. Am. Chem. Soc.* **102**, 7611-7612.

Padlan, E.A., Davies, D.R., Rudikoff, S., & Potter, M. (1976) *Immunochemistry* **13**, 945-949.

Pressman, D. & Grossberg, A. (1968) *The Structural Basis of Antibody Specificity*, Benjamin Press, New York.

Shokat, K.M. & Schultz, P.G. (1990) *Annu. Rev. Immunol.* **8**, 335-363.

Tanford, C. (1980) *The Hydrophobic Effect*, Wiley, New York.

Wüthrich, K. (1986) *NMR of Proteins and Nucleic Acids*, Wiley, New York.

Chapter 3: Mechanism of Immunoglobin Catalysis II Photosensitized C-C Bond Cleavage

The most prevalent product of UV photodamage to cellular DNA is a (*cis,syn*) thymine dimer (Patrick, 1977; Patrick & Snow, 1977). Thymine dimer formation can be reversed in solution by shorter wavelength UV light. Mechanistic studies of the photoreversal in solution indicate that indoles, quinones, or flavins can sensitize the cleavage at longer wavelengths through a free radical, electron transfer mechanism (figure 3.1; Lamola, 1972; Roth & Lamola, 1972; Helene & Charlier, 1977; Rokita & Walsh, 1984; Van Camp *et al.*, 1987; Jorns, 1987a). This lesion can be repaired in bacterial cells by the enzyme photolyase. This enzyme cleaves the thymine dimers when irradiated with visible light through the sensitizing cofactor FAD (Sutherland, 1981). Because immunogen-binding F_{ab} fragments of known structure often have tryptophan residues close to the binding site, particularly when the immunogen contains some polarized π electron density, it was hoped that an antibody specific for the thymine dimer could be isolated which would efficiently sensitize the photoreversal via serendipitous juxtaposition of the tryptophan indole with the thymine dimer binding site.

In fact, five out of six monoclonal antibodies raised against thymine dimers sensitized the photoreversal (Cochran, 1991). The most efficient of these was studied further, and it was found that the

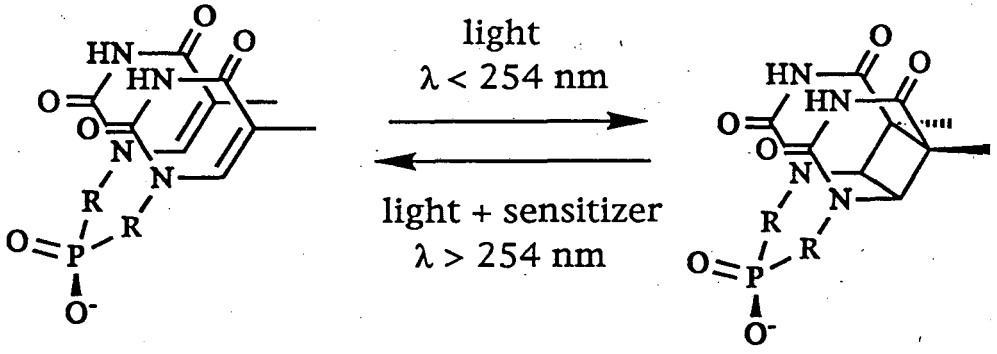

Figure 3.1a - Thymine dimer photochemistry. R = deoxyribose. Sensitizer = flavin, quinone, or indole.

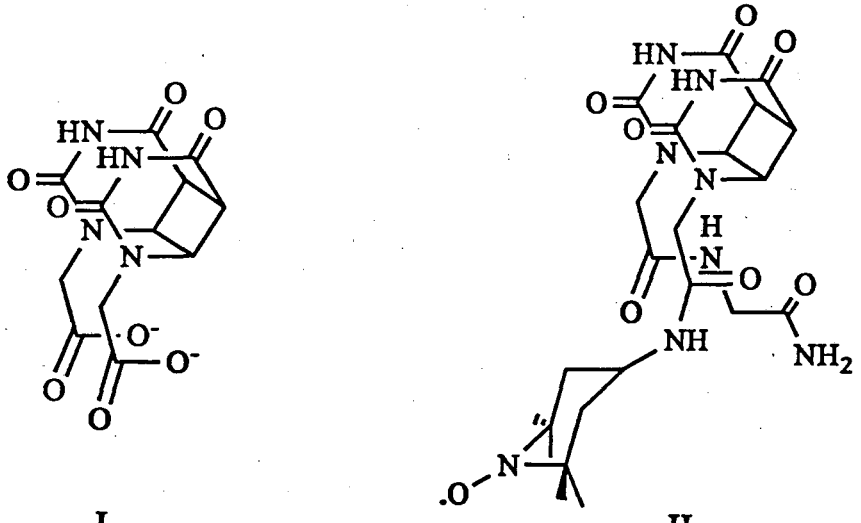

I II

Figure 3.1b - Haptens used in this chapter. I - Thymine dimer. II - Thymine dimer / spin label. The unpaired electron is on the nitroxide nitrogen.

reaction was first order in light intensity and followed Michaelis-Menten kinetics. The Michaelis-Menten constant k_{cat} was of similar magnitude to the turnover number for DNA photolyase from E. coli, and was 218 times faster than the first-order rate constant for the unsensitized reaction. The antibody mediated reaction showed exquisite specificity for thymine dimers. N,N-dimethylthymine dimers and uracil dimers were not substrates for this reaction, presumably because they did not bind (Cochran, 1991). The wavelength dependence of the photoreversal exhibited a shoulder at 300nm, and antibody fluorescence was partially quenched by the presence of thymine dimer. This suggests that photoreversal is sensitized by an antibody tryptophan-residue near the binding site. Chemical modification experiments of the denatured antibody revealed 10 tryptophan residues per antibody, yet none could be localized near the binding site by these techniques (Cochran, 1991).

Quantum yield experiments indicate that the quantum yield for the antibody-mediated reaction (0.05) is comparable to that for monomer formation from thymine dimer radical anions generated by pulse radiolysis (0.05; Lamola, 1972) and for dimer cleavage in linked indole-dimer photolysis (0.04; Van Camp *et al.*, 1987). This comparison assumes that only one tryptophan per antibody binding site is responsible for the photosensitization. Considering that there are 10 tryptophan residues per Ig allows the calculation of an approximate quantum yield of 0.4 for the formation of monomer (Cochran *et al*,, 1988). This is of the same order as the quantum yield for the bacterial photolyases (0.4-0.8; Sutherland, 1981).

The product monomer has a much lower affinity for the

antibody than the substrate dimer. When bound to the Ig the photoexcited intermediate would be expected to preferentially decay to the lower energy dimer ground state. This hypothesis predicts a reduced quantum yield for monomer formation in comparison to that for monomers formed by direct radical generation in the pulse radiolysis experiment. However, it would appear that the antibody favors the breakdown of this intermediate along the cleavage pathway. This unusual observation provoked further inquiry into the mechanism antibody mediated of photoreversal.

In an attempt to delineate the antibody-mediated photoreversal mechanism experiments were designed to determine the presence and number of tryptophan residues which might be responsible for catalysis. Chemical modification experiments designed to identify tryptophan residues in the binding/catalytic site were inconclusive (Cochran, 1991). However, the catalytic electron swapping or excitation transfer event can occur over as much as 20Å through the protein (Gray & Malmstrom, 1989; Boxer, 1990), in which case the photosensitizing indole may be buried and inaccessible to the modification reagents. Other means are necessary to demonstrate the involvement of tryptophan residues in the catalysis.

Evidence for the involvement of specific tryptophan residues in the catalytic event can be obtained indirectly by site-directed mutagenesis or directly through spectroscopic experiments designed and controlled to detect the interaction of the indole with the ligand. The first approach is time consuming and labor intensive, particularly in mammalian systems. Additionally, a single mutation

might cause structural changes which alter the specificity or mechanism in unanticipated ways. Some of these deleterious effects can be controlled, particularly with non-natural amino acids, yet this adds to the complexity of an already difficult experiment.

A more straightforward approach is to obtain direct spectroscopic evidence of the involvement of a specific tryptophan residue in binding and, by inference, catalysis. Measurement of the quantum yield for monomer formation as a function of wavelength revealed a broad shoulder extending out to 300nm (Cochran, 1991). Photochemistry at this wavelength cannot occur by direct absorption of light by the thymine dimer, and is suggestive of sensitization by a tryptophan indole. However, the identity and stoicheometry of the sensitizing chromophore(s) cannot by concluded from this optical data alone. NMR is exquisitely suited to this purpose, as it can discriminate nuclear spins on the basis of chemical functionality and environment. The binding of a ligand introduces new electron density and chemical functionalities to the binding pocket. This can introduce small changes in the chemical shift of nearby nuclei, which can be detected with modern high field, high resolution NMR spectrometers. ^{1}H-NMR is particularly useful in the study of proteins due to the ubiquity of protons in the constituent amino acids.

Discrimination of the residues involved in binding and catalysis can be obtained through the use of difference spectroscopy. The difference between spectra taken in the presence and absence of ligand will consist of only resonances arising from residues whose chemical environment is altered by the binding event. Crystallographic data on F_{ab} fragments do not show major structural

changes upon the binding of ligands (Padlan, 1977; Amzel & Poljak, 1979; Davies *et al.*, 1988; Padlan, 1990). Therefore, to a first approximation, only resonances arising from those residues in direct contact with the ligand will have their chemical environment altered by hapten binding, and only these should be observed in the NMR difference spectrum. Of course, this approximation must be verified since some effects, *e.g.* from aromatic rings, are exquisitely dependent on juxtaposition and may give relatively large spectral shifts for rather subtle structural reorientations (Becker, 1980).

If a particular type of amino acid is implicated in catalysis, as is tryptophan in the present instance, further spectral simplification can be obtained through the incorporation of isotopically labelled amino acids. Perdeuterated amino acids will not produce ^{1}H-NMR signals, allowing the selective detection of an amino acid type from others which have similar spectral characteristics. These experiments can be designed to show the involvement of a particular type of amino acid by the disappearance of signals in samples containing the ^{2}H-amino acid. Alternatively, by deuterating all other amino acids with spectral properties similar to the residue of interest, only signals from the desired type of amino acid will remain (Anglister *et al.*, 1984). The latter design invokes considerable expense in sample preparation, yet is advantageous in that the information content is positive.

The assumption that the observed differences arise from direct, nearby interaction with the ligand can be verified if paramagnetic spin-label, a stable free-radical, is attached to the ligand. In an NMR experiment, the large magnetic moment and fast

relaxation of the unpaired electron effect rapid magnetic relaxation of NMR-active nuclei within about a 20 Å radius, broadening these resonances and making them unobservable (Jardetzky & Roberts, 1981). A difference spectrum with and without a spin-labelled ligand will display only features from the unbound state; features of opposite sign due to the bound state will be broadened and not observed (Anglister *et al.*, 1984). The latter features can be made observable, in the case of nitroxide-based spin-labels described below, by mild reduction of the spin-label to its diamagnetic form. In this way the proximity to the ligand binding site of the residues observed in the difference spectrum is confirmed.

Materials and Methods

The hybridoma 15F1-3B1 was elicited to a thymine dimer-KLH conjugate in Balb/c mice. Hybridoma fusion and cloning were performed in accordance with standard protocols at IGEN, Inc., in Rockville, MD (Cochran *et al.*, 1988). Cell cultures were initiated in shallow stationary flasks with 5 x 10^6 cells in 25ml of RPMI-1640 or PFHM-II (Gibco BRL, Grand Island, NY) supplemented with 10% bovine fetal serum and gentimycin. Incubation took place at 37°C in a controlled atmosphere of 10% CO_2 and 100% humidity. Two days later, when the culture had attained a density of 6 x 10^5 cells/ml, they were expanded into 150ml of PFHM-II with deuterated phenylalanine and deuterated tyrosine substituted for the standard ^{1}H-amino acids, without additional FCS. The next day the cultures were expanded to a final volume of 1.5*l* in this same medium. Antibodies were harvested 7-10 days later by centrifugation of cells and cell debris followed by a single 50% ammonium sulfate

precipitation of the supernatent and Protein A chromatography (Jacobs, 1988 and appendix). Mild digestion with papain, quenched with a G-50 sephadex column, produced F_{ab} fragments. A second Protein A chromatography step separated the F_{ab}'s from the F_c's. The sample was concentrated after each step by vacuum dialysis. The F_{ab}'s were extensively dialyzed against 50mM NaCl and 5mM Na_2HPO_4 pH 7.2 and lyophilized overnight from 1.5ml of this buffer. The dried samples were resolubilized in 400µl ^2H_2O 12-24 hours prior to data collection. Final F_{ab} concentration was estimated by absorbance at 280nm by using $\varepsilon^{0.1\%}=1.37$ and was ~600µM.

^{1}H-NMR spectra were acquired on a Bruker AMX-600 at 25°C. 5000-6000 transients were averaged for each spectrum. 8333Hz were digitized into 16k points following 1sec. of solvent presaturation for a total recycle delay of 2.5 sec. Total data collection was ~3 hours per spectrum. Data were transferred to a VAX-4000/300 and processed using FTNMR (Hare Research). Samples were titrated with hapten in the NMR tube by the addition of 5-10 µl aliquots of 10-20mM thymine dimer stock solutions in ^2H_2O. The total volume of the sample increased by no more than 5% in these experiments. No correction was made for dilution in the data analysis. In experiments using the paramagnetic spin label/thymine dimer conjugate, the spin label was later reduced *in situ* by addition of a few µl of a fresh stock solution of 20mM sodium ascorbate. This ligand was then competed out of the binding site by the unconjugated thymine dimer. Total volume change over this experiment was 12%.

Results:

Representative spectra of the F_{ab} fragments with and without deuterated phenylalanine and tyrosine (dF,dY) are presented in figure 3.2. The aromatic region (6-9 ppm) of (dF,dY)F_{ab}'s is significantly reduced in intensity compared to unsubstituted F_{ab}'s due to the incorporation of the deuterated amino acids. This region contains only signals arising from tryptophan and histidine for the (dF,dY) sample. Figure 3.3 shows expansions of the aromatic region of (dF,dY) F_{ab}'s with and without the thymine dimer hapten and the difference spectrum of this region. In this difference spectrum positive signals appear at the position of a shifted resonance after binding of the ligand, whereas shifted resonances from the unliganded state appear as negative intensity. Unshifted resonances will not appear in this presentation of the data. Two broad features appear at 6.79 and 7.46 ppm, while several sharper features are seen in the 7.7 ppm region. All these features scale in intensity according to the amount of thymine dimer ligand added, without shifting position. This indicates the ligand binds with sufficient affinity to exchange slowly on the NMR timescale, and that these differences are not experimental artifacts. The linewidths and chemical shifts of the higher field resonances are consistent with a tryptophan residue (Wüthrich, 1986). As the linewidth of an aliphatic resonance for F_{ab} fragments is about 15Hz (data not shown) the breadth of these resonances likely reflects in part multiplet splittings inconsistent with the singlets of histidine residues. The lower field, sharper resonances may arise from histidine or the C_2H singlet of tryptophan. Other differences with lower intensity may arise from shifts of less than the linewidth, resulting in partial

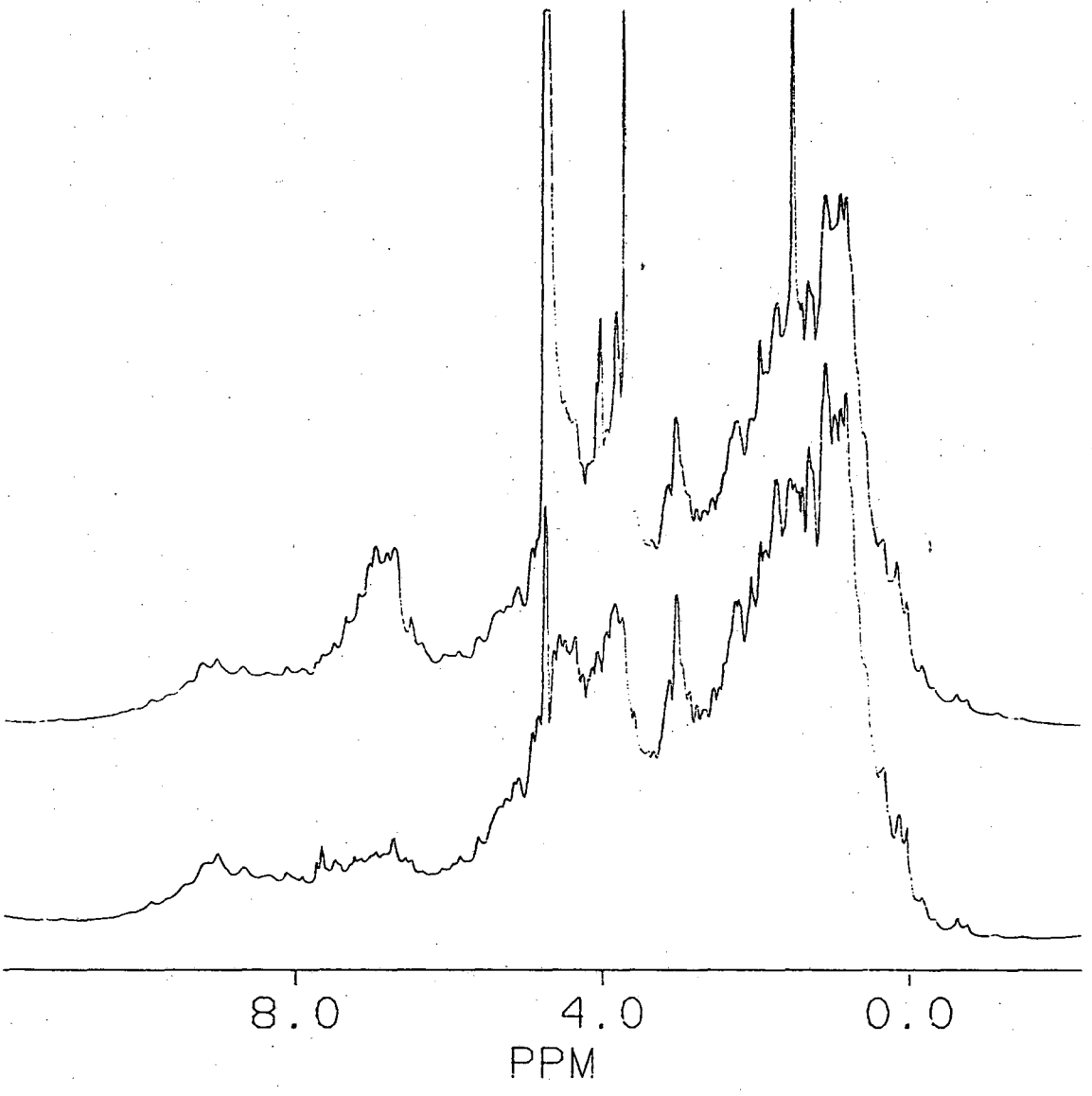

Figure 3.2 - 600 MHz ^{1}H-NMR spectra of thymine dimer Fab fragments. Top spectrum is of unsubstituted Fab's. Bottom spectrum is of Fab's substituted with deuterated phenylalanine and deuterated tyrosine. Note the reduced intensity between 6 and 8 ppm.

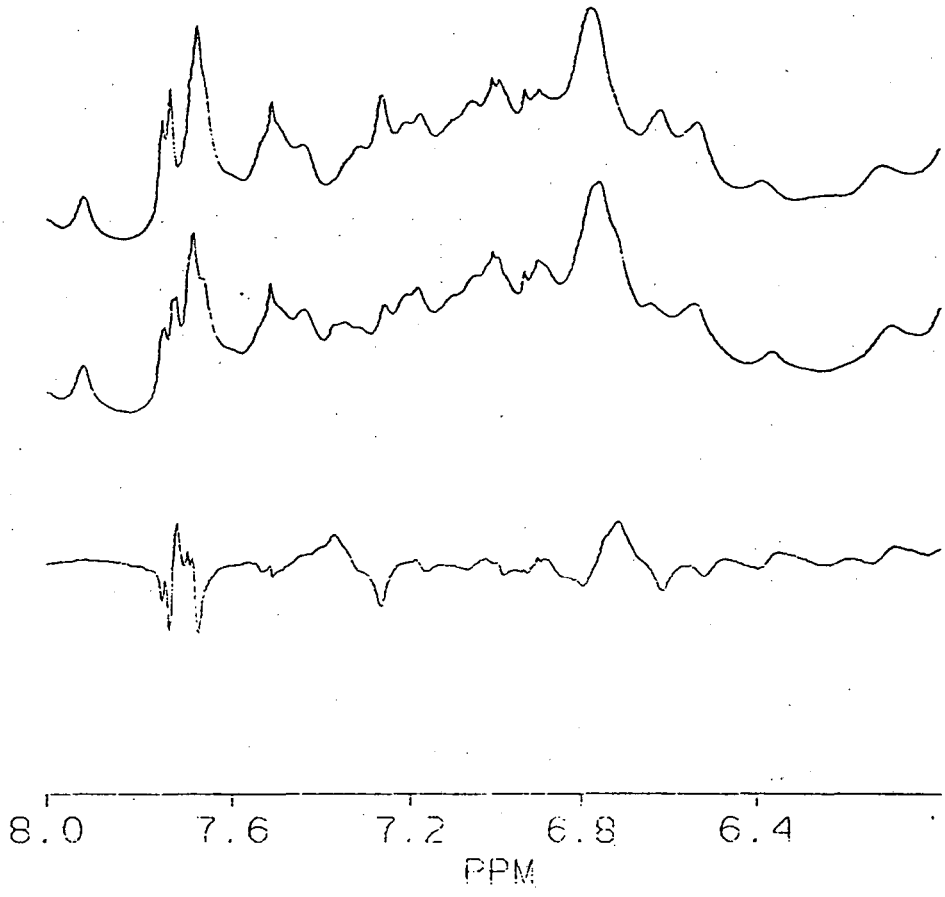

Figure 3.3 - Expansions of the aromatic region of the proton NMR spectra of (dF, dY)Fab's. Top is Fab in absense of the thymine dimer hapten. Middle spectrum is Fab with thymine dimer. Bottom is the difference spectrum: (with hapten) - (without).

cancellation of the signal in the difference spectra. Alternatively they may arise from residual protonated tyrosine or phenylalanine, or from imperfect cancellation of the relatively intense background.

Titrating F_{ab}'s with a thymine dimer conjugated to a nitroxide paramagnetic spin label gives rise to spectra complimentary to those discussed above and are shown in figure 3.4. The negative features at 6.69 and 7.35 ppm are present in these difference spectra, but the previously observed positive features downfield of these resonances are conspicuously absent. The two downfield resonances in the 7.7 ppm region appear only as negative features in the difference spectra, while a third resonance appears with somewhat reduced positive intensity. This resonance also appears at a slightly higher field than seen in the previous experiment. Several other differences are seen in this titration, particularly one at 7.04 ppm.

Ascorbate reduction of the spin label while still bound to the F_{ab} brings about the reappearance of the positive features at 6.84 and 7.50 ppm, as well as a new difference centered at 6.58 ppm. Three sharp, positive features also appeared near 7.7 ppm. The novel difference at 7.04 ppm was unaffected by reduction, indicating it arises from residues at a distance from the binding pocket. Additional ascorbate did not change this region of the spectrum.

Interestingly, the resonance observed at 7.74 ppm in the spin-label titration shifted to 7.78 ppm while the sample was stored for several days at 3°C. This indicates a slow structural equilibration of the complex with this larger ligand. The spin-labeled ligand is isosteric with the unconjugated ligand yet has at least a 5-fold lower

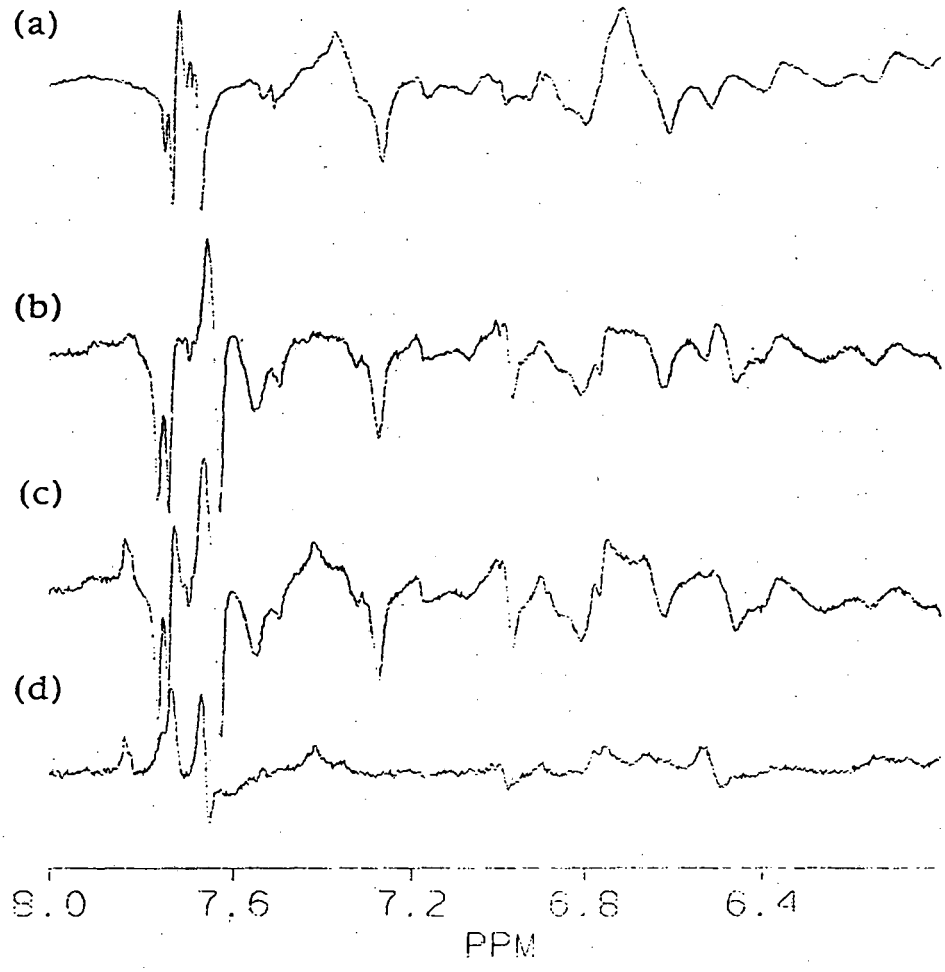

Figure 3.4 - Difference spectra of thymine dimer Fab's.
(a) (with dimer I) - (without hapten).
(b) (with dimer II [spin label]) - (without hapten)
(c) (with reduced dimer II) - (without hapten)
(d) (with reduced dimer II) - (with oxidized dimer II)

binding constant for this antibody. Typically larger ligands have higher affinity for immunoglobins due to a combination of increased van der Waals attractive forces and favorable gain in entropy from the release of protein-bound water. Because it binds less tightly, the larger spin labelled ligand likely introduces some steric interference to binding. It is reasonable to assume the thymine dimer might rest in the binding site in a somewhat different manner due to this strain, resulting in different spectral changes. A slow rearrangement of the F_{ab} to accommodate this strain might occur over the timescale of several days, accounting for the behavior of the 7.74 ppm feature. An orientational difference in the docking of the thymine dimer can also explain other differences between the titrations with the two ligands. In particular the 7.04 ppm difference, not seen with the unconjugated ligand, also shifted slightly while stored at 3°C. This difference signal was not affected by reduction of the spin label, indicating the proposed strain from the spin label causes reorientation of the F_{ab} framework far from the binding site.

This unusual chemical shift behavior is reflected in the upfield region, where a resonance originating near -0.2 ppm exhibited frequency shifts, the magnitude of which depended on the nature of the ligand. This resonance, too, shifted upon storage for one week at 3°C. The unusually low chemical shift of this resonance is most likely due to ring current shifts from a spatially adjacent aromatic residue; it is probable that the responsible residue gives rise to the 7.74 ppm feature. Many other difference features are observed with both ligands in the aliphatic region of the spectra. Interpretation of these spectral features is beyond the scope of this

work.

Discussion:

The difference features observed near 6.8 and 7.5 ppm when thymine dimer ligand is added indicated the perturbation in the environment of a tryptophan residue. These difference signals do not appear at exactly the same chemical shift as tryptophan in a solvent exposed, random coil conformation. Such changes in chemical shift are not uncommon in globular proteins such as F_{ab} fragments. The observation of just two broad difference features implies the perturbation of a single tryptophan upon binding of a thymine dimer. For two or more tryptophan residues to serendipitously have the same chemical shifts and the same change in chemical shift upon hapten binding is unlikely.

These difference signals are broadened by the paramagnetic spin-labelled ligand, but reappear upon reduction of the spin-label while still bound to the F_{ab}. This behavior localizes these residues to within 20Å of the spin label (Jardetzky & Roberts, 1981). The amplitude of the positive features at 6.84 and 7.50 ppm seen upon reduction with ascorbate is less than that seen without spin label. Competing out the reduced spin-labelled ligand with thymine dimer results in more positive amplitude near these chemical shifts. This implies that the reduced amplitude reflects binding or steric differences between the ligands rather than incomplete reduction of the spin-label.

Three difference features are seen in the 7.7 ppm region. These features are relatively intense and narrow, exhibiting a linewidth of about 7 Hz. While this may reflect partial cancellation of

the resonance due to a frequency shift less than the natural linewidth, the intensity of these lines argues against this interpretation. More likely these resonances arise from the singlets of histidine residues, or possibly the singlet C_2H from tryptophan. The two downfield resonances are completely broadened by the spin label, while the upfield-most of them is only partially broadened. This behavior again localizes the responsible residues to within 20Å of the spin label. While the singlets of histidine are separated by 1.08 ppm in fully exposed histidine residues (Wüthrich, 1986) no other differences were observed within <2 ppm with similar linewidth behavior. It is likely, therefore, that two of these signals reflect the close proximity to the binding site of one histidine residue, while the third may reflect a more distant histidine or, perhaps more likely, the C_2H of the aforementioned tryptophan residue.

These experiments confirm the proximity of one tryptophan residue to the binding site of thymine dimers. A second aromatic residue, most likely a histidine, is also observed to be close to the binding site. There are certainly other residues, in particular phenylalanine and tyrosine residues, which constitute the binding pocket but are not detected in the current experiment. The distance limit of 20Å for the identified tryptophan residue is well within range for photon-induced electron transfer and therefore implicates this tryptophan residue in the photoreversal mechanism for antibody mediated thymine monomer formation. This constitutes the first direct evidence for the proposed indole-mediated electron transfer mechanism. More experiments are necessary to explicate the

observed partitioning of the decay pathway, favoring monomer formation over back-electron transfer.

Amzel, L.M. & Poljak, R.J. (1979) *Ann. Rev. Biochem.* **48**, 961-997.

Anglister, J., Frey, T., & McConnell, H.M. (1984) *Biochemistry* **23**, 1138-1142.

Becker, E.D. (1980) High Resolution NMR 2nd ed., pp. 73-74, Academic Press, New York.

Boxer, S.G. (1990) *Ann. Rev. Biophys. and Biophys. Chem.* **19**, 267-299.

Cochran, A.G., Sugasawara, R., & Schultz, P.G. (1988) JACS **110**, 7888-7890.

Cochran, A.J. (1991) Ph.D. dissertation, UC Berkeley

Davies, D.R., Sheriff, S., & Padlan, E.A. (1988) *J. Biol. Chem.* **263**, 10541-10544.

Gray, H.B. & Malmstrom, B.G. (1989) *Biochemistry* **28**, 7499-7505.

Helene, C., & Charlier, M. (1977) *Photochem. Photobiol.* **25**, 429-434

Jacobs, J.A. (1988) Ph.D. dissertation, UC Berkeley.

Jardetzky, O. & Roberts, G.C.K. (1981) NMR in Molecular Biology pp. 99-100, Academic Press, New York.

Johnson, J.L., Hamm-Alvarez, S., Payne, G., Sancar, G.B., Rajagopalan, K.V., & Sancar, A. (1988) *Proc. Nat. Acad. Sci. USA* **85**, 2046-2050.

Jorns, M.S. (1987a) *J. Am. Chem. Soc.* **109**, 3133-3136.

Jorns, M.S., Baldwin, E.T., Sancar, G.B., & Sancar, A. (1987b) *J. Biol. Chem.* **262**, 486-491.

Lamola, A.A. (1972) *Mol. Photochem.* **4**, 107-133.

Padlan, E.A. (1977) *Quar. Rev. of Biophysics* **10**, 35-65.

Padlan, E.A. (1990) *Protiens* **7**, 112-124.

Patrick, M.H. (1977) *Photochem. and Photobiol.* **25**, 357-372.

Patrick, M.H. & Snow, J.M. (1977) *Photochem and Photobiol.* **25,** 373-384.

Payne, G. & Sancar, A. (1990) *Biochemistry* **29**, 7715-7727.

Rokita, S.E. & Walsh, C.T. (1984) *J. Am. Chem. Soc.* **106**, 4589-4595.

Roth, H.D. & Lamola, A.A. (1972) *J. Am. Chem. Soc.* **94**, 1013-1014.

Sancar, G.B., Smith, F.W., Reid, R., Payne, G., Levy, M., & Sancar, A. (1987a) *J. Biol. Chem.* **262**, 478-485.

Sancar, G.B., Jorns, M.S., Payne, F., Fluke, D.J., Rupert, C.S., & Sancar, A. (1987b) *J. Biol. Chem.* **262**, 492-498.

Sutherland, B.M. (1981) *The Enzymes*, Boyer PD, ed. **14**, 481-515.

Van Camp, J.R., Young, T., Hartman, R.F., & Rose, S.D. (1987) *Photochem. Photobiol.* **45**, 365-370.

Wüthrich, K. (1986) NMR of Proteins and Nucleic Acids p.17, Wiley, New York.

Chapter 4: Structure of a Hybrid Sequence Peptide

The peptide-bonded backbone of polypeptides often folds into regular patterns of repeating structure, called secondary structure (Richardson, 1981; Chothia, 1984). A result of steric, electronic, and hydrogen bonding constraints, these preferred conformations fall into two classes, helices and extended sheets. Linked together by a variety of turns and loops, helices and sheets form the basic motif for the majority of protein structures. Secondary structure is critical in determining the orientation and juxtaposition of the amino acid side chains. Because the function of a polypeptide is determined by these factors, maintaining the integrity of secondary structural elements is critical to preserving function. The remaining chapters will describe experiments which probe secondary structure stability, in particular helix propagation and termination (Presta & Rose, 1988).

Helices in polypeptides are formed via intrastrand hydrogen bonding of a peptide amide proton to a peptide carbonyl. The most prevalent helix, the α-helix, has a characteristic *i, i*+4 pattern in which the peptide carbonyl is hydrogen bonded to the peptide amide four residues towards the C-terminus (Barlow & Thornton, 1988). As shown in figure 4.1, this results in a periodicity of 3.6 residues per turn, with a rise of about 10Å per turn (Pauling *et al.*, 1951). In a right-handed helix of L-amino acids the side chains are directed radially and downward, towards the C-terminus. The dipole moment

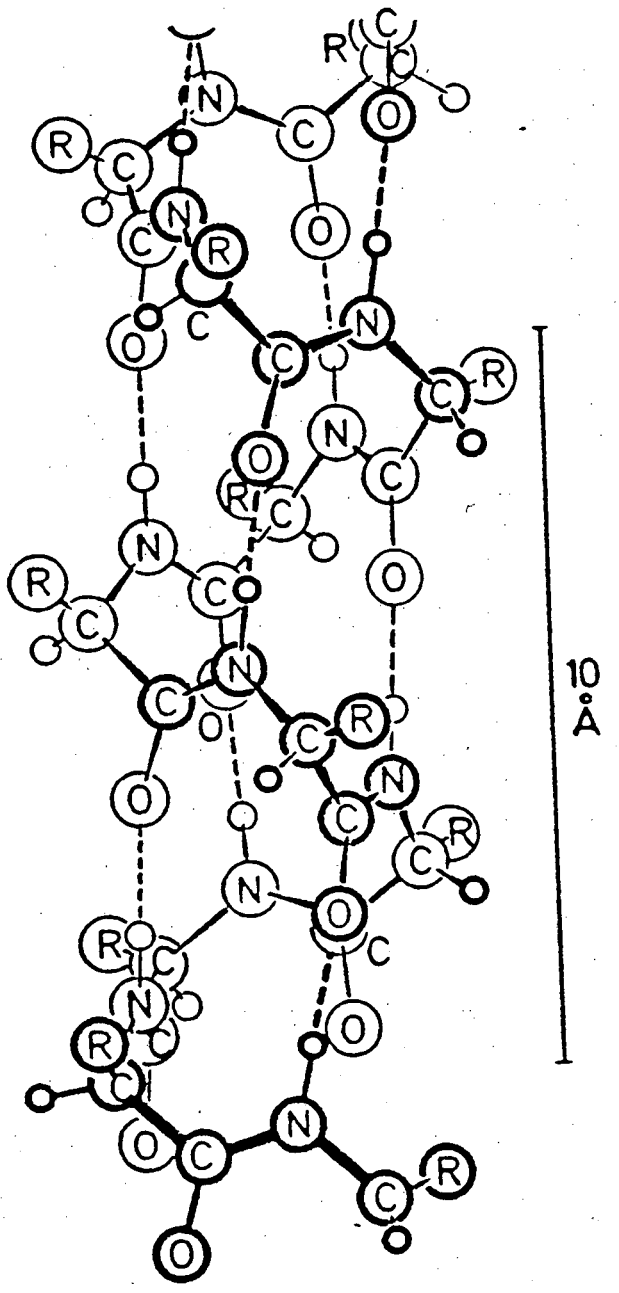

Figure 4.1 - Schematic drawing of an α-helix showing the characteristic *i, i*+4 hydrogen bonds. Drawing from Pauling and Corey (1953).

of each peptide bond is aligned with the helix axis. These add constructively to give the helix an overall dipole moment, with the positive pole at the N-terminus. This helix dipole moment has significance in determining helix stability as will be discussed below (Hol *et al.*, 1978). Often hydrophobic forces and favorable side-chain hydrogen bonding will contribute to the formation of specific interhelix interactions, resulting in bundles of helices or even mixed helix-sheet structures (Creighton, 1984).

Helices are also found in a variety of proteins with specific DNA affinity (Brennan & Matthews, 1989; Harrison & Aggarwal, 1990; Churchill & Travers, 1991). The dimensions of the α-helix are such that it fits snugly into the major groove of B-form DNA. Additionally the helix dipole moment can be oriented to favorably interact with the polyanionic phosphodiester backbone of the DNA. These proteins also respond to local chemical and conformational considerations of the DNA, resulting in exquisite specificity for binding particular sequences of DNA bases. The determinants of the sequence specificity in this class of proteins are complex. Based in the same chemical forces of hydrogen bonding, hydrophobic interaction, charge and steric complementarity, sequence specificity is the basis for control of gene regulation (Mitchell & Tjian, 1989). For this reason elucidating the relative importance of the various forces which determine sequence specificity is necessary for understanding and ultimately controlling gene regulation. In these proteins a helical conformation is necessary for sequence specific binding, and serves as a basis for investigation of other elements of DNA recognition.

One well studied example of a DNA binding polypeptide with a helical motif is the bacteriophage 434 repressor. This molecule consists of two domains which bind as a dimer to a nearly palindromic DNA sequence (Sauer *et al.*, 1982). An X-ray crystal structure has been published which hypothesizes conferral of sequence specificity by direct hydrogen bonding of glutamine amino acid side chains to the DNA base pairs in the major groove (Figure 4.2; Anderson *et al.*, 1987). X-ray crystallography, however, cannot directly observe the protons forming these hydrogen bonds, and the strength and specificity of these bonds must be inferred from chemical knowledge. The role of these putative hydrogen bonds in determining the sequence specificity of binding, particularly in relationship to other forces of interaction, remains a matter of considerable debate.

The study of this system is hampered by its large size. As with the immunoglobins discussed earlier, the local determinants of specific binding are shadowed by the larger structural domains orienting the recognition helix. Investigating the forces of interaction between the recognition helix and the DNA would be facilitated by reducing the size of the system. Unfortunately, helices in isolation are rarely stable (Marqusee *et al.*, 1989; Finkelstein *et al.*, 1991). Generally these structures unfold when isolated, adopting dynamic pseudo-random conformations.

In an attempt to stabilize the isolated 434 repressor recognition helix, a hybrid sequence peptide was designed in which this amino acid sequence is preceded by the N-terminal 8 amino acids from the bee venom peptide apamin. Apamin is an 18 residue

–3L	–2L	–1L	1L	2L	3L	4L	5L	6L	7L	7'R	6'R	5'R
T	A	T	A	C	A	A	G	A	A	A	G	T
	T	A	T	G	T	T	C	T	T	T	C	
	–2'L	–1'L	1'L	2'L	3'L	4'L	5'L	6'L	7'L	7R	6R	

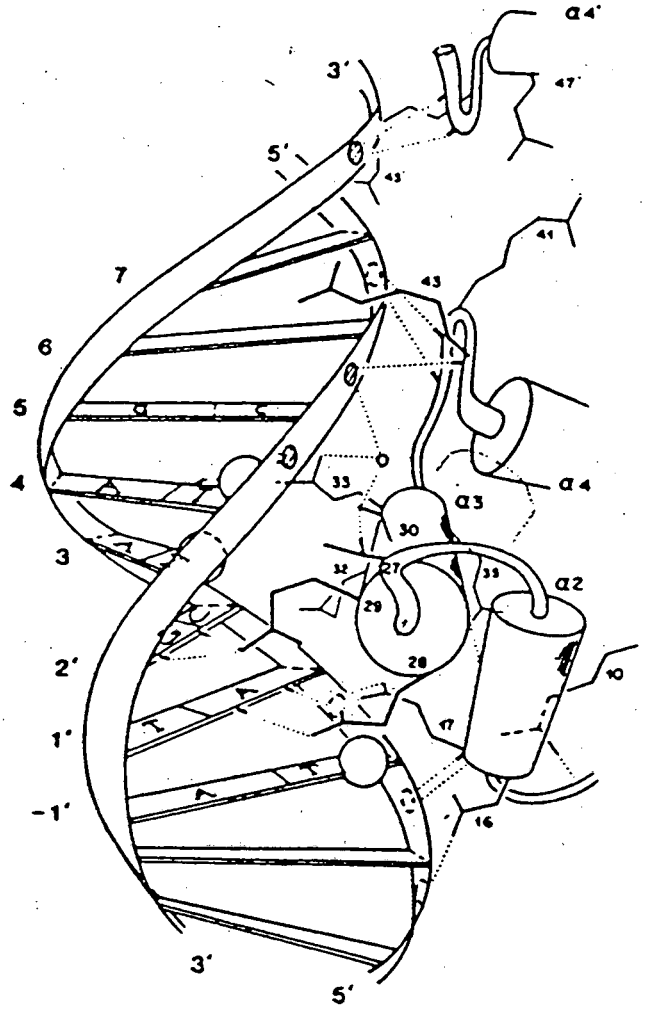

Figure 4.2 - DNA sequence recognized by 434 repressor and model of interaction between this DNA and the recognition helix of the repressor. From Aggarwal *et al* (1988).

peptide whose solution structure has been determined by NMR (Pease & Wemmer, 1987). As shown in figure 4.3a, the 8 N-terminal residues of apamin form a scaffold onto which two turns of helix are attached by disulfide bridges. These disulfide bridges covalently stabilize the otherwise isolated helix, which maintains its conformation under such extreme conditions as 6M urea or 70° C (Miroshnikov *et al.*, 1978). The two disulfide bridges of apamin always form in the correct 1-11, 3-15 orientation when the reduced peptide is exposed to mildly oxidizing conditions (Pease *et al.*, 1990; *vide infra*). The driving force for this unique orientation of disulfides is undetermined, but it was hoped to be based in the N-terminal scaffold. This would provide for an isolated helix of designed sequence.

As a first step towards the development of a small, sequence specific DNA binding peptide helix, experiments were designed to fabricate and characterize an apamin/434 repressor hybrid peptide. The sequences of apamin, the recognition helix from 434 repressor, and the hybrid peptide are shown in Figure 4.3b. The numbering of residues is based on the apamin sequence. Note the replacement of residues S30 and L34 of the 434 repressor sequence with cysteines to preserve the spacing of cysteine residues in native apamin. This places the critical Q28, Q29, and Q33 residues, which interact directly with the DNA bases (Andersen *et al.*, 1987), on the solvent exposed face of the helix. The -KRPR tail of the repressor sequence was included in the hybrid sequence to facilitate potential charged interactions between the positively charged K and R side chains with the negatively charged phosphodiester backbone of DNA (Mair *et al.*,

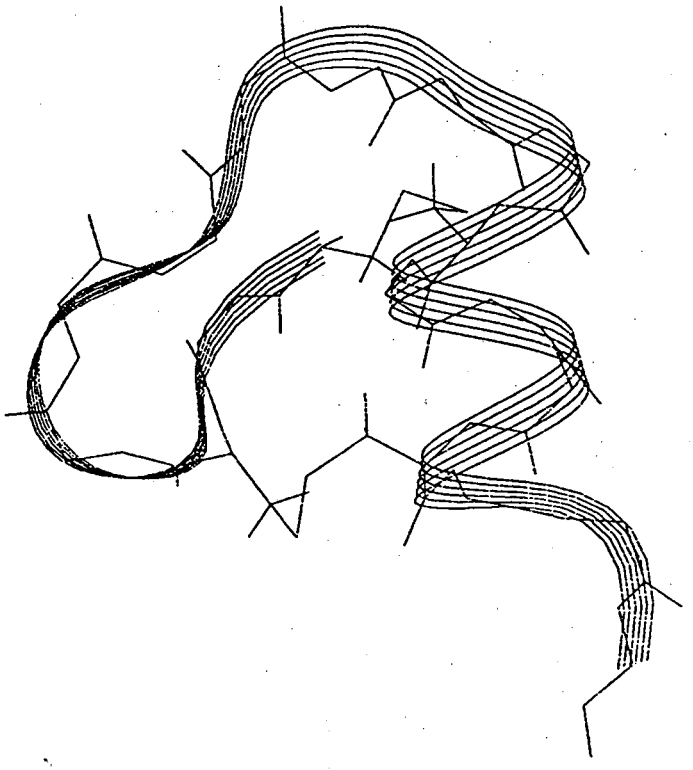

```
          1         5         10        15        20
          |         |         |         |         |
Apamin:   C N C K A P E T A L C A R R C Q Q H

434 repressor:          ...T Q Q S I E Q L E N G K T K R P R...

Apa-434:  C N C K A P E T Q Q C A A Q C Q N G K T K R P R
```

Figure 4.3 - Peptide backbone structure of apamin from Pease (1989) and one-letter codes for the peptide sequences of apamin, 434 repressor recognition helix, and the hybrid peptide.

1991).

Materials and Methods:

The hybrid sequence peptide was synthesized on an Applied Biosystems 430A solid phase peptide synthesizer using standard t-butoxycarbonyl (t-Boc) chemistry, utilizing double coupling cycles throughout. HF cleavage was performed by Applied Biosystems, yielding 946 mg of crude material (not all peptide). 200 mg of this material was dissolved in 10 ml of 50mM Tris·HCl (pH 8.0) and a molar excess of dithiothreitol. After incubating at room temperature for one hour to ensure complete reduction of all cysteine residues, this mixture was diluted to a final volume of 100 ml with distilled water in a 2 l flask. The peptide was allowed to air oxidize at room temperature for 1 week. The solution was reduced to 10 ml by ultrafiltration with an Amicon Diaflo UM2 membrane. The oxidized peptide was isolated via HPLC done on a Waters HPLC equipped with a Waters Delta Pak preparative column (C18 300Å; 19mm x 30cm). A two-buffer system was used: Buffer A, 0.1% trfluoroacetic acid/H_2O; buffer B, 0.1% trifluoroacetic acid/60% CH_3CN/40% H_2O. The run began with 100% buffer A at 5 ml/min for 5 minutes, then a linear gradient to 20% buffer B over 10 minutes, followed by a linear gradient to 30% buffer B over 30 minutes, then 100% buffer B over 15 minutes. Absorbance at 235 nm was monitored and the major peak, which eluted at 27% buffer B, was collected and dried by a Speed-Vac equipped with a dry ice/ethanol cold finger trap and molecular sieves. This fraction was confirmed to be the appropriate peptide by FAB-mass spectroscopy, with the major peak at 2661 Da. This is the expected mass for the fully oxidized peptide with two

disulfide bonds. The identity of the peptide was also confirmed by the ensuing NMR analysis.

NMR measurements were carried out on a General Electric GN-500 and a Bruker AMX-600 spectrometer operating at a proton frequencies of 500.13 MHz and 600.14 MHz, respectively. A 400 µl sample, ~10mM in peptide, was made by dissolving the dried HPLC fractions in 50mM NaCl, 5mM NaH_2PO_4, and 10% D_2O. The pH was adjusted to 4.0 with small additions of 1M NaOH.

Results:

The solution structure of the peptide was characterized by two-dimensional NMR as described in Chapter 1. Relevant sections of the two-dimensional NOESY spectrum are shown in Figure 4.4 and a summary of the sequential and helical connectivities is shown in Figure 4.5. The pattern of connectivities for residues 1-18 of the hybrid is identical to that observed for apamin (Pease & Wemmer, 1988), indicating that the overall folding is very similar. Most significant are the connectivities to P6. Centrally located in the apamin scaffold, the β,β', and γ protons display an NOE to the CαH of both A5 and A12. This pattern is indicative of the apamin fold, with the appropriate 1-11, 3-15 orientation of disulfide bridges.

The intensities of sequential $\alpha_iH\text{-}NH_{i+1}$ and intraresidue $\alpha_iH\text{-}NH_i$ connectivities from residues T8 through G18 are also similar to those seen in apamin (Pease & Wemmer, 1988). A strong sequential $\alpha_iH\text{-}NH_{i+1}$ connectivity coupled with a weak intraresidue $\alpha_iH\text{-}NH_i$ connectivity is highly indicative of a helical conformation. As in apamin, this helical pattern is observed extending as far as residue G18. These intensities become more similar beyond residue 16,

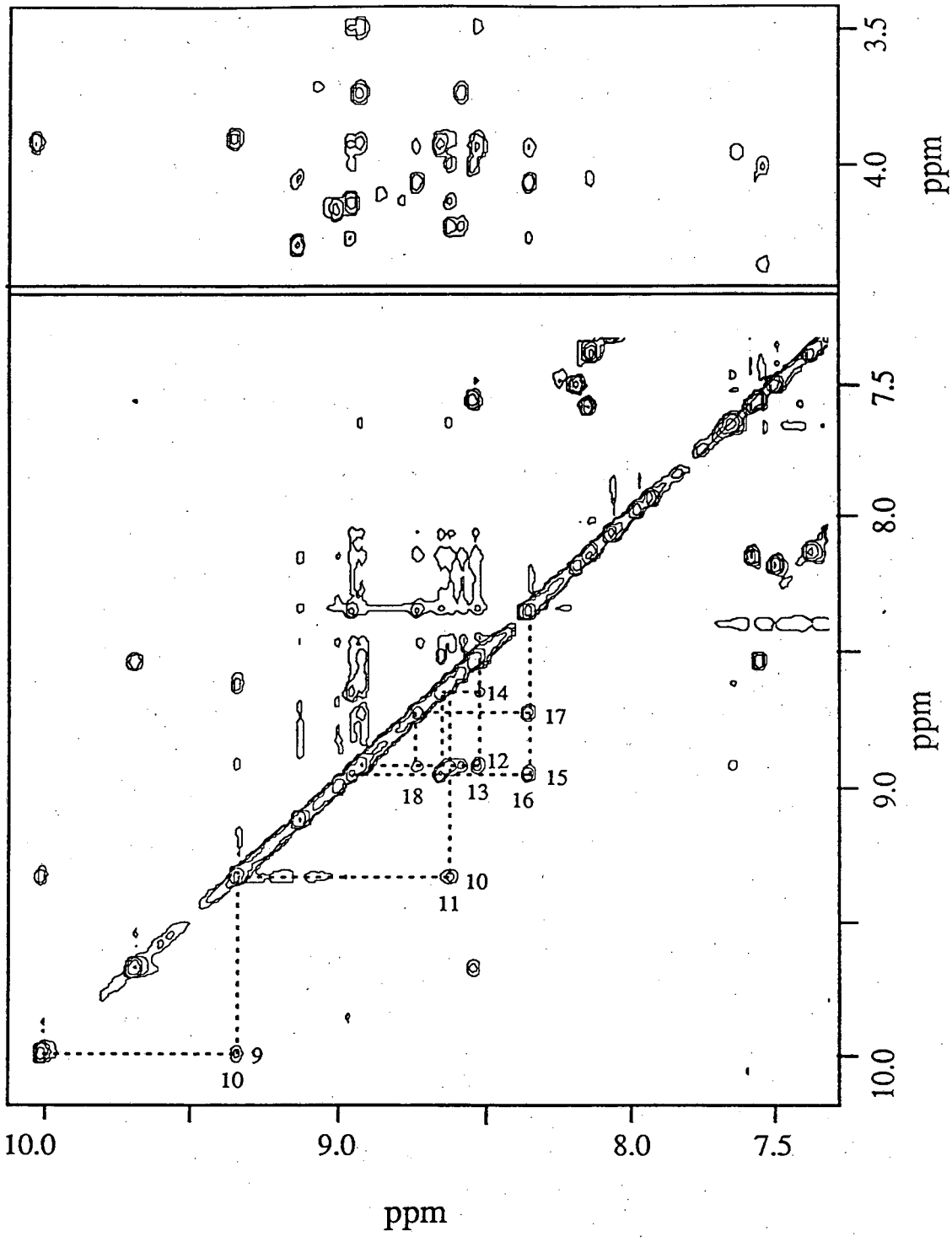

Figure 4.4 - Portions of a 300ms NOESY spectrum of the apamin-434 repressor hybrid peptide. The upper portion shows the αH - NH crosspeaks. The lower portion shows the NH - NH crosspeaks. The helical connectivites seen for residues 9-18 are shown in the lower portion.

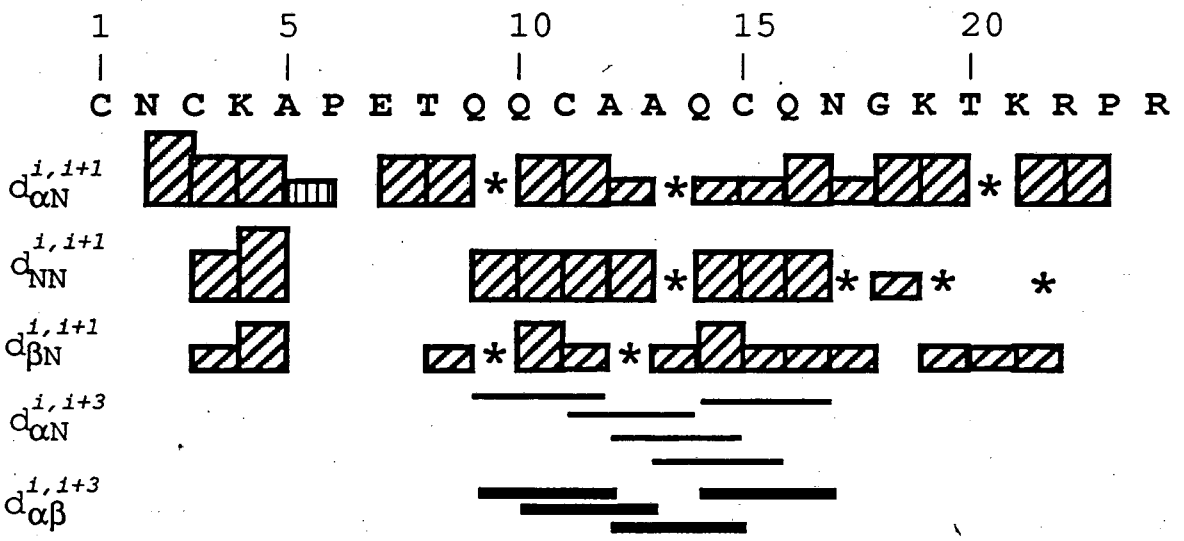

Figure 4.5 - Connectivities observed for the hybrid peptide in NOESY spectra with a 150 ms mixing time. Box height reflects sequential crosspeak intensity. The αH-NH(A5-P6) crosspeak was to the δ-proton of P6. * indicates crosspeaks which overlap with other crosspeaks or the diagonal. Long range helical connectivities are indicated with lines which do not reflect their intensities. Long range connectivities to the N-terminal scaffold are not shown.

which reflects the lowered stability of the helical conformation beyond the covalent disulfide bridge at residue C15. However, the $\alpha_i H\text{-}NH_{i+3}$-type connectivities, the hallmark of a helical conformation (Wüthrich, 1986), are clearly seen extending to residue N17.

That helical connectivities are absent beyond residue N17 is not surprizing in light of the low probability of finding glycine residues in helices (Richardson & Richardson, 1988). Indeed, glycines are often found at the C-terminus of helices. This observation can be explained in terms of the conformational flexibility of this amino acid. Lacking a side chain, glycine has fewer steric constraints on the conformation of the peptide backbone. This has two effects. It creates a larger entropic barrier to helix formation as the competing coil "state" consists of more conformers, and it allows added flexibility for the redirection of the peptide backbone to properly position the succeeding structural elements. In the present case the latter consideration is of no regard, but the former explains the rather abrupt termination of helical connectivities at this residue.

As the helix becomes less stable towards the C-terminus the correlation time describing local motions appears to decrease. This is reflected in the NOE intensities of protons with a fixed, short distance. Geminal methylene protons are constrained to a separation of about 1.8Å, and generally give rise to strong NOE's. For example the $\beta\beta'$ (and $\beta\gamma$) crosspeaks of P6 are easily observed, but the corresponding crosspeaks for P23 are not seen even at a mixing time of 400ms. On the other hand, the $NH\text{-}CH_3$ crosspeak of T8 is of similar magnitude to the corresponding crosspeak of T20. The $\beta\gamma$

crosspeaks of K19 and K21 are barely observable at 400ms, while this crosspeak is seen for Q14 and Q16.

These effects can all be explained by a local conformational equilibrium between the helix and more random conformations. When helical, a residue will tumble in concert with the whole apamin-stabilized core. In a random conformation the correlation time is no longer dependent entirely on molecular tumbling. The dynamics of random coil fluctuations as well as the dynamics of the helix-coil equilibrium contribute additional motions to these residues, shortening the correlation time (τ_c). As outlined in Chapter 1, the efficiency of the NOE effect is a function of this time. For apamin and this hybrid sequence peptide, the observed NOE's are negative, indicating that $\omega\tau_c>1$ (where ω is the Larmor or resonance frequency in the NMR experiment). As the correlation time is shortened and $\omega\tau_c\approx1$, the efficiency of NOE transfer weakens, as observed.

This study demonstrates that helix stabilization by the apamin scaffold (residues 1-8) is not dependent on the sequence of the helical portion of the molecule. As long as the proper juxtaposition of cysteine residues is maintained, these hybrid molecules will spontaneously fold to form the appropriate 1-11, 3-15 disulfide bond orientation and stabilize residues 8-16 in a rigid helix. Beyond the covalent bond at C15 the stability of the helix becomes subject to the entropic and enthalpic considerations of helix propagation. The extent of stabilization will then become sequence dependent. However, this model can be utilized to study these sequence dependent effects of helix propagation in the absence of

the confounding initiation events, as will be seen in the next chapter.

Anderson, J.E., Ptashne, M., Harrison, S.C. (1987) *Nature* **326**, 846-852.

Barlow, D.J. & Thornton, J.M. (1988) *J. Mol. Biol.* **201**, 601-619.

Brennan, R.G. & Matthews, B.W. (1989) *Trends in Biochemical Sciences* **14**, 286-90.

Chothia, C. (1984) *Ann. Rev. Biochem.* **53**, 537-572.

Churchill, M.E.A. & Travers, A.A. (1991) *Trends in Biochemical Sciences*, **16**, 92-97.

Creighton, T.E. (1984) *Proteins: Structures and molecular properties* W.H. Freeman, New York.

Finkelstein, A.V., Badritdinov, A.Y., & Ptitsyn, O.B. (1991) *Proteins*, **10**, 287-299.

Harrison, S.C. & Aggarwal, A.K. (1990) *Ann. Rev. Biochem.* **59**, 933-969.

Hol, W.G.J., van Duijnen, P.T., & Berendsen, H.J.C. (1978) *Nature* **273**, 443-446.

Marqusee, S., Robbins, V.H., & Baldwin, R.L. (1989) *Proc. Nat'l. Acad. Sci. USA* **86**, 5286-5290.

Miroshnikov, A.I., Elyakova, I.G., Kudelin, A.B., & Senyavina, L.B. (1978) *Bioorg. Khim.* **4**, 1022-1028.

Mitchell, P.J. & Tjian, R. (1989) *Science* **245**, 371-378.

Pauling, L., Corey, R.B., & Branson, H.R. (1951) *Proc. Natl. Acad. Sci. USA* **37**, 235-240.

Pauling, L. & Corey, R.B. (1953) *Proc. Royal Soc. London B* **141**, 21-33.

Pease, J.H.B. & Wemmer, D.E. (1988) *Biochemistry* **27**, 8491-8498.

Pease, J.H.B., Storrs, R.W., & Wemmer, D.E. (1990) *Proc. Nat. Acad. Sci.* **87**, 5643-5647.

Presta, L.G. & Rose, G.D. (1988) *Science* **240**, 1632-1641.

Richardson, J.S. (1981) *Adv. Prot. Chem.* **34**, 176-330.

Richardson, J.S. & Richardson, D.C. (1988) *Science* **240**, 1648-54.

Sauer, R.T., Yocum, R.R., Doolittle, R.F., Lewis, M., & Pabo, C.O. (1982) *Nature* **298**, 447-451.

Wüthrich, K. (1986) *NMR of Proteins and Nucleic Acids*, Wiley and Sons, New York.

Chapter 5: Helix Propagation in Trifluoroethanol Mixtures

Introduction:

It has been postulated that the folding of globular proteins begins with the formation of short helices or β-sheets which interact in a later step to produce the native three dimensional structure (Ptitsyn & Finkelstein, 1980; Richardson, 1981; Kim & Baldwin, 1982). Given this hypothesis, knowledge of how small units of secondary structure are formed is necessary for understanding how polypeptides fold uniquely into their native conformation. To elucidate the thermodynamics of helix formation many investigators have made use of 2,2,2-trifluoroethanol (TFE). TFE is a polar solvent which stabilizes the helical conformation of peptides with helix forming propensity. It is not well understood how TFE affects helix initiation, propagation, and termination to facilitate helix stabilization.

The S-peptide (residues 1-19) of Ribonuclease A has been extensively studied as a model for helix formation. The S-peptide exhibits a surprizing degree of helicity in water solution, up to 38% under optimal conditions (Rico *et al.*, 1984; Kim & Baldwin, 1982) TFE stabilizes additional helical structure in the S-peptide. The intensity of circular dichroism at 208nm and 222nm increases with added TFE, and the isodichroic point at 202nm indicates a two state transition for each residue between helical and coil conformations.

Circular dichroism studies, however, cannot distinguish between the effects of TFE on helix initiation and propagation.

The effects of TFE on the S-peptide helix have been investigated in a sequence-specific fashion by NMR chemical shifts (Nelson & Kallenbach, 1989). In this study the chemical shifts for the side chain resonances of residues 3-13 all moved proportionately with very small additions of TFE. Whether this reflects an all-or-none cooperativity for helix formation or a uniform probability for helix initiation within this sequence is still undetermined. The chemical shifts of residues 14-19 did not shift significantly when the peptide was titrated with TFE. The helix of the free S-peptide appears to terminate at residue 13, the same location as in native ribonuclease A. This indicates that an indigenous helix stop signal (Kim & Baldwin, 1982), encoded by the S-peptide sequence near residue 13, persists in TFE solutions.

An abrupt "helix stop" signal was not seen in the S-peptide sequence of a hybrid sequence peptide (Pease *et al.*, 1990). This hybrid peptide was designed such that the first turn of the S-peptide helix is covalently stabilized by disulfide bonds derived from the N-terminal sequence of the bee venom peptide apamin. The extent of helix propagation of the S-peptide sequence was examined in a hybrid sequence peptide using nuclear Overhauser effect spectroscopy (NOESY). Residues 11-20 of the S-peptide sequence (residues 16-25 of the hybrid peptide) are not conformationally constrained by the apamin-like part of the sequence, and may adopt either helical or random coil conformations. Rather than a discreet break in helicity at residue M13 (M18 of the hybrid), as suggested

by earlier NMR studies of S-peptide, this hybrid peptide exhibits a gradual decrease in helicity over several residues. There is no evidence for a single residue or pair of residues breaking the helix.

This hybrid peptide provides a unique opportunity to study helix propagation and termination in TFE solutions. Helix initiation can be separated from these events because the helix is essentially 100% nucleated through covalent disulfide bonds. In an attempt to further the understanding of the effects of TFE on helix propagation and termination, experiments were initiated to determine the extent of helical structure which can be favorably adopted by the apamin/S-peptide sequence in TFE solutions.

Materials and Methods

Design, synthesis, and purification of the hybrid peptide has been described previously (Pease *et al.*, 1990).

CD measurements were carried out on a Jasco J600 spectropolarimeter. Matched samples were made by dissolving lyophilized, buffered aliquots of a peptide stock solution with 300µl of the appropriate mixture of TFE and distilled water. Samples were placed immediately in a thermally jacketed 0.2-cm cell and were ~5mM peptide in 100mM NaCl and 10mM Na_2HPO_4, pH 5.0. Temperature was controlled via a recirculating constant temperature bath. 4 scans were averaged and are presented without further smoothing.

NMR measurements were carried out on a Bruker AMX-600 spectrometer. ~5mM samples were lyophilized from 500µl of 100mM NaCl and dissolved in 250µl distilled water and 250µl d_3-2,2,2-trifluoroethanol (MSD Isotopes). pH* was adjusted to 4.6 by

small additions of 1M NaOH and measured with an AgCl combination electrode without correction for the TFE. NOESY and TOCSY data were collected using the TPPI method, using the deuterium signal of TFE as a frequency lock. A NOESY spectrum (400ms mixing time) and TOCSY spectra (38ms and 50ms mixing times) were used for assigning NMR resonances, while a 150ms NOESY spectrum was used for structural analysis. The solvent resonance was reduced by 1 second of presaturation unless otherwise noted. 48-64 scans were averaged per t_1 value, with a recycle time of 2.5 sec. A 6024 Hz spectral width was used with 2048 points in t_2, and 512 t_1 values were collected for each spectrum.

Results:

As reported earlier, the ultraviolet circular dichroism (CD) spectrum in H_2O of the apamin/S-peptide hybrid closely resembles that of apamin (Pease *et al.*, 1990). The spectrum of the hybrid exhibits a minimum at 208nm and a pronounced shoulder at 222nm, features which are characteristic of an α-helix although there must be contributions from other parts of the peptide as well. As the proportion of TFE increases, both these spectral features increase in intensity with an isodichroic point at 202nm, indicating the stabilization of more residues in a helical conformation in a two-state, coil-to-helix process (figure 5.1). The coil state of each residue is in reality a collection of rapidly interconverting conformations which give rise to a single average spectrum. 80 vol. % (50 mol %) TFE gave rise to a 36% increase in the intensity of Θ_{222} at 20°C. Lowering the temperature to 3°C results in an additional 8% increase in ellipticity with 80% TFE.

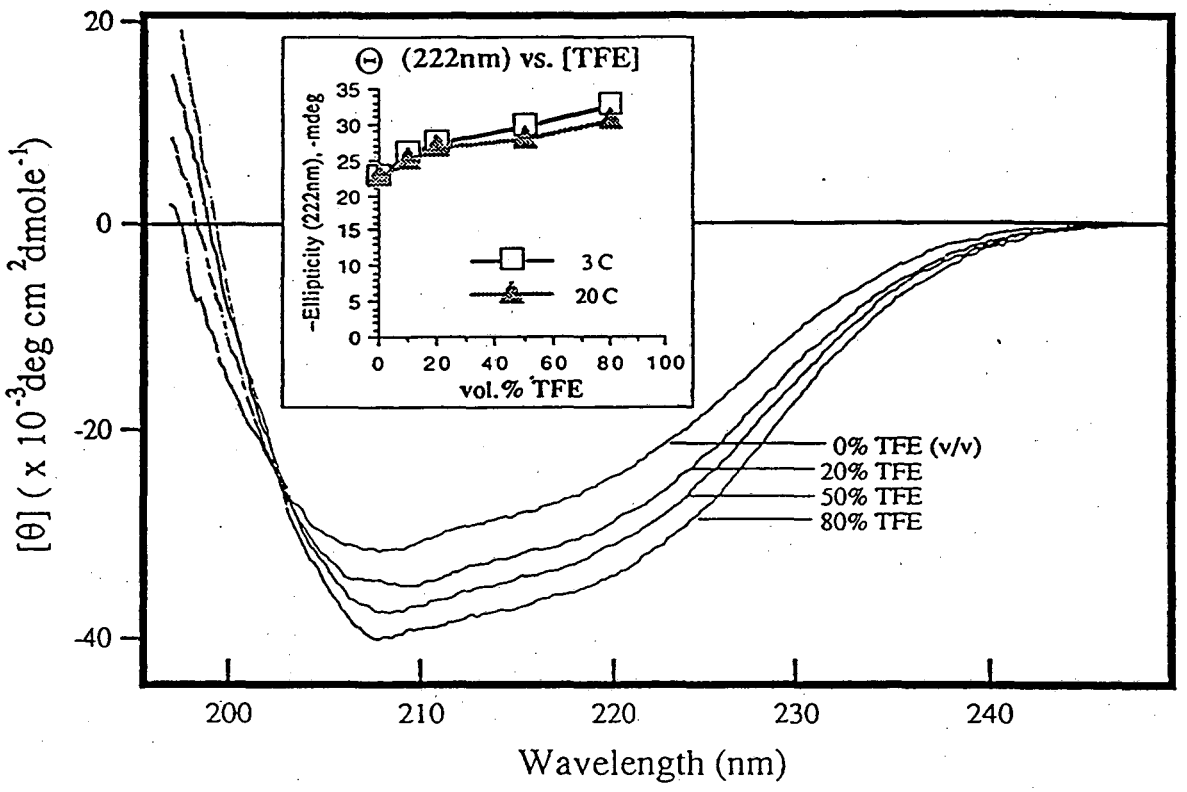

Figure 5.1 - Circular Dichroism spectra of the hybrid peptide at 3°C with increasing proportions of TFE. Sample concentration was the same in all samples, ~5μM. *Inset*: Negative ellipiticity at 222nm as a function of volume % TFE at 3°C(squares) and 20°C(triangles).

Unfortunately, the peptide is not amenable to analysis by NMR in 80% TFE at 3°C. Non-uniform broadening of the amide resonances was observed as the temperature is decreased. Furthermore, many $C_\alpha H$ chemical shifts were degenerate, a characteristic which has been seen with other helical peptides in TFE (Dyson *et al.*, 1988). Observation of crosspeaks due to the α protons was made additionally difficult by streaking from the residual ^1H-TFE signal.

A complete assignment of the 2D-NMR spectra is possible under the conditions of 50 vol.% TFE and 20°C using standard techniques (Wüthrich, 1986). As described above, the $C_\alpha H$ chemical shifts are closely grouped in the TFE/water mixture, and the chemical shifts of the NH resonances do not closely correspond to the spectrum in pure H_2O. However, the pattern of through-space connectivities reported previously for the hybrid peptide in water (Pease *et al.*, 1990) are preserved in 50% TFE. The turn/loop/helix motif of apamin is not disrupted by the solvent mixture, including the interaction of residue P6 with the $C_\alpha H$'s of C3 and K12. Many new crosspeaks were observed in 50% TFE which indicates the stabilization of additional secondary structure, as outlined below.

In comparison to H_2O, the peptide in 50% TFE exhibits new helical NOESY connectivities, and several with relatively greater intensity. These connectivities are summarized in figure 5.2. Sequential NH_i-NH_{i+1} crosspeaks, characteristic of the helical conformation, were strong and of nearly equal intensity from residue A9 through residue A25 in TFE (figure 5.3b). In water, these crosspeaks weakened at residue M18, and were unobservable

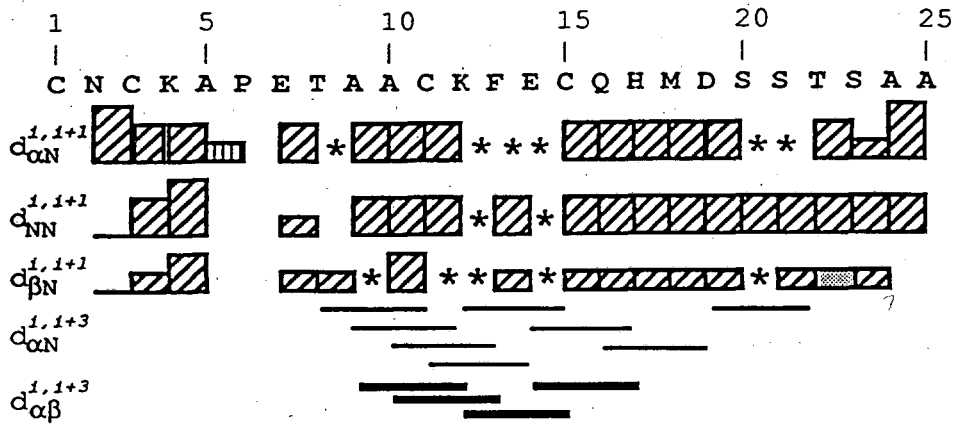

Figure 5.2 - Connectivities observed for the hybrid peptide in NOESY spectra with a 150ms mixing time. Box height reflects sequential crosspeak intensity. The αH-NH(A5-P6) crosspeak was to the δ-proton of P6. The β-NH(T21-S22) crosspeak was from the γ-CH_3 of T21. * indicates crosspeaks which overlap with other crosspeaks or the diagonal. Long range helical connectivities are indicated with lines which do not reflect their intensities. Long range connectivities to the N-terminal scaffold are not shown.

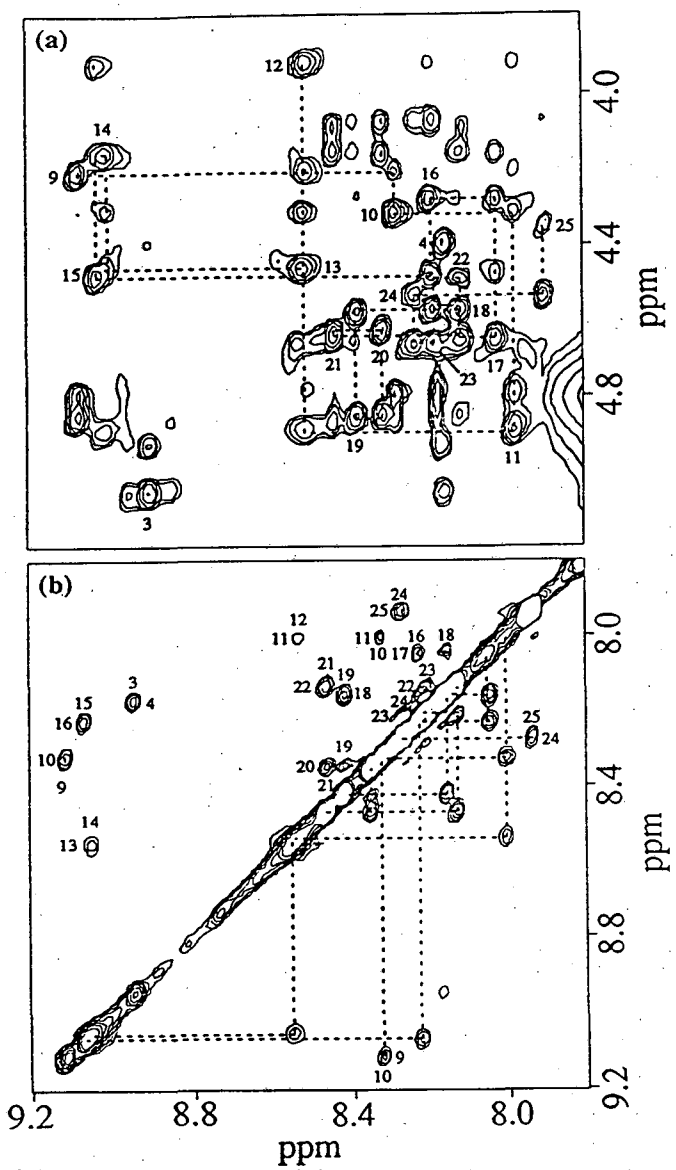

Figure 5.3 - Amide to α proton (a) and amide to amide proton (b) regions of NOESY spectra of the hybrid peptide in 50% TFE and at 20°C. The mixing time was 150ms in both spectra. The dashed lines trace the sequential connectivities from residue A9 through A25. In (a) the intraresidue crosspeak is identified with the residue number as designated in Figure 2. In (b) the numbers reflect the two residues from which the crosspeaks arise. In (a) the solvent resonance was reduced by a 1,1-jump return detection pulse, while in (b) the solvent resonance was reduced by presaturation.

beyond residue S20 (Pease *et al.*, 1990). Similarly, the intensities of both intraresidue α_iH-NH$_i$ and sequential α_iH-NH$_{i+1}$ NOESY crosspeaks are fairly uniform in the TFE spectrum (figure 5.3a), while in H_2O these crosspeaks first increase, then decrease in intensity near the C-terminus. For example, the intraresidue α_iH-β_iH crosspeaks for residues A24 and A25 are absent from the H_2O spectrum but are clearly observed as negative NOEs in the TFE spectrum. Local flexibility weakens this fixed distance NOE in H_2O because of a decrease in the internuclear correlation time. The C-terminus of this peptide is less dynamically disordered in the presence of TFE, lengthening the local correlation time and allowing the NOE to become observable. TFE clearly stabilizes helical structure in the C-terminus of this peptide, which is effectively random coil in pure aqueous solution.

Helical i,i+3 connectivities are observed for residues 8-22 in TFE; these crosspeaks were not observed beyond residue 19 in H_2O. The β_{19}H-NH$_{22}$ crosspeak observed in the TFE spectrum was weak, but a α_{19}H-NH$_{22}$ crosspeak was clearly observed in a 400ms 1,1-jump/return NOESY spectrum. The latter crosspeak was not observed in the NOESY spectrum collected with solvent presaturation due to overlap of the α_{19}H with the solvent resonance. Degeneracy of the α, β, and β' resonances for residues S20, S21, and S23 precludes observation of many long-range i,i+3 helical connectivities in the peptide's C-terminus. However, the expected α_{18}H-NH$_{21}$ and α_{20}H-NH$_{23}$ crosspeaks were conspicuously absent, even with a mixing time of 400ms.

Although a low temperature coefficient of chemical shift has been used as an indicator of hydrogen bonding (Dyson *et al.*, 1988), we do not observe any correlation between the temperature' dependence of the NH chemical shift with the characteristics of the helix. The NH temperature coefficients in H_2O vary with residue position in an irregular fashion (figure 5.4). For example, residue F13 has a much lower temperature coefficient, 1.5 ppb/K, than its neighbors, 5.3 ppb/K. All these residues are stabilized in a helical conformation by disulfide bonds to the apamin-like N-terminus and would be expected to have the similar hydrogen bonding stability. TFE increases the effects of temperature, but the pattern of relative magnitudes is generally conserved. Chemical shift temperature dependence does not seem to reflect the local environment nor degree of hydrogen bonding for this peptide.

Discussion:

The isodichroic point in the CD spectra indicates that TFE alters the conformational equilibrium of each residue in a two state fashion. An estimate of the number of helical residues in TFE solutions can be obtained by standardizing the ellipticity data at 0% TFE to the NMR data reported previously for this hybrid in H_2O (Pease *et al.*, 1990). Using the assumption of 10 helical residues, 8 turn-like residues, and 7 random coil residues indicated by the NMR structure in H_2O, combined with published molar ellipticity values (Θ_{222}) for helical, turn, and random coil conformations,[10-11] it is estimated that 3.2 (Brahms & Brahms, 1980) to 4.7 (Chang *et al.*, 1978) additional residues of helix are stabilized by 50 vol % TFE. Lowering the temperature to 3°C and increasing the proportion of

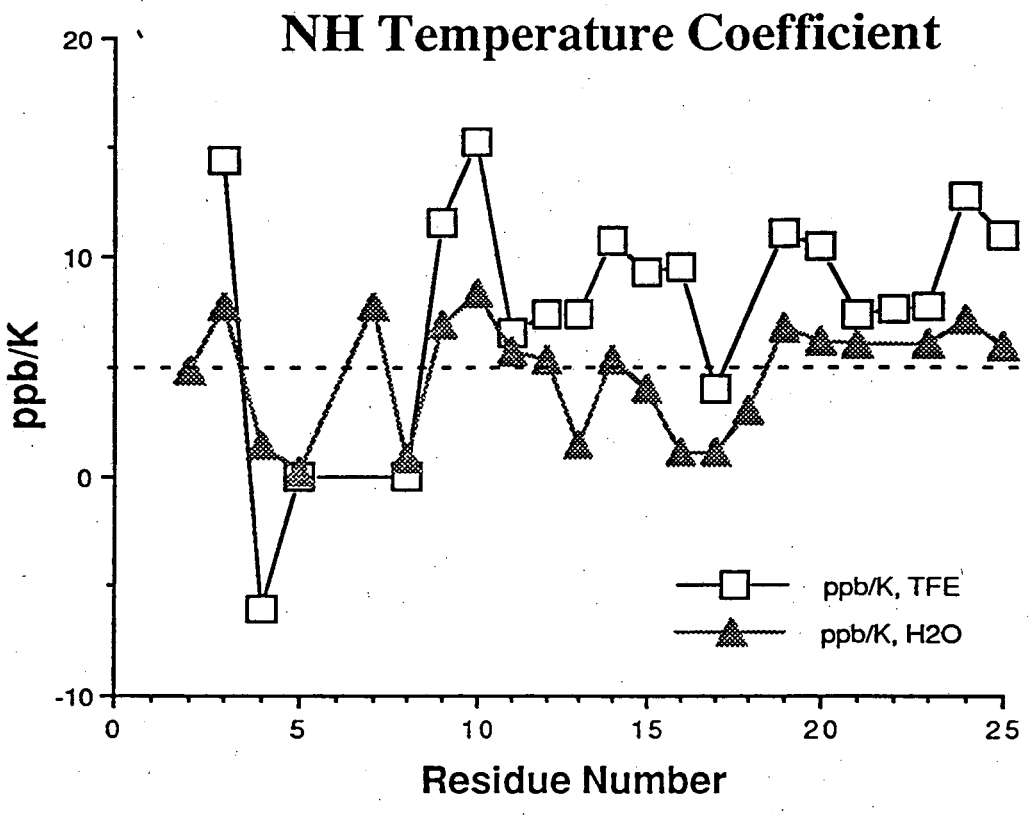

Figure 5.4 - Amide proton chemical shift temperature coefficients as a function of residue number in H_2O (triangles) and 50 volume % TFE (squares). A dashed line is drawn at 5ppb/K, above which value others suggest the amides are not hydrogen bonded intramolecularly.[9]

TFE to 80 vol. % stabilizes an estimated 3.9 (Brahms & Brahms, 1980) to 5.7 (Chang *et al.*, 1978) additional helical residues. If we consider only those residues whose conformation is not constrained by the disulfide bonds, these data indicate that seven residues between 16 and 25 of this hybrid peptide are helical under these conditions, or that these ten residues are helical 70% of the time.

The CD measurements indicate that the S-peptide sequence in 50% TFE at 20°C is not entirely in one conformational state. Additional TFE and decreased temperature further increase the helix content. Therefore under these conditions the helix as observed in the NOESY spectra is in equilibrium with some other structure(s). Helical NH_i-NH_{i+1} crosspeaks are seen throughout the S-peptide sequence, but the long-range α_i-NH_{i+3} crosspeaks are weak or unobservable beyond residue D19. The dynamics of the conformational equilibrium play an important role in the observation of long-range α_i-NH_{i+3} NOE connectivities. Six consecutive backbone ϕ and ψ angles must be restricted to maintain the short α_i-NH_{i+3} distance required for observation of the NOE, while only two such angles need adopt helical values for the observation of sequential NH_i-NH_{i+1} NOEs. Furthermore, the α_i-NH_{i+3} distance in a regular α-helix is 3.4Å, while the NH_i-NH_{i+1} separation is shorter, 2.8Å. Because the NOE intensity is proportional to the inverse sixth power of the internuclear separation, the long-range α_i-NH_{i+3} crosspeaks typically attain less than one third the intensity of the sequential NH_i-NH_{i+1} crosspeak in a regular helix. The uniform intensity of the sequential NH_i-NH_{i+1} connectivities indicates the helix persists to the

end of the peptide, yet long-range order is not maintained for a sufficient period to allow $\alpha_i H\text{-}NH_{i+3}$ connectivities to be detected.

Very weak $\alpha_i H\text{-}NH_{i+2}$ crosspeaks were observed for residues 15-17 and 16-18. The $\alpha_i H\text{-}NH_{i+2}$ distance is too great to give rise to an observable NOE in a regular helix, hence these crosspeaks arise from a non-helical conformation of the peptide. These i,i+2 crosspeaks reflect local order in the non-helical state and are indicative of turn-like conformations. Such interactions have been seen in "nascent" or incomplete helices (Dyson *et al.*, 1988). Beyond residue M18 these crosspeaks are not observed. This may indicate that the non-helical state is less ordered or more extended for these residues, or that additional conformers are accessible to the untethered C-terminus. However, the relatively great intensities of helical connectivities demonstrate that the preferred conformation of the entire S-peptide sequence in TFE solutions is helical.

It is difficult to isolate the effects of TFE on helix initiation, propagation, and termination. TFE and water differ in several chemical properties which may affect helix formation. For example, TFE might promote helix formation by facilitating charged interactions amongst side chains and with the macroscopic helix dipole moment. TFE should increase the magnitude of these effects as its dielectric constant, 26.67, is about one third that of water (Llinas & Klein, 1975). However, the additional helix stabilized by TFE in the current work contains no ionized groups save the terminal carboxylate. TFE should diminish any helix promoting effect of this group by virtue of its unfavorable interaction with the negative terminus of the helix dipole. Furthermore, charge effects should be

reflected in the enthalpic term of the free energy of helix stabilization, yet thermodynamic studies indicate the stabilizing effects of TFE are entropic in origin (Conio *et al.*, 1970). Finally, CD studies show that TFE does not magnify the helix stabilizing properties of ionizable side chains in the free S-peptide (Nelson & Kallenbach, 1986).

The helix stabilizing effects of TFE might also be due to specific interactions of TFE with the helix. The NOESY spectrum should be affected by such specific interactions, yet nothing unusual was observed with this peptide in TFE. The amide protons of the apamin-like part of the hybrid broaden selectively as the temperature is decreased, an effect also seen with apamin itself in 50% TFE (data not shown). The helical portions of both peptides, however, do not behave unusually. Furthermore, as shown in figure 5.3, conditions of 50% TFE and 3°C stabilize the same proportion of helix as 80% TFE and 20°C. The CD spectra under these conditions are nearly superimposable. Taken together, these NMR and CD results would indicate that the effect of TFE is strictly thermodynamic in origin, not a result of direct interaction of TFE with the helix state of the peptide. Therefore, as suggested by others (Conio *et al.*, 1970) helix stabilization by TFE is likely the result of altered hydrogen bonding in the coil state.

The intramolecular hydrogen bonds of peptide NH and CO groups in the helix form in competition with intermolecular hydrogen bonds with solvent in the coil state. TFE should have the most profound effect on the hydrogen bonding in the coil state, as the activity of H_2O is lowered and TFE can become a direct partner in

forming these bonds. It is likely that the coil state of the peptide is destabilized by TFE relative to the helix, with the consequent shift in helix-coil equilibrium. Because TFE is more acidic than water, it can donate to hydrogen bonds with the peptide carbonyls more readily (Nelson & Kallenbach, 1986). In this event the destabilizing effects of TFE on the coil state are due to the less effective hydrogen bonding of the backbone NH. This implies that satisfying the hydrogen bonding potential of the peptide NH plays a more important role in stabilizing the helix conformation than that of the backbone carbonyl.

The relative importance of peptide amide and carbonyl groups in stabilizing helical conformations can be addressed by observing the effects of residues contiguous with a helical segment. The N-terminal three amides and the C-terminal three carbonyls of a helix are not involved in the regular intramolecular hydrogen bonding array, and therefore do not contribute to helix stability. However, helical sequences in proteins are often flanked with amino acids whose side chains can satisfy the hydrogen bond potentials at the ends of helix (Presta & Rose, 1988). The ends of helices can be stabilized by interaction with the side chains of contiguous amino acids, which will in turn contribute to overall helix stability. By studying the effects of such groups on helix formation, the relative importance of these hydrogen bonds can be asessed.

This "helix hypothesis" was demonstrated in studies of isolated peptides incorporating helical sequences derived from native proteins, along with 3-4 flanking amino acids (Bruch *et al.*, 1991). These peptides show some helical structure in aqueous solution,

which is diminished by removing the hydrogen bonding capabilities of the amino acids adjacent to the helical sequence. In this study, however, the residues at both termini were changed in concert. If the "helix-amide hypothesis" stated above is correct, a greater reduction in helicity should be realized by removal of the N-terminal hydrogen bonds than removal of those at the C-terminus. It would be interesting to study the effects of helix flanking residues at the N-terminus and C-terminus independently. In this way the relative importance of hydrogen bonding the amide and carbonyl groups can be assessed.

We had previously observed that in water the "helix-stop" signal for this peptide is distributed over several residues. Only the N-terminus is altered in our hybrid, resulting in the near perfect nucleation of the α-helix. Once initiated, the helix would be expected to propagate similarly in both peptides, as the sequence of C-terminal amino acids is the same. This hybrid peptide does not exhibit the discreet helix stop signal around residue M18 (M13 of S-peptide) as observed by others (Kim & Baldwin, 1982; Nelson & Kallenbach, 1986; Nelson & Kallenbach, 1989). The NOE data presented herein unequivocally show that the entire S-peptide sequence can favorably adopt a helical conformation at high concentrations of TFE.

This study demonstrates the helix propagating effects of TFE on marginally stable peptide helices. Using a covalently initiated turn of helix, we have shown that the helix-stabilizing effects of this solvent are due at least in part to facilitated propagation of an extant helix. We also provide evidence that this stabilizing effect is a

general solvation effect and not a specific interaction of the helical peptide with TFE. Specifically we propose that TFE destabilizes the coil state by less effective hydrogen bonding of the peptide amide. Furthermore, TFE stabilized a helical conformation in this peptide sequence which is helical neither in water nor in the native protein from which it is derived.

Brahms, S & Brahms, J. (1980) *J. Mol. Bio.* **138**, 149-178.

Bruch, M. D., Dhingra, M. M., & Gierasch, L. M. (1991) *Proteins* **10**, 130-139.

Chang, L. T., Wu, C. C., & Yang, J. T. (1978) *Analytical Biochemistry* **91**, 13-31.

Conio,G., Patrone, E., & Brighetti, S. (1970) *J. Biol. Chem.* **245**(13), 3335-3340.

Dyson, H. J., Rance, M., Houghten, R. A., Wright, P. E., & Lerner, R. A., (1988) *J. Mol. Bio.* **201**, 201-207.

Dyson, H. J., Rance, M., Houghten, R. A., Lerner, R. A., & Wright, P. E. (1988) *J. Mol. Bio.* **201**, 161-200.

Kim, P. S. & Baldwin, R. L. (1982) *Ann.Rev.Bioc.* **51**, 459-489.

Llinas, M. & Klein, M. P. (1975) *J. Am. Chem. Soc.* **97**, 4731-4737.

Nelson, J. W. & Kallenbach, N. R. (1986) *Proteins* **1**, 211-217.

Nelson, J. W. & Kallenbach, N. R. (1989) *Biochemistry* **28**, 5256-5261.

Pease, J. H. B., Storrs, R. W., & Wemmer, D. E., (1990) *Proc. Nat. Acad. Sci.* **87**, 5643-5647.

Presta, L. G. & Rose, G. D. (1988) *Science* **240**, 1632-1641.

Ptitsyn, O. B. & Finkelstein, A. V. (1980) *Quart.Rev.Biophys.* **10**, 339-386 .

Richardson, J. S. (1981) *Advances in Prot.Chem.* **34**,167-339.

Rico, M., Gallego, E., Santoro, J., Bermejo, F. J., Nieto, J. L., & Herranz, J. (1984) *Biochem. and Biophys. Research Comm.* **123**(2), 757-763.

Wüthrich, K. (1986) *NMR of Proteins and Nucleic Acids*, Wiley and Sons, New York.

Chapter 6: Activity of the Hybrid Peptides

Introduction:

The helical sequences of the apamin hybrids are intimately involved in the biochemical function of the proteins from which they are derived. In these examples the juxtaposition of the amino acid side chains lies at the root of the proper function. A helical backbone conformation is necessary but not sufficient to properly orient the side chains. Often the native side chain conformation is determined by interaction with other parts of the protein and is not well defined in the isolated helix. For the stabilized helix to effect chemistry the side chains must adopt a well defined orientation when associated with their biochemical partners. In the "lock and key" theory of protein interaction the proper, functional orientation is adopted prior to association (Neubig & Thomsen, 1989). In contrast, the hypothesis of "induced fit" calls for the binding energy to alter the equilibrium conformation distribution to allow close fit (Jorgensen, 1991). While normally applied to the overall protein fold, these concepts are equally applicable to the consideration of side chain orientation. The ability of the side chains to adopt their functional orientation is not a forgone conclusion of the helicity of the backbone. In this chapter the ability of these peptides to replace their cognate sequences in biochemical processes will be investigated.

The Apamin/434 repressor hybrid was designed so that the face of the helix which contacts the major groove of the operator DNA

would be solvent exposed. Binding of the full 434 repressor to DNA is achieved by a combination of charge complementarity and hydrophobic and van der Waals forces as well as hydrogen bonding between the protein and the DNA (Aggarwal *et al.*, 1988). Sequence specificity in this system is thought to be conferred by direct hydrogen bonding of three glutamine side chains from the recognition helix directly with the bases of the operator DNA.

While the total binding energy is realized by interaction of many residues in the protein with the DNA, only a subset of these are possible with the truncated 434 sequence in the hybrid peptide. However, it was hoped that the hydrogen bonding characteristics of the glutamine side chains would be sufficient to mediate sequence specific recognition of the operator DNA. This would afford a sequence-specific DNA recognition system of a size amenable to NMR structural characterization, and would allow for delineation of the various interactions which determine the sequence specificity. In particular, it is of interest to know the relative importance of the aforementioned forces in determining affinity in aqueous solutions. This knowledge could then be used to design peptides with altered specificity, with obvious ramifications in the study of gene regulation and expression, and possibly in medicinal gene therapy.

As the full-sized 434 repressor binds as a symmetric dimer to a 14 base pair palindromic DNA sequence (Koudelka *et al.*, 1987), the hybrid peptide should bind as a monomer to half this sequence. Attempts to observe binding of the Apamin/434 peptide to half of the operator DNA sequence by enzymatic and chemical footprinting techniques met with repeated failure. This result motivated a

modeling study of the proposed peptide/DNA complex. In the 434/DNA cocrystal structure the recognition helix sits within the major groove to allow the proper amino acid contacts with the nucleotides (Anderson *et al.*, 1987). In the high resolution crystal structure of the complex now available the methylenes of the glutamine residues, presumed to be extended in our initial design, were shown in fact to fold back along the helix axis in the protein/DNA complex (Aggarwal *et al.*, 1988). This allows close hydrophobic contacts of these methylenes with the base pairs in the major groove. This requires that the recognition helix of 434 to be completely buried within the major groove, where the apamin part of the hybrid simply won't fit.

When the helix backbone from the apamin structure is superimposed on the backbone of the recognition helix of the native complex (Aggarwal *et al.*, 1988), the backbone of residues 1, 2, and 3 of the apamin scaffold overlapped with both phosphodiester backbones of the duplex DNA (figure 6.1). Altering the position of the cysteine residues along the helical segment causes overlap with the phosphodiester backbone on other strand of DNA (figure 6.2). While the overlap of the second hybrid construction is less severe, the sequence of this hybrid replaces residue T8 from the apamin scaffold with Q27 from the 434 repressor sequence. The latter residue makes direct contact with the bases of the operator DNA, and must be maintained for sequence specificity. Threonine 8, however, forms the "helix cap" (Richardson & Richardson, 1988). Without this residue there is no guarantee the peptide would fold into the desired conformation, with the correct 1-11, 3-15 orientation of disulfide

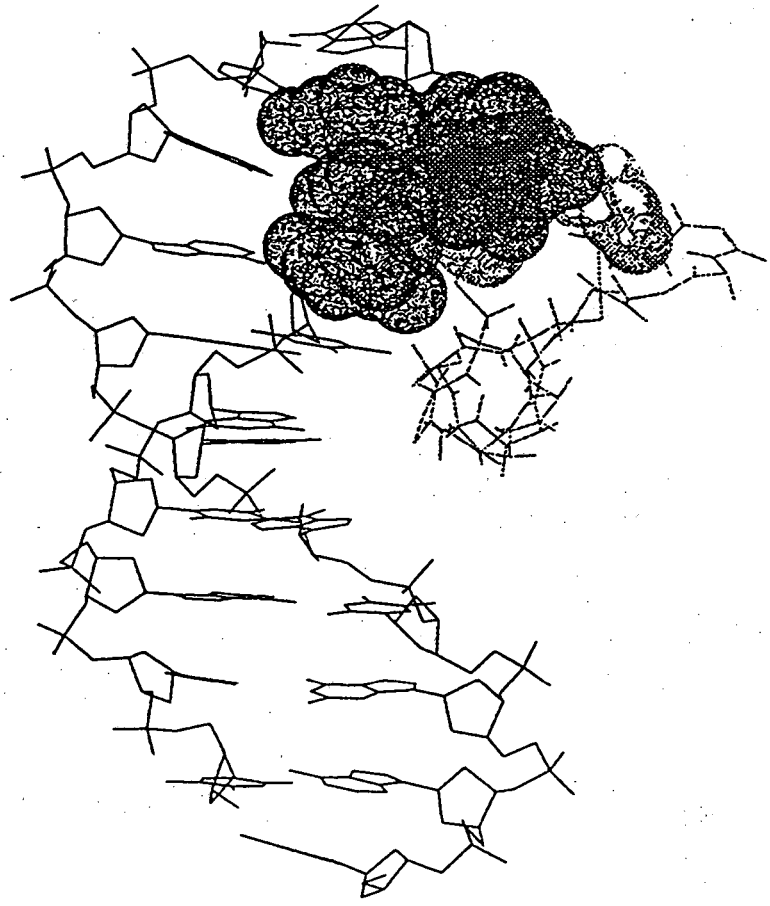

Peptide sequence: CNC KAP ETQ QCA AQC QNG KTK RPR

Figure 6.1 - Model of the apamin/434 hybrid peptide described in Chapter 4 with the operator DNA. The backbone of residues 8-16 of this hybrid peptide were superimposed on the backbone of residues 27-35 of the 434 repressor protein from the crystal structure of Aggarwal *et al.* (1988). Van der Waals surfaces of residues 1-3 of the hybrid and residues B13-14 of the operator DNA are shown to demonstrate the steric interference to binding.

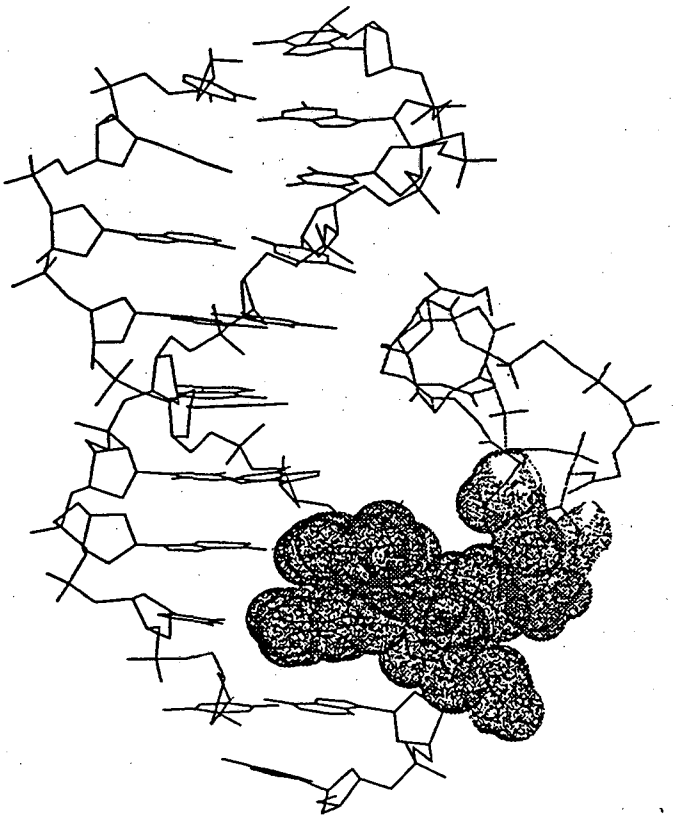

Peptide sequence: CNC KAP EQQ SCE QLC NGK TKR PR

Figure 6.2 - Model of an apamin/434 hybrid peptide (not investigated experimentally) with the operator DNA. The backbone of residues 8-16 of this hybrid peptide were superimposed on the backbone of residues 28-36 of the 434 repressor protein from the cocrystal structure of Aggarwal *et al.* (1988). Van der Waals surfaces of residues 4-6 of the hybrid and residues A4-5 of the operator DNA are shown to demonstrate the steric interference to binding. The helix and DNA are in the same orientation as the previous figure - the apamin scaffold is rotated due to the altered sequence.

bonds. Only by the addition of an extra turn of peptide helix could the apamin scaffold be accommodated in the complex, while maintaining the proper DNA contacts of the glutamine side chains. This would result in a larger peptide whose structure at the functional residues is less well determined by the stabilizing disulfide bonds.

In contrast to the depth of the major groove of B-form DNA, the site of association on the S-protein of ribonuclease A for the S-peptide is relatively shallow (Wlodawer & Sjölin, 1983). In a modeling study analogous to that described above, the helical portion of the S-peptide backbone from the Apamin/S-peptide structure was superimposed with the same residues of S-peptide in the crystal structure of ribonuclease A (figure 6.3). This model demonstrated the potential for favorable interaction between the hybrid peptide and S-protein. No rearrangement of either polypeptide backbone was necessary, suggesting that the apamin/S-peptide hybrid and S-protein should form a stable complex.

Because the S-peptide is necessary for the endoribonuclease activity (Richards & Vithayathil, 1959), this system could be utilized to demonstrate the functional relevance of the apamin-stabilized helices. Removal of the S-peptide from ribonuclease A creates the inactive S-protein. The loss of endoribonuclease activity is due to the separation with S-peptide of a histidine residue, H12, from the active site. Histidine has been implicated in a charge-shuttling mechanism of catalysis for this enzyme. Adding S-peptide to the inactive S-protein results in an active complex, called ribonuclease S, which is indistinguishable from ribonuclease A by kinetic parameters

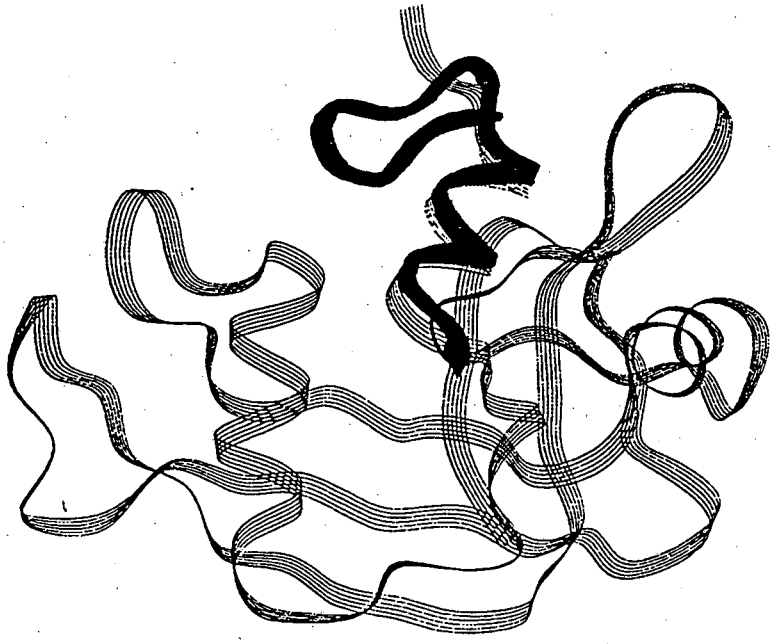

Figure 6.3 - Ribbon diagram of the peptide backbone of apamin/S peptide hybrid (solid) superimposed on residues 3-11 of ribonuclease A (stripes). There is no overlap of the apamin scaffold with the S-protein.

(Richards & Vithayathil, 1959). Since the apamin/S-peptide hybrid possesses the necessary histidine residue, it was hoped that the apamin/S-peptide hybrid would associate with S-protein and reconstitute endoribonuclease activity.

Materials and Methods

2µl of either authentic S-peptide (200 or 2µM), the hybrid (200 or 2µM), or water (control) was mixed with 2µl of S-protein (3.6µM; Sigma). These were mixed and allowed to stand at room temperature for 10 minutes to allow association of the peptide with the protein. Following this incubation 10µl of RNA (18S and 23S; Boehringer Mannheim) at 80µg/ml in 0.1 M NaOAc (pH 5) at 0°C was added and quickly mixed. After a reaction time of 15-60 seconds, the reaction was quenched by adding 50 µl of phenol/chloroform (1:1) and mixing. The water layer was separated and the RNA precipitated with three volumes of cold ethanol. Following centrifugation, the RNA was resuspended in 30% (v/v) glycerol and run on 1.2% agarose gels. The reaction products were visualized with ethidium bromide and UV light.

Results:

The gel is presented in figure 6.4. The initially separate bands of 18S and 23S RNA components of the reactants are replaced by broad bands of cleavage products running faster on the gel in those lanes loaded with active RNase. No cleavage products were observed for unreacted RNA or RNA incubated with either peptide in the absence of S-protein. However, incubation of the RNA with S-protein in combination with native S-peptide resulted in the expected smear of cleavage products which ran much faster on the gel. Incubating

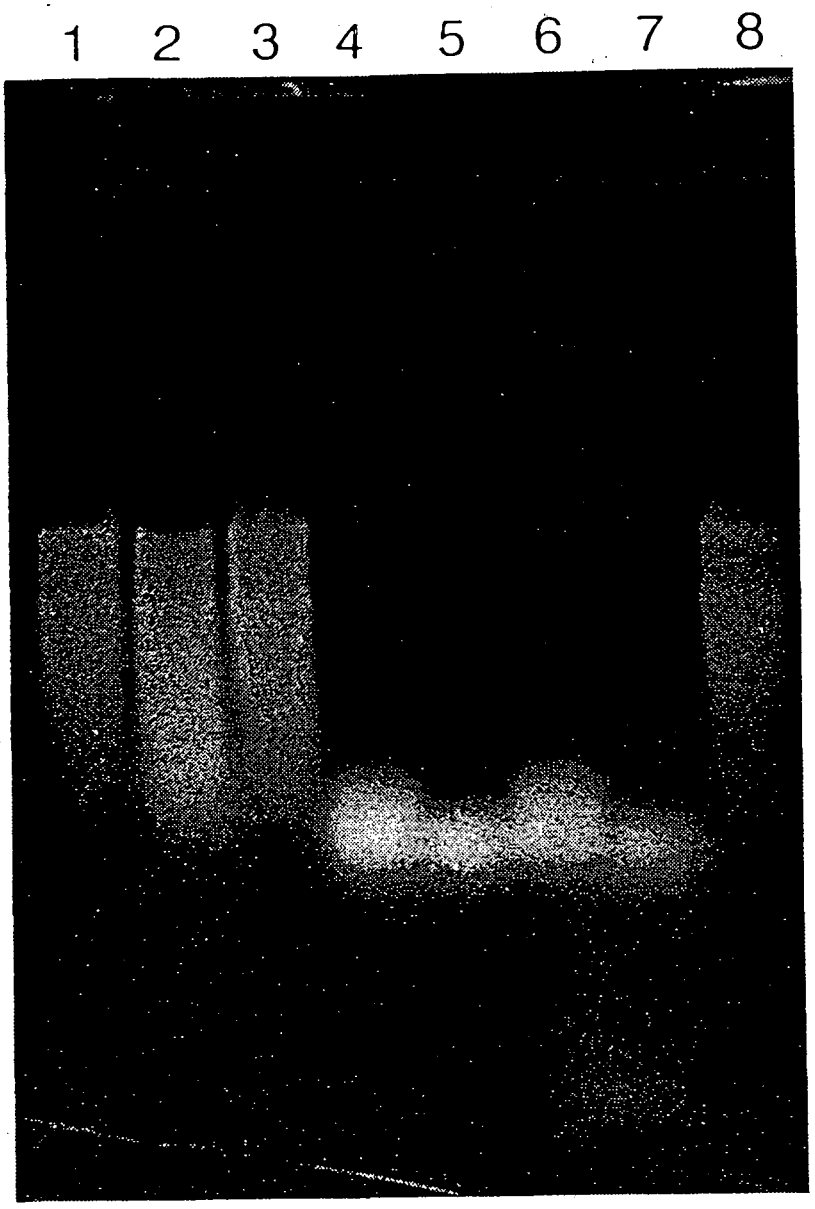

Figure 6.4 - Ethidium-stained agarose gel showing hydrolysis of a mixture of 16S and 23S RNA by reconstituted RNase. Lanes: 1, RNA only; 2, S protein only, 15 sec. reaction; 3, S protein only, 60 sec. reaction; 4, S protein + apamin/S-peptide hybrid, 15 sec. reaction; 5, S protein + apamin/S-peptide hybrid, 60 sec. reaction; 6, S protein + S peptide, 15 sec. reaction; 7, S protein + S peptide, 60 sec. reaction; 8, apamin/S-peptide hybrid only, 60 sec. reaction.

RNA with S-protein in association with the apamin/S-peptide hybrid showed a similar extent of cleavage. No difference in endoribonuclease activity could be detected with this assay, even at short reaction times. Some cleavage was detected when RNA was incubated with S-protein alone, however this reaction did not proceed consistently to a significant extent when compared to RNA incubated with S-protein complexed with either native S-peptide or the apamin/S-peptide hybrid. This background cleavage is likely due to residual ribonuclease A and/or ribonuclease S known to be present in the S-protein reagent (used as supplied with no further purification).

Discussion:

This experiment demonstrates that the helix stabilized by the apamin scaffold is biologically relevant, capable of being recognized by the cognate site on the S-protein. This interaction constrains the side chains in an orientation which facilitates endoribonuclease activity. Whether this occurs via a lock-and-key or an induced fit mechanism is unclear. The side chains of the hybrid peptide are dynamically disordered as evidenced by their lack of significant NOE's. There is a family of side chain conformers in solution, only some of which are appropriate for functional association with S-protein. It is possible that each peptide molecule visits the functionally relevant conformation immediately prior to collision with a molecule of S-protein. This hypothesis requires multiple unfavorable collisions prior to successful association, yet this is possible given the 10 minutes of incubation prior to the addition of RNA. Once associated the peptide is constrained to maintain its

conformation by the binding energy.

The alternative possibility is that the peptide first associates with the S-protein in a somewhat random conformation, and then reorganizes to the active conformation by adjusting its side chain conformation while associated. This hypothesis invokes a high energy binding mode, where the peptide is associated with the protein but in a suboptimal fashion from both energetic and functional perspectives. The additional binding energy due to optimal side chain interactions drives the side chains into the functionally relevant conformation while associated with the protein. The side chain's conformation is driven in a concerted fashion, rather than a stochastic one, which is more aesthetic description but may not be correct (Jorgensen, 1991).

The latter description is supported by studies of the association and refolding of S-peptide with S-protien. The kinetics of this process have been investigated in detail, and are complicated by several unfolded forms with different refolding kinetics (Labhardt & Baldwin, 1982). However, only two kinetic processes are observed for the peptide component of this reaction. The faster component displayed second order kinetics, while the slower component displayed first order kinetics (Labhardt *et al.*, 1983). These components were assigned to association and structuring of the S-peptide, respectively. The structuring of the S-peptide was later shown to involve the formation of α-helix (Labhardt, 1984). Helix formation is a more gross structural change than occurs with the hybrid sequence peptide in this work, where the helix is already stabilized by the apamin scaffold. That association with S-protein

occurs prior to helix formation in the S-peptide supports the hypothesis that the apamin/S-peptide hybrid similarly associates with S-protien prior to the functional reorientation of the amino acid side chains.

Some insight into the mode of binding can be had from thermodynamic studies of the binding event. In collaboration with Patrick Connelly, working with Prof. Sturdevant at Yale University, precision titration calorimetric analysis was done on the association of S-protein with both S-peptide and the apamin/S-peptide hybrid (figure 6.5). The free energies of binding to S-protein for the two peptides were remarkably similar, in agreement with the kinetic data presented above. However, this agreement was a consequence of a decrease in both enthalpy and entropy of binding for the hybrid peptide, effects which serendipitously cancel at room temperature. The drop in the entropy contribution to the overall free energy of binding is very close to the theoretical gain predicted by restricting the conformational ensemble of unassociated states. This comparison assumes that nine amino acid residues become helical upon association of the random coil S-peptide.

The reduced enthalpy of the hybrid association is harder to explain. In the modelling study described above several side chains of the S-protein would need to reorient to accommodate the apamin scaffold. This alone should not require a great amount of free energy because it is known from NMR studies that solvent exposed side chains on the surface of globular proteins are generally mobile or dynamically disordered. However, one of these side chains is a lysine, which could interact unfavorably with residue K4 of the

	$\Delta G_{binding}$	$\Delta H_{binding}$
S-peptide	-9.5 kcal/mol	-39 kcal/mol
Apa-S hybrid	-9.4 kcal/mol	-29 kcal/mol

$$-T\Delta\Delta S = -10 \text{ kcal/mol}$$

expected $$-T\Delta\Delta S = -RT \ln (N_2/N_1) = -11.7 \text{ kcal/mol}$$

Figure 6.5: Titration calorimetric data of peptide binding to S-protein. Expected entropic gain calculated assuming 3 rotamers at each φ and ϕ peptide backbone dihedral for 9 residues ($N_2 = 3^{*9}$) are constrained to a single conformational state ($N_1 = 1$) in the hybrid. Data from Patrick Connelly (Yale).

hybrid and account for the decreased enthalpy. Of course this is only speculation, and is likely just one of many contributors to the overall binding energy.

Addition of S-peptide to S-protein results in circular dichroism changes which can be time resolved on a timescale of several hundred milliseconds (Labhardt, 1984). The spectral characteristics of the CD changes are consistent with the formation of additional α-helix. This additional helix likely results from the restructuring to the S-peptide from the unassociated, mostly random coil state to the associated, helical conformation. With the apamin construct there is no such transition, and therefore there would be little or no change in CD to be measured. This assay then cannot be used to monitor the kinetics of association of our hybrid with the S-protein. Such analysis will require a new technique, and will be left for future investigators.

Aggarwal, A.K., Rodgers, D.W., Drottar, M., Ptashne, M., & Harrison, S.C.; (1988) *Science*, **242**, 899-907.

Anderson, J.E., Ptashne, M., & Harrison, S.C.; (1987) *Nature*, **326**, 846-852.

Jorgensen, W.L.; (1991) Science, **254**, 954-955.

Koudelka, G.B., Harrison, S.C., & Ptashne, M.; *Nature*, **326**, 886-888.

Labhardt, A.M.; (1984) *Proc. Nat'l. Acad. Sci.* **81**, 7674-7678.

Labhardt, A.M. & Baldwin, R.L.; (1982) *J. Mol. Biol.*, **135**, 231-244.

Labhardt, A.M., Ridge, J.A., Lindquist, R.N., & Baldwin, R.L.; (1983) *Biochemistry*, **22**, 321-327.

Neubig, R.R. & Thomsen, W.J.; (1989) *Bioessays*, **11**, 136-141.

Richards, F.M. & Vithayathil, P.J.; (1959) *J. Biol. Chem.*, **234**, 1459-1465.

Richardson, J.S. & Richardson, D.C. (1988) *Science*, **240**, 1648-54.

Wlodawer, A. & Sjölin, L.; (1983) *Biochemistry*, **22**, 2720-2728.

APPENDIX: Cell culture and Ig purification

Thawing cells: The cells were thawed in the freezing/shipping vial by gently swirling in a 37°C water bath. *Once the thawing process has begun it is critical to thaw and wash the cells as quickly as possible.* As soon as the media is fluid it is quickly pipetted into a waiting 15ml conical tube containing 10ml RPMI-1640/gent with 10% FCS warmed to 37°C. *I found washing with this media gave the cells a "jump-start", and used this regardless of the composition of the freezing or desired growth media.* This tube is immediately placed in a desktop clinical centrifuge and the cells gently pelleted by spinning for 5-7 minutes at a speed setting of 3. The medium was decanted from the pellet of cells, which were resuspended in the remaining drop of medium by rapping the tube on the countertop. The cells were then suspended in the desired amount of the desired media. *There is a lag phase of growth lasting 1-3 days following thawing. Do not be lulled into complacency or discouraged because viable cell density does not increase during this period. The only reliable indicator of unsuccessful thawing is decreasing cell viability.*

Cell counts: The density of cells is determined with a cytometer, a microscope slide with a defined area grid inscribed. With the coverslip in place, the resulting volume per large division (which nearly fills the field of view at moderate magnifications) is 10^{-4}ml. A suspension of cells is introduced by pipetting 10µl into the groove under one end of the coverslip. Capillary action will draw the cells into the defined volume if the cytometer is clean. If the

suspension does not quickly and evenly fill the area, remove the coverslip and clean it and the cytometer with 70% ethanol. Dry and repeat. Counting the number of cells (X) in the large area will immediately translate into a cell density of X x 10^4 cells/ml. If X is less than 10, the count will not be statistically significant. In this event, count the cells in the four large grids off each apex of the center large grid (you will have to move the cytometer around on the stage to do this) and divide the total by four. Healthy cells will appear smooth and nucleated. An irregular shape or grainy texture are signs of a suffering cell. They should not be clumped, although actively dividing cells are often observed during log phase growth.

Viable cell counts can be obtained by a similar procedure, preceded by diluting the cell suspension 1:1 with Trypan Blue. Intact cell membranes are impermeable to this dye, but dead cells and cell debris are quickly stained blue. Microscopic inspection in the cytometer of such a suspension allows enumeration of both live, unstained cells and dead, stained cells in the manner described above. The counts, however, must be multiplied by two to account for dilution by the dye solution. A good culture will have greater than 95% live cells except, perhaps, just after it is thawed.

Cell growth: Every hybridoma is unique in its growth behavior. Optimal cell densities and media composition will vary for each, as will the manipulations required to adapt the cells to new media conditions. Hybridomas are grown in shallow, stationary culture flasks in a 37°C water jacketed incubator with a controlled atmosphere of 7-10% CO_2 and 100% humidity. *To facilitate gas exchange (critical to mammalian cell growth) the cultures can be no*

deeper than 1cm. The caps on each culture flask must be loose. Additionally I have found that stacking the flasks inhibits growth. The flasks must be separated both vertically and horizontally from their neighbors. Humidity is maintained by pans of water in the bottom of the incubator. Make sure these do not go dry. In general hybridomas grow best at cell densities in the range of 8 x 10^4 to 8 x 10^5 cells/ml and with at least 5% FCS. When the cell density nears the top of this range the culture is either expanded or cut back. Expansion is merely diluting the culture into more media, pre-warmed to 37°C and preferably pre-equilibrated with the atmosphere of the incubator. Cutting back involves removing a prescribed volume of cell suspension and replenishing it with fresh, prewarmed media. *I have found that large dilutions of growing cultures promotes most rapid growth. For instance, expanding a cell culture from* 8 x 10^5 cells/ml *to* 8 x 10^4 cells/ml *in one step resulted in an order of magnitude increase in cell density in 26 hours for* IGEN #5, *or a doubling time of 8 hours. Smaller expansions resulted in a doubling time of about 16 hours for this cell line.*

Suspending cells: Hybridomas will sink to the bottom of the culture flask. Some will adhere to the flask. For accurate cell counts and uniform expansion these cells must be evenly resuspended by rapping the flask on the countertop. For smaller flasks up to 25ml culture volume this is best accomplished by horizontal rapping against the lip of the hood or other vertical object. For T-175 75ml culture flasks, better results are obtained by sharply rapping in a vertical motion from a height of 5 cm. In either case, frothing of the media is to be avoided as is unnecessary

rapping. To check for complete suspension swirl the culture gently while looking through it at the overhead lights. The macroscopic hybridoma cells should swirl with the media. The flask should not look fuzzy or clouded.

Adapting cell cultures to new media conditions, for instance minimal FCS, is best done slowly by serial 1:1 dilution of the old media into the new. Some cell lines are very forgiving: IGEN #5 for instance can be expanded from RPMI/10% FCS to PFHM/2% FCS in a single 1:10 expansion without a break in doubling time. Others, like the *anti*-JWJ/1 cell line 4A1-G5, requires more coddling with no greater than a two-fold change in FCS concentration. Until familiarity with a particular cell line is achieved, it is necessary to monitor cell density and viability at least daily, and maintain a culture in known high-growth conditions as a control.

Antibody production Hybridomas are screened and selected for high constitutive production of antibodies. Antibodies will be produced throughout the growth cycle, yet during the log phase of culture expansion much of the cellular machinery is harnessed for cell division. More metabolic energy can be directed towards antibody production in the stationary phase, once the culture has attained its maximum viable density. This is usually in the range of 1-3 x 10^6 cells/ml, but again is unique to each hybridoma. Once cell division is suspended antibody production can begin in earnest, however, dying cells can release proteolytic enzymes that both digest antibodies and attack viable cells. The balance between production and degradation is, once again, unique to each cell line.

There are a plethora of enhancer supplements to both

protect stationary phase cultures from proteolysis and induce more antibody production. These, too, have different effects on different cell lines. I have tried products from BMB (Nutridoma) and Gibco/BRL (ObtiMab) and found neither to have any impact on IGEN #5 production levels. However, this cell line routinely produces a healthy 15 mgs Ig/liter. Antibody production by the cell line 4A1-G5 is boosted by an average of 30% by either of these supplements. My choice for this cell line would be the BMB product due to its ease of use. The enhancement proffered by either of these products is variable, however, probably because of the additional manipulation required for administration to the stationary phase culture. The supplements require pelleting the cells and resuspending them in new media after reaching stationary phase. Pelleting large cultures is best done in 500ml GS-3 rotor bottles. The suspension is spun for 10 minutes at 500 rpm, slower than the Sorvall ratemeter is calibrated. Therefore one must estimate the proper speed by trial and error. I have found that slower spins for longer times give the best results. The Jouan desktop centrifuge can also be used, however the swinging bucket rotor does not pellet the cells well causing large losses when the media is removed. Resuspension is accomplished by adding 20ml of the desired media to each bottle and gently swirling. Generally 20-30% of the viable cells are lost in the pelleting/resuspension step.

Harvesting antibodies: Once cell viability is less than 50%, or the antibody ELISA titer ceases to increase (whichever comes first) the antibody should be harvested. Typically this occurs 7-14 days after stationary phase has been achieved. First pellet the cells

in the GS-3 rotor by centrifugation at 10,000 x g for 15 min. Decant the supernatent and discard the cells. To a gently stirring flask of supernatent slowly add an equal volume of saturated ammonium sulfate. At no time should foam develop on the surface; this indicates the protein is being denatured by too vigorous stirring. It should take no less than 10 minutes to add one liter of ammonium sulfate. The suspension will appear only slightly translucent. Allow the suspension to stir gently for one hour, then centrifuge at 10,000 x g for 15 minutes. Discard the supernatent and allow the pellets to drain completely. The pellets will readily resuspend in a few milliliters of any buffer near neutral pH with more than 50mM NaCl. Covering the pellet with the buffer for an hour makes this a facile task. That which won't resuspend is precipitated cell debris and should be pelleted and discarded before continuing.

Protein A affinity chromatography: Protein A is a cell membrane associated protein from Staphalococcus which selectively binds IgG in a pH dependent fashion. Recombinant Protein A covalently linked to agarose beads is readily available from a number of manufacturers; other solid supports are also available. The agarose supports are easily crushed, therefore take heed of flow rates and column height to preserve this rather costly chromatography medium. Columns should never be taller than 5cm and should freely flow at rates not to exceed one drop every 3-4 seconds. A protein A column has an enormous capacity for IgG binding. One ml of Protein A/agarose will bind 6-10 mgs IgG. The small flow rate is more than compensated by the small column volume, making this an efficient one-step isolation.

The following buffers are used with Protein A/agarose:

Binding Buffer: 1.5M Glycine
3.0M NaCl
0.05% (w/v) NaN_3
pH 8.9

Elution Buffer: 0.1M Citrate
0.05% (w/v) NaN_3
pH 3.0

Collection Buffer: 1M Tris pH 9.0

Regeneration Buffer: 1.5M NaSCN

Storage Buffer (PBS): 50mM NaH_2PO_4
150mM NaCl
0.05% NaN_3
pH 7.2

The columns should be kept refrigerated, but chromatography may be done at room temperature. The Elution Buffer will slowly degrade the column material; the column should always be quickly regenerated following elution.

Begin by equilibrating the column with Binding Buffer at a flow of no more than one drop every 3-4 seconds, or as fast as the column will flow under a 10cm potential. If the column has been stored for a long period, this often elutes some specie which absorbs at 280nm. After the baseline has stabilized or 5-7 column volumes have passed the sample can be applied directly to the top of the column material. Very slow flow rates are recommended for sample application, one drop every 6 seconds. I have also pumped the sample through the peristaltic pump with good results. Flush the column with Binding Buffer at 4-6 sec./drop until the absorbance

at 280nm is no more than 0.05.

Elute the column with Elution Buffer, again at one drop every 3-4 seconds. When the Ig peak appears collect it in 7 ml aliquots in tubes which have 1 ml of Collection Buffer in them. This immediately neutralizes the acidic pH of the Elution Buffer and prevents acid denaturation of the Ig. Some manual mixing will be required initially due to the different specific gravities of the Elution and Collection Buffers. One can also collect the Ig in a single fraction provided that the Collection Buffer is added in 1 ml aliquots maintaining a 1:7 volume ratio.

Immediately regenerate the column by running 5-7 column volumes of Regeneration Buffer at one drop every 3-4 seconds. Repeat with Storage Buffer (PBS) and refrigerate the column for storage. If the column is going to be reused immediately the Storage Buffer can be skipped and the column reequilibrated with Binding Buffer. The column is stable in Binding Buffer for several days.

LAWRENCE BERKELEY LABORATORY
TECHNICAL INFORMATION DEPARTMENT
1 CYCLOTRON ROAD
BERKELEY, CALIFORNIA 94720